

NONLINEAR DYNAMICS AND SYSTEMS THEORY

An International Journal of Research and Surveys

Volume 24

Number 3

2024

CONTENTS

Improved Power Quality with Active Shunt Power Filter Based on Optimized PI Controller and Flying Squirrel Search MPPT Technique Applied to the WECS.....	217
<i>A. Abbadi, F. Hamidia, A. Morsli, M. R. Skender and A. Tlemçani</i>	
Optimization of Hotel W Management through Performance Comparison of Support Vector Machine and Linear Regression Algorithm in Forecasting Occupancy.....	228
<i>M. Y. Anshori, T. Herlambang, V. Asy'ari, H. Arof, A. A. Firdaus, K. Oktafianto and B. Suharto</i>	
Numerical Solution of Neutral Double Delay Volterra Integral Equations Using Taylor Collocation Method.....	236
<i>H. Bouzeraieb, H. Laib and A. Boulmerka</i>	
Stability Analysis of a Coupled System of Two Nonlinear Differential Equations with Boundary Conditions.....	246
<i>Besma Fadlia, Abdelwahab Zarour, Rima Faizi and Mohamed Dalah</i>	
Trajectory Estimation of Amphibious Aircraft Using H -Infinity and Ensemble Kalman Filter Methods.....	259
<i>T. Herlambang, S. Syamsuar, F. Yudianto, A. Basuki, G. Wijiatmoko, A. Roschyntawati, H. Hendrato, K. Oktafianto and R. S. Marjianto</i>	
Numerical Solution for Benjamin-Bona-Mahony-Burgers Equation Using Septic B -Spline Galerkin Method.....	267
<i>Ali M. Jasim, Adham A. Ali, Isam H. Halil, Fatima Z. Ahmed and Muhannad A. Shallal</i>	
A New Chaotic Supply Chain Model, Its Bifurcation Analysis, Multi-Stability and Synchronization Using Backstepping Control.....	275
<i>M. D. Johansyah, A. Sambas, S. Vaidyanathan, S. S. Abas, H. Hassan, M. Makhtar, S. Purnama and B. Foster</i>	
On Unique Solvability and a Generalized Newton Method for Solving New General Absolute Value Equations.....	286
<i>M. Khaldi and M. Achache</i>	
Adaptive Control for the Stabilization, Synchronization and Anti-Synchronization of New Chaotic System with a Line Equilibrium.....	298
<i>K. Mesbah and N. E. Hamri</i>	
Properties of MDTM and RDTM for Nonlinear Two-Dimensional Lane-Emden Equations.....	309
<i>N. Teyar</i>	

NONLINEAR DYNAMICS & SYSTEMS THEORY

Volume 24, No. 3, 2024

Nonlinear Dynamics and Systems Theory

An International Journal of Research and Surveys

EDITOR-IN-CHIEF A.A.MARTYNYUK

*S.P.Timoshenko Institute of Mechanics
National Academy of Sciences of Ukraine, Kiev, Ukraine*

MANAGING EDITOR I.P.STAVROULAKIS

Department of Mathematics, University of Ioannina, Greece

REGIONAL EDITORS

S.G. GEORGIEV, Paris, France

A.OKNIŃSKI, Kielce, Poland
Europe

M.BOHNER, Rolla, USA
HAO WANG, Edmonton, Canada
USA and Canada

T.A.BURTON, Port Angeles, USA
C.CRUZ-HERNANDEZ, Ensenada, Mexico
Central and South America

M.ALQURAN, Irbid, Jordan
Jordan and Middle East

T.HERLAMBANG, Surabaya, Indonesia
Indonesia and New Zealand

Nonlinear Dynamics and Systems Theory

An International Journal of Research and Surveys

EDITOR-IN-CHIEF A.A.MARTYNYUK

The S.P. Timoshenko Institute of Mechanics, National Academy of Sciences of Ukraine,
Nesterov Str. 3, 03057, Kyiv-57, UKRAINE / e-mail: journalndst@gmail.com

MANAGING EDITOR I.P.STAVROULAKIS

Department of Mathematics, University of Ioannina
451 10 Ioannina, HELLAS (GREECE) / e-mail: ipstav@cc.uoi.gr

ADVISORY EDITOR A.G.MAZKO,

Institute of Mathematics of NAS of Ukraine, Kiev (Ukraine)
e-mail: mazko@imath.kiev.ua

REGIONAL EDITORS

S.G. GEORGIEV, France, e-mail: svetlingeorgiev1@gmail.com

A. OKNINSKI, Poland, e-mail: fizao@tu.kielce.pl

M. BOHNER, USA, e-mail: bohner@mst.edu

HAO WANG, Edmonton, Canada, e-mail: hao8@ualberta.ca

T.A. BURTON, USA, e-mail: taburton@olypen.com

C. CRUZ-HERNANDEZ, Mexico, e-mail: ccruz@cicese.mx

M. ALQURAN, Jordan, e-mail: marwan04@just.edu.jo

T. HERLAMBANG, Indonesia, e-mail: teguh@unusa.ac.id

EDITORIAL BOARD

Adzkiya, D. (Indonesia)

Artstein, Z. (Israel)

Awrejcewicz, J. (Poland)

Braiek, N. B. (Tunisia)

Chen Ye-Hwa (USA)

De Angelis, M. (Italy)

Denton, Z. (USA)

Djemai, M. (France)

Dshalalow, J. H. (USA)

Gajic Z. (USA)

Georgiou, G. (Cyprus)

Honglei Xu (Australia)

Jafari, H. (South African Republic)

Khusainov, D. Ya. (Ukraine)

Kloeden, P. (Germany)

Kokologiannaki, C. (Greece)

Kouzou A. (Algeria)

Krishnan, E. V. (Oman)

Kryzhevich, S. (Poland)

Limarchenko, O. S. (Ukraine)

Lopez Gutierrez R. M. (Mexico)

Lozi, R. (France)

Peterson, A. (USA)

Radziszewski, B. (Poland)

Shi Yan (Japan)

Sivasundaram, S. (USA)

Staicu V. (Portugal)

Vatsala, A. (USA)

ADVISORY COMPUTER SCIENCE EDITORS

A.N.CHERNIENKO and A.S.KHOROSHUN, Kiev, Ukraine

ADVISORY LINGUISTIC EDITOR

S.N.RASSHYVALOVA, Kiev, Ukraine

INSTRUCTIONS FOR CONTRIBUTORS

(1) General. Nonlinear Dynamics and Systems Theory (ND&ST) is an international journal devoted to publishing peer-refereed, high quality, original papers, brief notes and review articles focusing on nonlinear dynamics and systems theory and their practical applications in engineering, physical and life sciences. Submission of a manuscript is a representation that the submission has been approved by all of the authors and by the institution where the work was carried out. It also represents that the manuscript has not been previously published, has not been copyrighted, is not being submitted for publication elsewhere, and that the authors have agreed that the copyright in the article shall be assigned exclusively to InforMath Publishing Group by signing a transfer of copyright form. Before submission, the authors should visit the website:

<http://www.e-ndst.kiev.ua>

for information on the preparation of accepted manuscripts. Please download the archive Sample_NDST.zip containing example of article file (you can edit only the file Samplefilename.tex).

(2) Manuscript and Correspondence. Manuscripts should be in English and must meet common standards of usage and grammar. To submit a paper, send by e-mail a file in PDF format directly to

Professor A.A. Martynyuk, Institute of Mechanics,

Nesterov str.3, 03057, Kiev-57, Ukraine

e-mail: journalndst@gmail.com

or to one of the Regional Editors or to a member of the Editorial Board. Final version of the manuscript must typeset using LaTeX program which is prepared in accordance with the style file of the Journal. Manuscript texts should contain the title of the article, name(s) of the author(s) and complete affiliations. Each article requires an abstract not exceeding 150 words. Formulas and citations should not be included in the abstract. AMS subject classifications and key words must be included in all accepted papers. Each article requires a running head (abbreviated form of the title) of no more than 30 characters. The sizes for regular papers, survey articles, brief notes, letters to editors and book reviews are: (i) 10-14 pages for regular papers, (ii) up to 24 pages for survey articles, and (iii) 2-3 pages for brief notes, letters to the editor and book reviews.

(3) Tables, Graphs and Illustrations. Each figure must be of a quality suitable for direct reproduction and must include a caption. Drawings should include all relevant details and should be drawn professionally in black ink on plain white drawing paper. In addition to a hard copy of the artwork, it is necessary to attach the electronic file of the artwork (preferably in PCX format).

(4) References. Each entry must be cited in the text by author(s) and number or by number alone. All references should be listed in their alphabetic order. Use please the following style:

Journal: [1] H. Poincare, Title of the article. *Title of the Journal* volume (issue) (year) pages. [Language]

Book: [2] A.M. Lyapunov, *Title of the Book*. Name of the Publishers, Town, year.

Proceeding: [3] R. Bellman, Title of the article. In: *Title of the Book*. (Eds.). Name of the Publishers, Town, year, pages. [Language]

(5) Proofs and Sample Copy. Proofs sent to authors should be returned to the Editorial Office with corrections within three days after receipt. The corresponding author will receive a sample copy of the issue of the Journal for which his/her paper is published.

(6) Editorial Policy. Every submission will undergo a stringent peer review process. An editor will be assigned to handle the review process of the paper. He/she will secure at least two reviewers' reports. The decision on acceptance, rejection or acceptance subject to revision will be made based on these reviewers' reports and the editor's own reading of the paper.

NONLINEAR DYNAMICS AND SYSTEMS THEORY

An International Journal of Research and Surveys
Published by InforMath Publishing Group since 2001

Volume 24

Number 3

2024

CONTENTS

Improved Power Quality with Active Shunt Power Filter Based on Optimized PI Controller and Flying Squirrel Search MPPT Technique Applied to the WECS	217
<i>A. Abbad, F. Hamidia, A. Morsli, M. R. Skender and A. Tlemçani</i>	
Optimization of Hotel W Management through Performance Comparison of Support Vector Machine and Linear Regression Algorithm in Forecasting Occupancy	228
<i>M. Y. Anshori, T. Herlambang, V. Asy'ari, H. Arof, A. A. Firdaus, K. Oktafianto and B. Suharto</i>	
Numerical Solution of Neutral Double Delay Volterra Integral Equations Using Taylor Collocation Method	236
<i>H. Bouzeraieb, H. Laib and A. Boulmerka</i>	
Stability Analysis of a Coupled System of Two Nonlinear Differential Equations with Boundary Conditions	246
<i>Besma Fadlia, Abdelwahab Zarour, Rima Faizi and Mohamed Dalah</i>	
Trajectory Estimation of Amphibious Aircraft Using H -Infinity and Ensemble Kalman Filter Methods	259
<i>T. Herlambang, S. Syamsuar, F. Yudianto, A. Basuki, G. Wijiatmoko, A. Roschyntawati, H. Hendrato, K. Oktafianto and R. S. Marjianto</i>	
Numerical Solution for Benjamin-Bona-Mahony-Burgers Equation Using Septic B -Spline Galerkin Method	267
<i>Ali M. Jasim, Adham A. Ali, Isam H. Halil, Fatima Z. Ahmed and Muhannad A. Shallal</i>	
A New Chaotic Supply Chain Model, Its Bifurcation Analysis, Multi-Stability and Synchronization Using Backstepping Control	275
<i>M. D. Johansyah, A. Sambas, S. Vaidyanathan, S. S. Abas, H. Hassan, M. Makhtar, S. Purnama and B. Foster</i>	
On Unique Solvability and a Generalized Newton Method for Solving New General Absolute Value Equations	286
<i>M. Khaldi and M. Achache</i>	
Adaptive Control for the Stabilization, Synchronization and Anti-Synchronization of New Chaotic System with a Line Equilibrium	298
<i>K. Mesbah and N. E. Hamri</i>	
Properties of MDTM and RDTM for Nonlinear Two-Dimensional Lane-Emden Equations	309
<i>N. Teyar</i>	

Founded by A.A. Martynyuk in 2001.

Registered in Ukraine Number: KB No 5267 / 04.07.2001.

NONLINEAR DYNAMICS AND SYSTEMS THEORY

An International Journal of Research and Surveys

Impact Factor from SCOPUS for 2022: SJR – 0.293, SNIP – 0.784 and CiteScore – 1.5

Nonlinear Dynamics and Systems Theory (ISSN 1562–8353 (Print), ISSN 1813–7385 (Online)) is an international journal published under the auspices of the S.P. Timoshenko Institute of Mechanics of National Academy of Sciences of Ukraine and Curtin University of Technology (Perth, Australia). It aims to publish high quality original scientific papers and surveys in areas of nonlinear dynamics and systems theory and their real world applications.

AIMS AND SCOPE

Nonlinear Dynamics and Systems Theory is a multidisciplinary journal. It publishes papers focusing on proofs of important theorems as well as papers presenting new ideas and new theory, conjectures, numerical algorithms and physical experiments in areas related to nonlinear dynamics and systems theory. Papers that deal with theoretical aspects of nonlinear dynamics and/or systems theory should contain significant mathematical results with an indication of their possible applications. Papers that emphasize applications should contain new mathematical models of real world phenomena and/or description of engineering problems. They should include rigorous analysis of data used and results obtained. Papers that integrate and interrelate ideas and methods of nonlinear dynamics and systems theory will be particularly welcomed. This journal and the individual contributions published therein are protected under the copyright by International InforMath Publishing Group.

PUBLICATION AND SUBSCRIPTION INFORMATION

Nonlinear Dynamics and Systems Theory will have 6 issues in 2024, printed in hard copy (ISSN 1562–8353) and available online (ISSN 1813–7385), by InforMath Publishing Group, Nesterov str., 3, Institute of Mechanics, Kiev, MSP 680, Ukraine, 03057. Subscription prices are available upon request from the Publisher, EBSCO Information Services (<mailto:journals@ebSCO.com>), or website of the Journal: <http://e-ndst.kiev.ua>. Subscriptions are accepted on a calendar year basis. Issues are sent by airmail to all countries of the world. Claims for missing issues should be made within six months of the date of dispatch.

ABSTRACTING AND INDEXING SERVICES

Papers published in this journal are indexed or abstracted in: Mathematical Reviews / MathSciNet, Zentralblatt MATH / Mathematics Abstracts, PASCAL database (INIST–CNRS) and SCOPUS.



Improved Power Quality with Active Shunt Power Filter Based on Optimized PI Controller and Flying Squirrel Search MPPT Technique Applied to the WECS

A. Abbadi^{1*}, F. Hamidia¹, A. Morsli¹, M. R. Skender² and A. Tlemçani¹

¹ *Research Laboratory in Electrical Engineering and Automatic (LREA), University of Medea, Algeria.*

² *Renewable Energy and Materials Laboratory (REML), University of Medea, Algeria.*

Received: October 14, 2023; Revised: May 3, 2024

Abstract: This paper aims to improve power quality issues following the IEEE 519 power quality standard recommendations. Indeed, the existing electrical distribution system employs highly nonlinear loads, which raises concerns about the quality of electrical energy. To solve these problems, an optimized PI controller and a bio-inspired MPPT controller are applied to a Wind Energy Conversion System (WECS) integrated with a Shunt Active Power Filter (SAPF). The MPPT controller is used for extracting maximum power from the WECS using the Flying Squirrel Search (FSS) algorithm. In order to overcome the problem of the dynamic performance of DC Link voltage that occurs when using the traditional PI control, an adaptive PI controller using the Sliding Mode Extremum-Seeking (SMES) algorithm is adopted. The SMES algorithm is utilized here to reduce a selected cost function that brings the required performance aspects. The dynamic performance of the SAPF is optimized using the direct power control technique. Simulation results are provided to confirm the effectiveness of the proposed controllers. They clearly demonstrate that the applied control algorithms are effective in eliminating harmonic currents and injecting the available active power of the wind turbine into the load and power grid.

Keywords: *SAPF; THD; WECS; MPPT controller; FSS algorithm; adaptive PI controller; SMES technique.*

Mathematics Subject Classification (2010): 93E11, 93-XX, 93B12, 90C59.

* Corresponding author: <mailto:amel.abbadi@yahoo.fr>

1 Introduction

With substantial advancements in power electronics and microelectronics technology in recent years, the propagation of nonlinear loads such as static power converters has impaired the power quality in transmission systems energy distribution. Indeed, the current waveform is not purely sinusoidal on the network mainly due to high harmonic currents. This results in a reduced power factor, decreased efficiency, and decreased system performance which is not allowed according to the recommendations of the IEEE 519 power quality standard [1–3].

Using passive LC has always been the simplest way to reduce current harmonics and boost the power factor. However, there are numerous drawbacks to using a passive filter [4, 5]. Because of the rapid advancement of modern power electronic technology, earlier efforts have primarily focused on active filters rather than passive filters. One of the most common active filters is the shunt active power filter (SAPF). It injects currents that are equal and at the same time opposite to the harmonic components, allowing only the fundamental components to flow through the point of common coupling (PCC) [5].

DC-link voltage directly affects the performance of shunt active power filters (SAPFs). Maintaining voltage stability of the DC-link voltage has a direct impact on the system output and is critical to ensuring the converters operate properly. In SAPFs, DC-link voltage regulators are critical for mitigating fluctuations in instantaneous active power [6].

The shunt active power filter is powered by a DC voltage source or a capacitor which is expensive [1]. In our case, we propose another free continuous source, which is the wind energy. The Wind Energy Conservation System (WECS) based on the SAPF is used to improve power quality. It ensures bidirectional energy flow while extracting maximum energy under different wind speeds [4, 5]. As we know, the MPPT controller can extract the maximum energy from the WECS by adjusting the duty cycle of the boost converter. MPPT offers a variety of control strategies, such as perturbation and observation (P&O), fuzzy logic, neural network, etc. [5]. However, there are only a few publications on bio-inspired MPPT techniques for the WECS [7, 8]. The most significant advantage of bio-inspired MPPT algorithms is that they do not require mathematical modeling of the process to improve control; their convergence speed is appreciable; and they are robust to load variations [9, 10].

In this paper, two regulators are proposed to ensure the maintenance of the THD of current sources according to the IEEE 519 standard in the SAPF connected to a WECS. The first controller is the flying squirrel search optimization (FSSO) MPPT controller. This MPPT technique is proposed to extract the maximum power from the WECS. The second controller is the DC-link voltage controller based on an adaptive PI controller which uses the sliding-mode extremum-seeking technique to enhance compensation adaptability for fluctuation in wind speed.

This paper is structured as follows. Section 2 describes the system under consideration. Control strategies of a shunt active power filter in a grid-integrated wind system are presented in Section 3. Section 4 employs simulations to assess the efficacy of the proposed controllers. Finally, the conclusions are presented in Section 5.

2 Configuration of the System

The structure of the shunt active power filter connected to the wind energy conversion system (WECS) is presented in Figure 1. In this system, a permanent magnet syn-

chronous generator (PMSG) wind turbine is coupled to the grid and a nonlinear load via a shunt active power filter. The inverter converts power from the wind turbine in addition to compensating for harmonic currents.

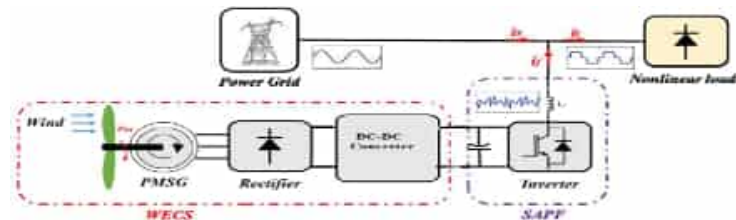


Figure 1: Block Diagram of the SAPF connected to the WECS.

2.1 Wind energy conversion system

As shown in Figure 1, the wind energy conversion system is formed up of a wind turbine that transforms wind energy into mechanical energy. A gearbox connects the wind turbine shaft to the shaft of the permanent magnet synchronous generator. The generator generates nominal three-phase voltages and currents, which are then fed into a three-phase rectifier. The resulting DC signal is amplified in a DC/DC boost converter [7].

2.2 Shunt active power filter

The operation of the SAPF is based on the fact that the harmonic currents are produced equally in amplitude and in phase opposite to these harmonics generated by the nonlinear loads and circulating in the network. As a result, the SAPF current is generated in such a way that the network current's sinusoidal shape is retained. The typical structure of a SAPF includes a converter, a DC-link capacitor and a filter inductor, as illustrated in Figure 1 [1, 3].

3 Control Strategies of Shunt Active Power Filter in Grid-Integrated Wind System

Figure 2 depicts the different control strategies adopted for the integrated wind system with a grid-connected shunt active power filter. In this section, we will describe in detail the MPPT flying squirrel search controller of the WECS and the adaptive PI controller of the DC Link voltage control loop.

3.1 Flying Squirrel Search MPPT controller

3.1.1 Overview of the FSSO algorithm

The search process begins when flying squirrels start looking for food. During the warm season (fall), squirrels glide from one tree to the next in quest of food. They shift their location and explore different regions of the forest while doing so. They can achieve their daily energy requirements more quickly on a diet of abundantly accessible acorns since the climatic conditions are warm enough and hence consume the acorns promptly

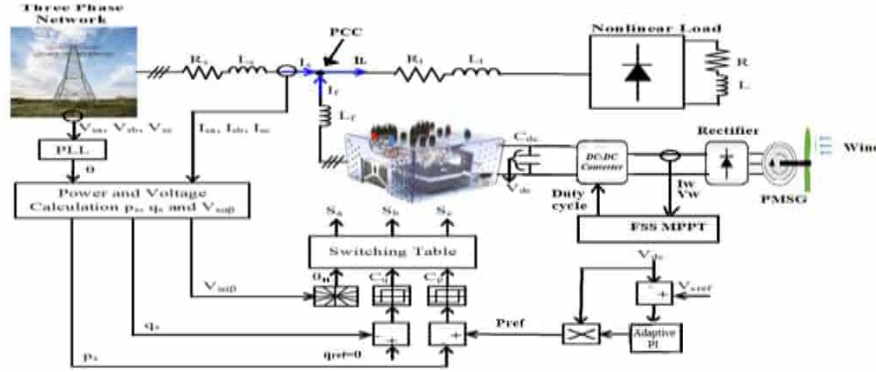


Figure 2: General control structure of the SAPF and the WECS.

after finding them. Once they have met their daily energy requirements, they begin looking for winter food sources (hickory nuts). Storing hickory nuts will help them meet their energy needs in difficult weather conditions, avoid costly foraging trips, and hence boost their chances of survival. Indeed, in the winter, the lack of leaf cover in deciduous woods increases the risk of predation, and as a result, they become less active but do not hibernate. As the winter season ends, flying squirrels become active again (Figure 3). This is a repetitive process that continues during a flying squirrel's foraging for food [11].

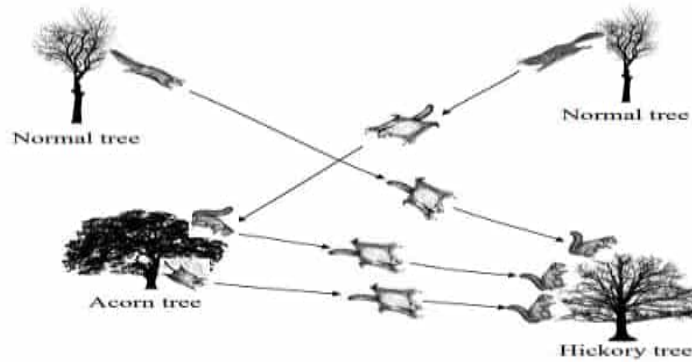


Figure 3: Flying Squirrel foraging habit.

3.1.2 FSSO algorithm steps for global maximum power point tracking

The power output of the WECS is used as the objective (food source) in MPPT, while the duty ratio ' d ' of the boost converter is used as the decision variable (position).

To minimize the convergence time to global maximum power point (GMPP), the existing FSSO algorithm is modified with the elimination of the presence of predators. The various phases and processes of the FSSO algorithm to follow the GMPP are described as follows [12].

1. Initialization: Initially, the Nfs FS are positioned at different positions, which represent different values of the duty cycle of the boost converter in a limited duty cycle space solution : $0 < d_i < 0.5$.

2. Fitness Assessment: The boost converter acts sequentially with each duty cycle (i.e., the position of each FS) in this step. The quality of the food source is determined by the instantaneous wind power $P_{wind}(d)$ for each duty cycle ‘ d ’. This phase is performed for all duty cycles, and the MPPT objective fitness function is $f(d) = Max(P_{wind}(d))$.

3. Declaration and sorting: The hickory tree is declared to have the duty cycle with the maximum wind power output. The next best FS position is supposed to be on an acorn tree. The remaining FSs are presumed to be on normal trees.

4. Position update: The duty cycle update is performed after the seasonal monitoring condition has been verified. Duty cycles are updated using (a) if $(S_C^k < S_{min})$, other duty cycles are updated using (b). Following that, the fitness is assessed.

(a). Seasonal monitoring condition: Introducing seasonal monitoring conditions ensures that the algorithm does not get stuck in the LMPP. The seasonal constant (S_C) and its minimum value (S_{min}) for a one-dimensional space are calculated as follows:

$$S_C^k = |d_{at}^k - d_{ht}^k|, \tag{1}$$

$$S_{min} = \frac{10e^{-6}}{(365)^{k/(k_m/2.5)}}, \tag{2}$$

where d_{ht} and d_{at} represent the squirrel position at the hickory and acorn trees, respectively; k is the current iteration number and k_m is the maximum number of iterations allowed. The duty ratios (FSs on normal trees) NTFS are relocated using the Lévy distribution for better search space exploration

$$d_{nt}^{k+1} = d_{nt}^k + s, \tag{3}$$

where d_{nt} represents the squirrel position at the normal tree and the step length s using the Lévy distribution is presented as

$$s \approx K \left(\frac{u}{|v|^{1/\beta}} \right) (d_{ht} - d_{nt}), \tag{4}$$

where the Lévy index β and step coefficient K are taken as 1.5 and 1.25, respectively, and u and v are determined from the normal distribution curve as

$$u \approx N(0, \sigma_u^2) \quad v \approx N(0, \sigma_v^2) \tag{5}$$

if Γ denotes the integral gamma function, then the variables σ_u and σ_v are defined as

$$\sigma_u = \left(\frac{\Gamma(1 + \beta) \sin(\pi\beta/2)}{\Gamma\left(\frac{1+\beta}{2}\right) \beta(2)^{\left(\frac{\beta-1}{2}\right)}} \right)^{1/\beta} \quad \text{and} \quad \sigma_v = 1, \tag{6}$$

where $\Gamma(n) = (n - 1)!$.

(b). Routine update: The squirrel on the hickory tree is not allowed to move. The squirrel on the acorn tree is making its way toward the hickory tree. Some squirrels from normal trees move toward the hickory tree, whereas the others move toward the acorn tree. The corresponding duty cycles are updated according to the following equations:

$$d_{at}^{k+1} = d_{at}^k + g_d G_c (d_{ht}^k - d_{at}^k), \tag{7}$$

$$d_{nt}^{k+1} = d_{nt}^k + g_d G_c (d_{ht}^K - d_{nt}^k), \quad (8)$$

$$d_{nt}^{k+1} = d_{nt}^k + g_d G_c (d_{at}^K - d_{nt}^k), \quad (9)$$

where G_c and g_d represent the gliding constant and gliding distance, respectively. The value of G_c is taken as 0.0019. The gliding distance g_d is expressed as

$$\begin{cases} g_d = \frac{h_g}{s_f \tan \phi}, \\ \tan \phi = \frac{F_D}{F_L}, \end{cases} \quad (10)$$

where the value of the height loss after gliding (h_g) is taken to be 0.01m; the scaling factor s_f is selected as 0.18. F_D and F_L are the drag and the lift forces, respectively, which are calculated as

$$\begin{cases} F_D = \frac{1}{2} \rho V^2 S C_D, \\ F_L = \frac{1}{2} \rho V^2 S C_L, \end{cases} \quad (11)$$

where ρ is the air density, V is the velocity of the squirrel, and S is the surface area of the body. The drag coefficient C_D is taken as 0.006 and the lift coefficient C_L is selected as 0.007.

5. Convergence determination: If the change in the position of all FSs is less than a threshold, or if the maximum number of iterations is achieved, the algorithm optimization is ended, and the duty cycle at which the boost converter works while tracking GMPP is selected as the output.

6. Re-initialization: The MPPT is a time variation optimization algorithm in which the fitness value varies with the weather. In such circumstances, the FSs positions (duty ratios) are re-initialized to look for the new GMPP. In this paper, the duty cycles are reinitialized after detecting the change in wind power through the following constraint equation:

$$\frac{P_{wind}^{k+1} - P_{wind}^k}{P_{wind}^{k+1}} \geq \Delta P(\%). \quad (12)$$

3.2 DC Link voltage PI controller tuned using sliding mode extremum seeking algorithm

The DC Link voltage controller is synthesized in this section. In the DC Link voltage control loop, the suggested adaptive PI controller is employed to reduce DC capacitor fluctuation voltages. As shown in Figure 4, the optimized PI controller is used to maintain the DC Link voltage at a specified value using the error between the measured DC Link voltage and its reference to control the output active power of the inverter. The proposed sliding-mode extremum seeking (SMES) technique is employed to adjust the parameters of the PI controller with the aim of minimizing a specified cost function [13, 14].

The block diagram for the overall control loop with the proposed sliding-mode extremum seeking PI controller is shown in Figure 4. The cost function is utilized to quantify the effectiveness of the PI controller.

In general, the Integrated Squared Error (ISE) is used as a cost function [13]:

$$J(\theta) = \frac{1}{T} \int_0^T [e(t, \theta)]^2 dt \quad (13)$$

and $\theta = [k_p \ k_i]^T$ contains the PI parameters. The SMES algorithm updates the PI controller parameters θ to minimize the cost function $J(\theta)$.

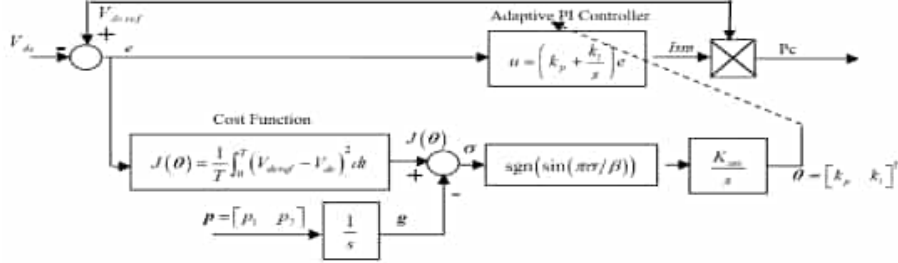


Figure 4: Block diagram for the overall control loop with the proposed multivariable sliding-mode extremum seeking PI controller.

The proposed sliding-mode extremum seeking algorithm applies two switching functions

$$\sigma = [\sigma_1 \quad \sigma_2] \tag{14}$$

to determinate the gains k_p and k_i of the PI controller. Each switching function is defined as

$$\sigma_i = J(\theta) - p_i t, \tag{15}$$

$p_i > 0$ ($i = 1, 2$) represents the slope of the i -th sliding surface. The vector of driving signals is determined as

$$\mathbf{p} = [p_1 \quad p_2]. \tag{16}$$

According to Figure 4, g_i is an increasing reference function defined as $\dot{g}_i = p_i$. The parameter θ_i is considered as the optimal control law. It is designed to satisfy

$$\dot{\theta} = K_{ses_i} \text{sgn}(\sin(\pi\sigma_i/\beta_i)), \tag{17}$$

where K_{ses_i} and β_i are positive.

The proposed scheme adopts a minimal search method with a periodic switching function since the performance function is not known. This technique adapts the parameters of the PI controller to achieve the minimum point of the cost function and this by forcing the function $J(\theta)$ to rest on the increasing sliding surface vector.

4 Simulations Results

A MATLAB/Simulink model merging SAPF and WECS has been developed to validate the suggested control strategies under non-linear load conditions and wind speed variation.

We have adressed two cases: with and without the WECS. The WECS is not connected in the first case. Figure 5 depicts the source voltages, source current I_{as} , filter current I_{af} , and load current I_{aL} before and after SAPF compensation.

The source voltage waveform is sinusoidal and balanced, as seen in Figure 5. Before filtering, the source current waveform was distorted, but once the active filter was applied to the configuration ($t = 0.25$ s), the waveform immediately became sinusoidal.

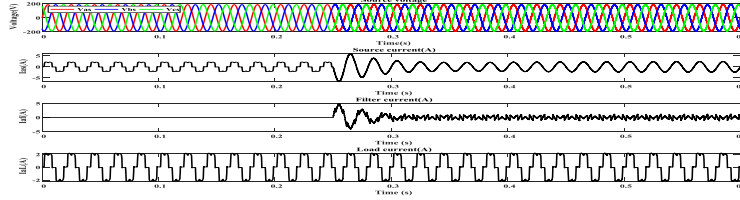


Figure 5: Source voltages, the source current I_{as} , the filter current I_{af} , and the load current I_{aL} before and after compensation by the shunt APF.

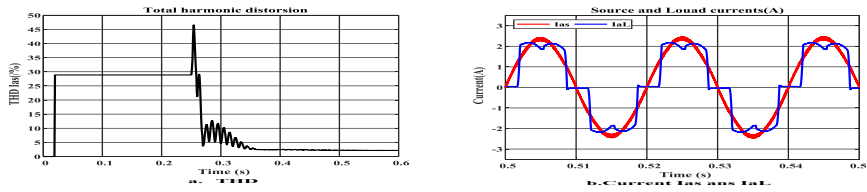


Figure 6: a. Temporal pattern of the THD without and with SAPF of the source current I_{as} . b. Source current I_{as} , and the load current I_{aL} with SAPF.

As shown in Figure 6a, the THD (Total Harmonic Distortion) decreases significantly after activating the filter on the electrical network, confirming the high quality of the filtering. Figure 6b shows that the source current meets the load requirement (I_{aL}).

In the second case, the WECS is connected to the shunt active power filter. We employed two wind speed profiles for the wind turbine, one at 5 m/s and the other at 9m/s. For both wind speed profiles, the form of the source current is clearly sinusoidal (Figure 7).

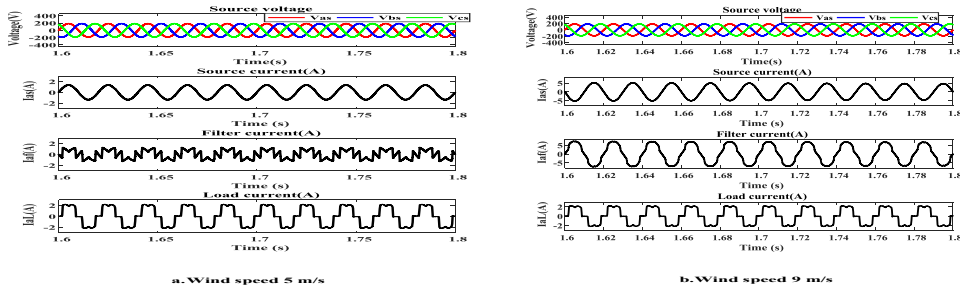


Figure 7: The source voltages, the source current I_{as} , the filter current I_{af} , and the load current I_{aL} for both wind speed.

According to Figure 8a, the charging current is supplied by the two sources (WECS and network); however, as illustrated in Figure 8b, part of the wind energy satisfies the load demand and the additional energy is injected into the power grid, which is justified

by the fact that there is a phase π between V_{as} and I_{as} (Figure 8b). In addition, the THD (Total Harmonic Distortion) complies with IEEE 519 standard, as seen in Figure 9.

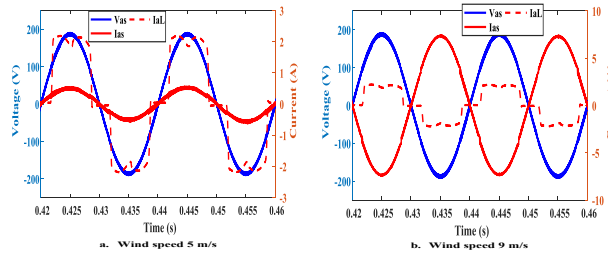


Figure 8: The source current I_{as} and the load current I_{aL} for both wind speeds.

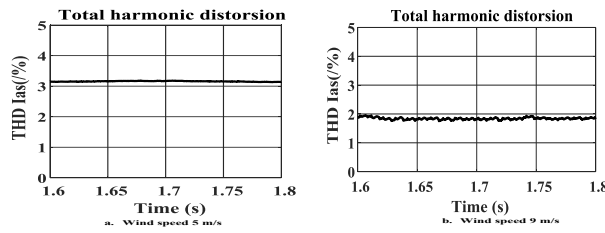


Figure 9: Temporal pattern of the THD for both wind speeds.

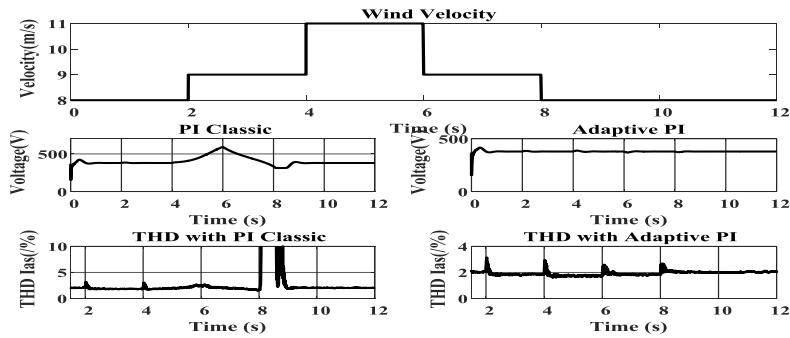


Figure 10: Dynamic performance of the classic DC Link PI controller and the adaptive PI controller with their associated THD.

As demonstrated in Figure 10, the adaptive PI controller considerably improves the dynamic performance of the DC Link voltage regulator as well as the THD of the source currents.

5 Conclusion

This paper focuses on the application of two regulators to control an active shunt power filter in order to improve the compensation of current harmonics injected by nonlinear charges. The first is an MPPT controller based on the flying squirrel search algorithm. The advantage of the proposed method is that it requires only the instantaneous current and voltage generated by the wind turbine to generate the duty cycle of the boost controller. The second regulator is an adaptive PI controller based on the sliding mode extreme search technique. It is used to control the dynamic performance of the DC Link voltage regulator. The proposed optimizer modifies the PI gains by minimizing a cost function based on the feedback error term. The resulting PI controller can exhibit fast and accurate tracking response as well as excellent disturbance rejection. The two proposed controllers are considered model-free algorithms. The three-phase inverter of the SAPS is controlled using a Direct Power Control (DPC) technique. According to the simulation results, the proposed system works efficiently. Indeed, the combination of the proposed control strategies makes it possible to reduce current harmonics according to the standard recommendations of the electrical energy quality (IEEE519) while injecting all the available power of the PMSG into the load and, in certain cases, into the power grid, particularly when the wind speed increases.

References

- [1] M. Morsli, A. Tlemceni, A. Krama, A. Abbad L. Zellouma and H. Nouri. Application of the Direct Power Control Strategy in a Shunt Active Filter by Exploiting the Solar Photovoltaic Energy as a Continuous Source. *Nonlinear Dynamics and Systems Theory* **20** (4) (2020) 410–424.
- [2] H. Wayne Beaty, M.F. McGranaghan, R. C. Dugan and S. Santoso. *Electrical Power Systems Quality, Second Edition*. McGraw-Hill, New York, 2008.
- [3] M. Morsli, A. Tlemceni and M.S. Boucherit. Shunt Active Power Filter Based Harmonics Compensation of a Low-Voltage Network Using Fuzzy Logic System. *Nonlinear Dynamics and Systems Theory* **17** (1) (2017) 70–85.
- [4] N. Mesbahi, A. Ouari, D. Ouldabdeslam, T. Djamah and A. Omeiri. Direct power control of shunt active filter using high selectivity filter (HSF) under distorted or unbalanced conditions. *Electric Power Systems Research* **108** (2014) 113–123.
- [5] T. Trivedi, R. Jadeja and P. Bhatt. Improved direct power control of shunt active power filter with minimum reactive power variation and minimum apparent power variation approaches. *Journal of Electrical Engineering & Technology* **12** (3) (2017) 1124–1136.
- [6] Juan Zhou, Yalei Yuan and Hao Dong. Adaptive DC-Link Voltage Control for Shunt Active Power Filters Based on Model Predictive Control. *IEEE Access* **8** (2020) 208348–208357.
- [7] H. Gaied, M. Naoui, H. Kraiem, B. Srikanth Goud, A. Flah, L. M. L. Alghaythi, H. Kotb, S. G. Ali and K. Aboras. Comparative analysis of MPPT techniques for enhancing a wind energy conversion system. *Frontiers in Energy Research* (2022) 1–15.
- [8] L. Xuan Chau M. Quan Duong and K. Hung Le. Review of the Modern Maximum Power Tracking Algorithms for Permanent Magnet Synchronous Generator of Wind Power Conversion Systems. *Energies* **16** (1) (2023) 1–25.
- [9] M. H. Zafar, N. Mujeeb Khan, A. Feroz Mirza and M. Mansoor. Bio-inspired optimization algorithms based maximum power point tracking technique for photovoltaic systems under partial shading and complex partial shading conditions. *Journal of Cleaner Production* **309** 127279 (2021) 1–18.

- [10] F. Hamidia and A. Abbadi. SOFC-PV System with Storage Battery Based on Cuckoo Search Algorithm. *Nonlinear Dynamics and Systems Theory* **22** (4) (2022) 367–378.
- [11] Y. Wang and T. Du. An Improved Squirrel Search Algorithm for Global Function Optimization. *Algorithms* **12** (80) (2019) 1–29.
- [12] N. Singh, K. K. Gupta, S. K. Jain, N. K. Dewangan and P. Bhatnagar. A Flying Squirrel Search Optimization for MPPT Under Partial Shaded Photovoltaic System. *EEE Journal of Emerging and Selected Topics in Power Electronics* **9** (4) (2021) 4963–4978.
- [13] T. Roux-Oliveira, L. R. Costa, A. V. Pino and P. Paz. Extremum Seeking-based Adaptive PID Control applied to Neuromuscular Electrical Stimulation. *Anais da Academia Brasileira de Ciências* **91** (1) (2019) 1–20.
- [14] N. J. Killingsworth and M. Krstic. PID tuning using extremum seeking: online, model-free performance optimization. *IEEE Control Systems Magazine* **26** (1) (2006) 70–79.



Optimization of Hotel W Management through Performance Comparison of Support Vector Machine and Linear Regression Algorithm in Forecasting Occupancy

M. Y. Anshori¹, T. Herlambang², V. Asy'ari², H. Arof³, A. A. Firdaus⁴,
K. Oktafianto⁵ and B. Suharto^{6*}

¹ Department of Management, Universitas Nahdlatul Ulama Surabaya, Indonesia.

² Department of Information System, Universitas Nahdlatul Ulama Surabaya, Indonesia.

³ Department of Electrical Engineering, University of Malaya, Malaysia.

⁴ Department of Engineering, Faculty of Vocational, University of Airlangga, Indonesia.

⁵ Department of Mathematics, University of PGRI Ronggolawe, Indonesia.

⁶ Department of the Tourism and Hospitality, Faculty of Applied Sciences, University of Airlangga, Indonesia.

Received: September 5, 2023; Revised: April 19, 2024

Abstract: The hospitality industry continues to grow globally. More and more people are traveling for various purposes such as leisure, business, or special events. This growth has created a huge opportunity for hotels to increase revenue and profits. Due to the growth of the industry, competition among hotels has also intensified. So, this condition encourages hotels to look for efficient ways of managing hotel resources. One way to efficiently manage a hotel is by forecasting the hotel occupancy. The study in this paper is aimed to optimize hotel management through the application of occupancy forecasting by the SVM and linear regression methods. The results indicated that the linear regression method had a higher accuracy and a smaller error than the SNM for two cases. When compared, as a whole, using linear regression in case 2 had the smallest RMSE value, in which the difference in RMSE by the linear regression method is around 0.3 -0.9 smaller than that by the SVM method.

Keywords: hotel management; SVM; linear regression algorithm; forecasting occupancy.

Mathematics Subject Classification (2010): 62J05, 70-10, 90Bxx.

* Corresponding author: <mailto:bambang.suharto@vokasi.unair.ac.id>

1 Introduction

Hospitality industry continues to grow globally. More and more people are traveling for various purposes such as leisure, business, or special events. This growth has created a huge opportunity for hotels to increase revenues and profits. Due to the growth of the industry, competition among hotels has also intensified [1]. Hotels must compete to attract the attention of potential customers and retain existing guests. This encourages hotels to find innovative ways to improve their services and operational efficiency. On the other hand, hotel operating costs, including employee salaries, raw materials, energy, and property maintenance, continue to increase. Such condition compels them to find any possible efficient ways of managing hotel resources.

One way to efficiently manage a hotel is by forecasting the hotel occupancy [2]. Before the 1980s, forecasting was still seen as a technical activity in the western world. While in the 1990s, the same view was still felt among Indonesian business people and those in other developing countries. Whereas in its place of origin (the United States), the scope of forecasting has grown rapidly beyond its technical nature, encompassing an extensive use in planning, decision-making, and other managerial disciplines [3].

The main purpose of the forecasting process in general is to make estimates or predictions about future events or data based on available historical information. The function of forecasting is among others to assist organizations in a long-term and short-term strategic planning by providing a view of future demand, sales, production, or other needs and to support the development of business strategies by providing a better understanding of market trends, customer behavior, and several other business development and research studies used forecast methods to help predict the desired figures or data. Several publications related to forecasting were applied in the health sector for forecasting the spread of Dengue Fever (DHF) [4]. Forecasting was also used to detect coffee aroma [5]. Forecasting researches using the Backpropagation Neural Network [6, 7], ANFIS and Linear Support Vector Machine methods were also applied for forecasting in the economic [8, 9] and tourism fields to support government policies related to tourism development.

Some reliable forecasting methods include Support Vector Machine (SVM) and linear regression. SVM is a machine learning method which can be used to analyze data and sort it into one of two categories. SVM was originally developed for classification problems. It can be used to separate data into two classes. However, SVM can also be applied to regression problems whose goal is to predict numerical values. In the context of data forecasting, SVM is used for both classification (e.g., predicting whether an event will occur or not) and regression (e.g., predicting stock prices). Linear regression analysis is an approach for modeling the relationship between one dependent variable and one independent variable. The main purpose of the Linear Regression method is to model the linear relationship between one or more independent variables (also referred to as predictor variables or features) and the dependent variable (also referred to as the target variable) so as to make predictions or estimates. And, in this paper, it is for optimizing hotel management through the application of occupancy forecasting by the SVM and linear regression methods.

2 Occupancy Data of Hotel W

The following tables present the occupancy data of Hotel W.

	2017			2018			2019		
	Room Available	Occ (%)	Room Sold	Room Available	Occ (%)	Room Sold	Room Available	Occ (%)	Room Sold
Jan				2,201	27.1%	596	2,201	50.3%	1,108
Feb				1,988	32.3%	643	1,988	76.3%	1,516
Mar				2,201	51.7%	1,139	2,201	82.8%	1,822
Apr				2,130	43.0%	916	2,130	71.3%	1,518
May				2,201	52.8%	1,162	2,201	74.6%	1,641
Jun				2,130	40.7%	866	2,130	72.0%	1,533
Jul				2,201	41.7%	918	2,201	63.1%	1,389
Aug				2,201	57.5%	1,265	2,201	69.8%	1,536
Sep				2,130	49.4%	1,052	2,130	68.9%	1,468
Oct	1,988	36.8%	732	2,201	58.6%	1,290	2,201	68.3%	1,504
Nov	2,130	53.1%	1,132	2,130	53.4%	1,137	2,130	66.5%	1,416
Dec	2,201	52.9%	1,164	2,201	47.7%	1,050	2,201	66.4%	1,461

Table 1: The occupancy data of Hotel W for 2017-2019.

	2020			2021			2022		
	Room Available	Occ (%)	Room Sold	Room Available	Occ (%)	Room Sold	Room Available	Occ (%)	Room Sold
Jan	2,201	55.8%	1,229	2,201	37.3%	820	2,201	31.2%	687
Feb	2,059	65.4%	1,346	1,988	36.6%	728	1,988	35.0%	695
Mar	2,201	46.5%	1,023	2,201	39.6%	871	2,201	43.0%	947
Apr	2,130	9.9%	210	2,130	41.0%	874	2,130	37.5%	798
May	2,201	0.0%	0	2,201	37.6%	827	2,201	47.2%	1,038
Jun	2,130	12.2%	259	2,130	44.8%	955	2,130	34.8%	741
Jul	2,201	28.7%	632	2,201	36.2%	797	2,201	53.2%	1,170
Aug	2,201	25.4%	560	2,201	38.0%	836	2,201	48.0%	1,056
Sep	2,130	24.1%	514	2,130	46.9%	1,000	2,130	44.0%	938
Oct	2,201	27.1%	597	2,201	48.6%	1,070	2,201	52.9%	1,165
Nov	2,130	33.4%	711	2,219	34.1%	756	2,130	52.5%	1,118
Dec	2,201	45.0%	990	2,201	39.5%	870	2,201	61.4%	1,352

Table 2: The occupancy data of Hotel W for 2020-2022.

	2023		
	Room Available	Occ (%)	Room Sold
Jan	2,201	58.4%	1,286
Feb	1,988	52.2%	1,038
Mar	2,201	43.0%	947
Apr	2,130	60.1%	1,280
May	2,201	52.6%	1,158

Table 3: The occupancy data of Hotel W for 2023.

3 Algorithm of Support Vector Machine

SVM was invented in [11]. Since then, SVMs have been used in text, hypertext, and image classification. SVMs can work with handwritten characters, and the algorithm has been used in biology labs to perform tasks such as protein sorting. SVMs work to find the best hyperplane or decision boundary function to separate two or more classes in the input space. The hyperplane can be a line in two dimensions and can be a flat plane in multiple planes.

The algorithm of SVM is shown in Figure 2.

3.1 Linear Regression method

Simple linear regression analysis is an approach method for modeling the relationship between one dependent variable and one independent variable. In regression, the independent variable explains the dependent variable. In a simple regression analysis, the relationship between variables is linear, in which the changes in the variable X are followed by those in the variable Y in a fixed manner. While in a non-linear relationship, the changes in the variable X are not followed by those in the variable Y proportionally [10].

A simple linear regression analysis model is

$$Y = a + bX + \varepsilon, \quad (1)$$

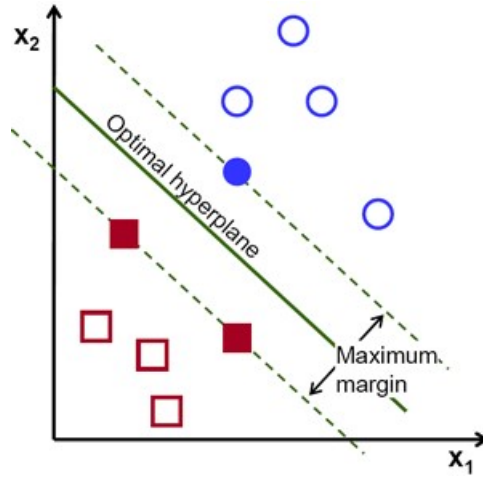


Figure 1: Support Vector Machine Model [1].

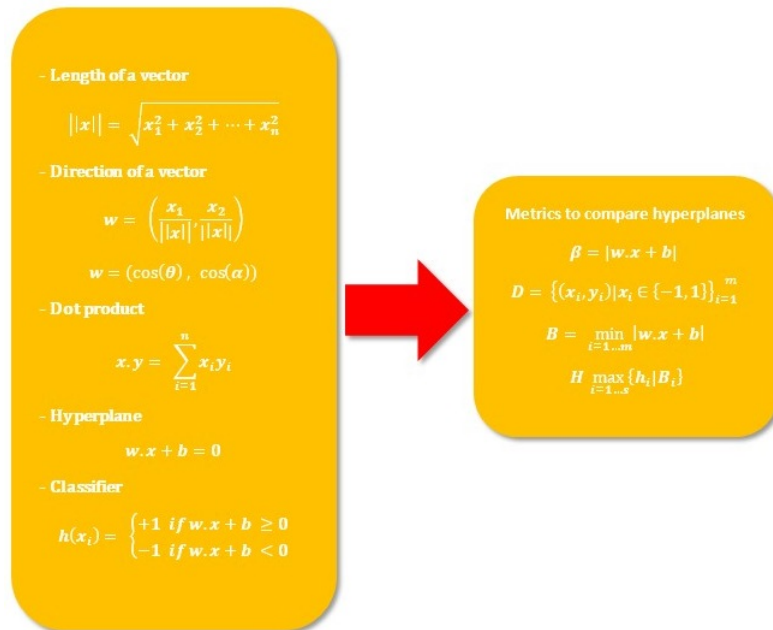


Figure 2: Algorithm of Support Vector Machine.

where Y is the predicted value, a is the constant, b is the regression coefficient, X is the independent variable, ε is the residual value.

The value $a = \frac{\Sigma Y - b(\Sigma X)}{n}$, $b = \frac{n(\Sigma XY) - (\Sigma X)(\Sigma Y)}{n(\Sigma X^2) - (\Sigma X)^2}$.

4 Simulation Results

4.1 Implementation of SVM and linear regression algorithms on data

Below is the implementation of the SVM and linear regression algorithms for hotel occupancy data in the RapidMiner software.

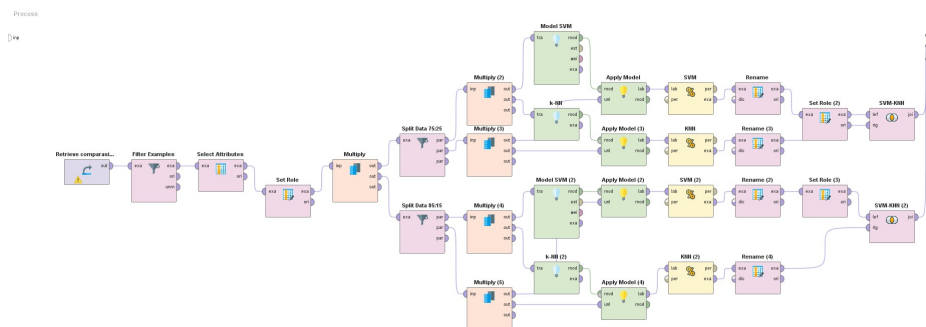


Figure 3: Implementation of the SVM and linear regression algorithms for hotel occupancy.

4.2 Simulation results

In the simulation, this study used two algorithms, the SVM and linear regression algorithms, the results of which were compared for several types of training data and testing data. There were 2 types of training and testing data grouping cases, that is, case 1 with 75% of training data and 25% of testing data and case 2 (the second case) with 85% of training data and 15% of testing data. After modeling in the RapidMiner software, using Hotel W occupancy data, the SVM and linear regression methods were then implemented, resulting in Figures 4 and 5.

Figure 4 is an explanation related to case 1 with 70% of training data and 30% of testing data, indicating that the H-infinity forecasting results by the SVM method have a bigger error than those by the linear regression method because the simulation results graph shows that the SVM method still has a difference from the real data. It can be seen in Table 4 that the RMSE produced by the SVM method is 0.946 and that by the linear regression method is 0.005. Thus, the linear regression method has a smaller error of about 0.9.

Figure 5 is an explanation related to case 2 with 85% of training data and 15% of testing data. It shows that the forecasting results by the SVM method have a bigger error than those by the linear regression method because the simulation results graph shows that the SVM method still has a difference from the real data. It can be seen in Table 4 that the RMSE produced by the SVM method is 0.371 and that by the linear regression method is 0.004. Thus, the linear regression method has a smaller error of about 0.3.

Based on Table 4, it can be seen that the linear regression method has a higher accuracy and a smaller error than the SVM for both cases. When compared, as a whole, the linear regression method for case 2 has the smallest RMSE value. When considering the SVM method alone, case 2 has the smallest RMSE value because the training data

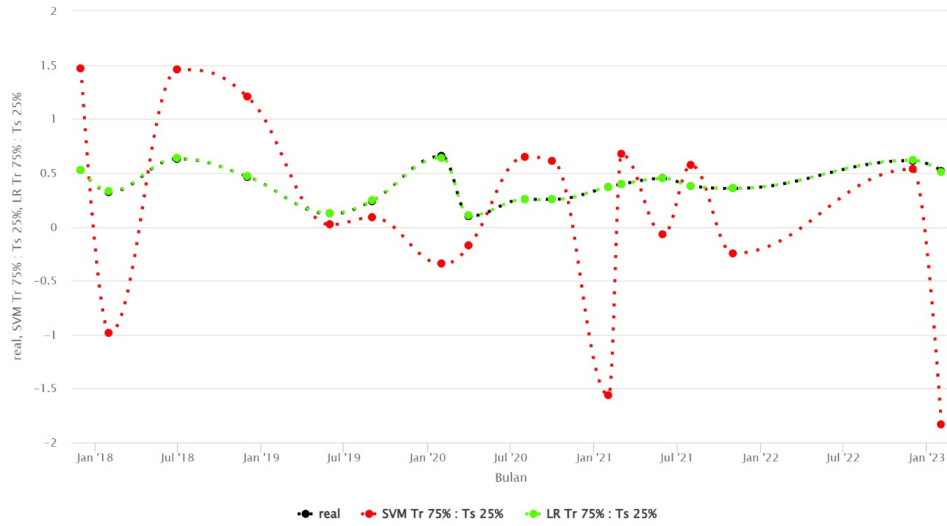


Figure 4: Hotel Y occupancy forecast simulation results with 70% of training data and 30% of testing data.



Figure 5: Simulation results of Hotel Y occupancy forecast with 80% of training data and 20% of testing data.

is larger than that in case 1. Likewise, the linear regression method in case 2 has a smaller RMSE value than that in case 1. The Linear Regression method is often used in various fields such as economics, social science, natural science, finance, and engineering. However, it is important to remember that the Linear Regression has certain assumptions

	SVM		Linear Regression	
	75% Training data and 30% Testing data	85% Training data and 15% Testing data	75% Training data and 30% Testing data	85% Training data and 15% Testing data
RMSE of Forecasting results	0.946	0.371	0.005	0.004

Table 4: Comparison of RMSE generated by the SVM and linear regression methods.

to be met for valid results, for example, the assumption that the relationship between the variables is linear and normally distributed. At the same time, the main advantage of the SVM is its ability to handle non-linear data, in this case, using hotel occupancy data which is classified as linear data. So, the linear regression method has a higher accuracy than the SVM method.

5 Conclusion

Based on the results of the discussion above and the forecasting results graph above, it can be concluded that the linear regression method has a higher accuracy and a smaller error than the SNM for two cases. When compared, as a whole, the linear regression in case 2 has the smallest RMSE value. When considering the SVM method alone, in case 2, it has the smallest RMSE value because the training data is larger than that in case 1. Likewise, the linear regression for case 2 has a smaller RMSE value than it has for case 1. The Linear Regression is often used in various fields such as economics, social science, natural science, finance, and engineering. However, it is important to remember that Linear Regression has certain assumptions to be met for the results to be valid, for example, the assumption that the relationship between the variables is linear and normally distributed. At the same time, the main advantage of the SVM is its ability to handle non-linear data, in this case, using hotel occupancy data which are classified as linear data, therefore the linear regression method is more accurate than the SVM. However, the SVM method is very reliable for forecasting hotel occupancy.

Acknowledgment

High appreciation to the Kemdikbudristek for the very fund support for the research conducted in the year of 2023 with contract number 183/E5/PG.02.00.PL/2023,049/SP2H/PT/LL7/2023 and 1287/UNUSA-LPPM/Adm-I/VII/2023.

References

- [1] M. Y. Anshori, I. H. Santoso, T. Herlambang, D. Rahmalia, K. Oktafianto and P. Katias. Forecasting of Occupied Rooms in the Hotel Using Linear Support Vector Machine. *Non-linear Dynamics and Systems Theory* **23** (2) (2023) 129–140.
- [2] F. A. Susanto, M. Y. Anshori, D. Rahmalia, K. Oktafianto, D. Adzkiya, P. Katias and T. Herlambang. Estimation of Closed Hotels and Restaurants in Jakarta as Impact of

- Corona Virus Disease (Covid-19) Spread Using Backpropagation Neural Network. *Nonlinear Dynamics and Systems Theory* **22** (4) (2022) 457–467.
- [3] M. Y. Anshori, T. Shawyun, D. V. Madrigal, D. Rahmalia, F. A. Susanto, T. Herlambang and D. Adzkiya. Estimation of closed hotels and restaurants in Jakarta as impact of corona virus disease spread using adaptive neuro fuzzy inference system. *International Journal of Artificial Intelligence (IJAI)* **11** (2) (2022).
- [4] F. S. Rini, T. D. Wulan and T. Herlambang. Forecasting The Number of Demam Berdarah Dengue (DBD) Patients Using The Fuzzy Method At The Siwalankerto Public Health Center. In: *The 1st International Conference on Neuroscience and Learning Technology (ICONSATIN 2021)* Jember, Indonesia, 18-19 September 2021.
- [5] D. B. Maghfira, R. Sarno, F. A. Susanto, T. Herlambang, K. Oktafianto, W. Hartawan and I. W. Farid. Electronic Nose for Classifying Civet Coffee and Non-Civet Coffee. *Nonlinear Dynamics and Systems Theory* **23** (3) (2023) 323–337.
- [6] M. Y. Anshori, D. Rahmalia and T. Herlambang. Comparison Backpropagation (BP) and Learning Vector Quantification (LVQ) on classifying price range of smartphone in market. In: *The 4th International Conference on Combinatorics, Graph Theory, and Network Topology (ICCGANT) 2020* East Java, Indonesia, 22-23 August 2020.
- [7] M. Y. Anshori, D. Rahmalia, T. Herlambang and D. F. Karya. Optimizing Adaptive Neuro Fuzzy Inference System (ANFIS) parameters using Cuckoo Search (Case study of world crude oil price estimation). In: *The 4th International Conference on Combinatorics, Graph Theory, and Network Topology (ICCGANT) 2020* East Java, Indonesia, 22-23 August 2020.
- [8] M. Y. Anshori, T. Herlambang, P. Katias, F. A. Susanto and R. R. Rasyid. Profitability estimation of XYZ company using H-infinity and Ensemble Kalman Filter. In: *The 5th International Conference of Combinatorics, Graph Theory, and Network Topology (ICCGANT 2021)* Jember, Indonesia, 21-22 August 2021.
- [9] D. Rahmalia, T. Herlambang, A. S. Kamil, R. A. Rasyid, F. Yudianto, L. Muzdalifah and E. F. Kurniawati. Profitability estimation of XYZ company using H-infinity and Ensemble Kalman Filter. In: *The Third International Conference on Combinatorics, Graph Theory and Network Topology* University of Jember-Indonesia, 26-27 Oct 2019.
- [10] A. Muhith, I. H. Susanto, D. Rahmalia, D. Adzkiya and T. Herlambang. The Analysis of Demand and Supply of Blood in Hospital in Surabaya City Using Panel Data Regression. In: *Nonlinear Dynamics and System Theory* **22** (5) (2022) 550–560.
- [11] V. N. Vapnik and A. Y. Lerner. Pattern recognition using generalized portraits. In: *Automation and Remote Control* **24** (1963) 709–715.



Numerical Solution of Neutral Double Delay Volterra Integral Equations Using Taylor Collocation Method

H. Bouzeraieb, H. Laib* and A. Boulmerka

*Laboratory of Mathematics and Their Interactions,
University Center Abdelhafid Boussouf, Mila, Algeria.*

Received: October 16 , 2023; Revised: April 26, 2024

Abstract: In this paper, we employ a direct collocation method using Taylor polynomials to estimate the solution of linear Volterra integral equations with two constant delays within the polynomial spline $S_{m-1}^{(-1)}(\Pi_N)$. This approach is well-suited for capturing the dynamics inherent in age and size-structured population models (Gurtin–MacCamy model), epidemiological models, chemical engineering processes (heat equation with delay in control and in state) and control theory (Roesser model). We derive an iterative formula to compute the approximate solution and prove its convergence. We confirm the validity and efficacy of this convergent algorithm by presenting numerical results.

Keywords: *neutral double delay Volterra integral equation; collocation method; Taylor polynomials; error analysis.*

Mathematics Subject Classification (2010): 34K28, 45L05, 65R20, 70K99, 93A99.

1 Introduction

Delay Volterra integral equations pose a significant mathematical challenge across various scientific and engineering domains, encompassing biology [1], epidemiology [2,3], chemical engineering [4], control theory [5], physics [6] and social sciences [7]. In [8,9], double delay Volterra integral equations (DDVIEs), which incorporate memory and delayed effects, apply to model age-structured populations, where two distinct age groups within a single population are considered. The dual delays in equation (1) correspond to the time required for maturation and reaching the maximum age, rendering analytical solutions impractical for many problems. As a result, developing efficient and precise numerical

* Corresponding author: <mailto:hafida.laib@gmail.com>

methods for solving such equations has become a significant area of research in recent years.

The study of DDVIEs is driven by their widespread applicability, addressing problems that involve multiple delays and intricate memory effects. Including two distinct delays introduces additional complexity to the equations, making their numerical analysis intellectually stimulating and practically crucial.

The numerical investigation of equation (1) has only recently garnered attention, and the existing specialized literature on this subject still needs to be expanded. A numerical method developed to resolve equation (1) is elaborated in [10].

This research explores the Taylor collocation method [11] applied to the solution of linear DDVIEs. The method leverages the versatility of Taylor polynomials and the precision of collocation schemes, providing an advantageous approach for addressing the challenges posed by this class of integral equations.

We consider the linear Volterra integral equation with two constant delays τ_1, τ_2 of the form

$$x(t) = g(t) + x(t - \tau_1) + x(t - \tau_2) + \int_{t-\tau_2}^{t-\tau_1} K(t, s)x(s)ds \tag{1}$$

for $t \in [\tau_2, T]$ and $x(t) = \phi(t)$ for $t \in [0, \tau_2]$. In the following, we assume that the given functions g, K and ϕ are sufficiently smooth. Furthermore, we suppose that

$$\phi(\tau_2) = g(\tau_2) + \phi(\tau_2 - \tau_1) + \phi(0) + \int_0^{\tau_2 - \tau_1} K(\tau_2, s)\phi(s)ds.$$

Bellour et al. [12] provide a proof regarding the existence and uniqueness of results for equation (1).

The structure of this paper is as follows. Section 2 presents a description of the Taylor collocation method for our problem (1). Section 3 introduces the analysis of convergence. Subsequently, in Section 4, we present the results obtained using our proposed approach. Finally, in Section 5, we discuss the implications of our work and suggest potential avenues for the future.

2 Description of the Method

We suppose that $T = (r + 1)\tau_2$, where $r \in \{1, 2, 3, \dots\}$. Let Π_N be a uniform partition of the interval $I = [\tau_2, T]$ defined by $t_n^i = (i + 1)\tau_2 + nh$, $n = 0, 1, \dots, N$, $i = 0, 1, \dots, r - 1$, where the step size is given by $h = t_{n+1}^i - t_n^i$, and assume that $h = \frac{\tau_1}{N_1} = \frac{\tau_2}{N}$ with N and N_1 being positive and integer. Define the subintervals $\sigma_n^i = [t_n^i; t_{n+1}^i)$, $n = 0, 1, \dots, N - 1$, $i = 0, 1, \dots, r - 2$ and $\sigma_{N-1}^{r-1} = [t_{N-1}^{r-1}, t_N^{r-1}]$. Moreover, denote by π_m the set of all real polynomials of degree not exceeding m . We define the real polynomial spline space of degree $m - 1$ as follows:

$$S_{m-1}^{(-1)}(\Pi_N) = \{u(I, \mathbb{R}) : u|_{\sigma_n^i} \in \pi_{m-1}, n = 0, \dots, N - 1, i = 0, 1, \dots, r - 1\}.$$

This is the space of piecewise polynomials of degree (at most) $m - 1$. Its dimension is rNm , i.e., the same as the total number of the coefficients of the polynomials $u_n^i, n = 0, \dots, N - 1, i = 0, 1, \dots, r - 1$. To find these coefficients, we use the Taylor polynomial on each subinterval.

First, to approximate x by u_n^0 ($n \in \{0, 1, \dots, N-1\}$) on the interval σ_n^0 , x must be approximated by u_k^0 ($0 \leq k < n$) on each interval σ_k^0 so that

$$u_n^0(t) = \sum_{j=0}^{m-1} \frac{\hat{u}_{n,0}^{(j)}(t_n^0)}{j!} (t - t_n^0)^j; \quad t \in \sigma_n^0, \quad (2)$$

where $\hat{u}_{0,0}(\tau_2) = x(\tau_2)$ and $\hat{u}_{n,0}$ is the exact solution of the integral equations

$$\hat{u}_{n,0}(t) = g(t) + \phi(t - \tau_1) + \phi(t - \tau_2) + \int_{t-\tau_2}^{t-\tau_1} K(t, s)\phi(s)ds, \quad n \in \{0, \dots, N_1 - 1\}, \quad (3)$$

and

$$\begin{aligned} \hat{u}_{n,0}(t) &= g(t) + u_{n-N_1}^0(t - \tau_1) + \phi(t - \tau_2) + \int_{t-\tau_2}^{\tau_2} K(t, s)\phi(s)ds \\ &+ \sum_{i=0}^{n-N_1-1} \int_{t_i^0}^{t_{i+1}^0} K(t, s)u_i^0(s)ds + \int_{t_n^0-\tau_1}^{t-\tau_1} K(t, s)u_{n-N_1}^0(s)ds, \quad n \in \{N_1, \dots, N-1\}. \end{aligned} \quad (4)$$

Now, for all $j = 1, \dots, m-1$, the formula for computing the values of the coefficients $\hat{u}_{n,0}^{(j)}(t_n^0)$ can be obtained by differentiating (3) and (4), respectively, we get the following formulas:

$$\begin{aligned} \hat{u}_{n,0}^{(j)}(t_n^0) &= g^{(j)}(t_n^0) + \phi^{(j)}(t_n^0 - \tau_1) + \phi^{(j)}(t_n^0 - \tau_2) \\ &+ \left(\int_{t-\tau_2}^{t-\tau_1} K(t, s)\phi(s)ds \right)^{(j)}(t_n^0), \quad n \in \{0, \dots, N_1 - 1\}, \end{aligned}$$

and

$$\begin{aligned} \hat{u}_{n,0}^{(j)}(t_n^0) &= g^{(j)}(t_n^0) + \hat{u}_{n-N_1,0}^{(j)}(t_{n-N_1}^0) + \phi^{(j)}(t_n^0 - \tau_2) + \left(\int_{t-\tau_2}^{\tau_2} K(t, s)\phi(s)ds \right)^{(j)}(t_n^0) \\ &+ \sum_{i=0}^{n-N_1-1} \sum_{l=0}^{m-1} \frac{\hat{u}_{i,0}^{(l)}(t_i^0)}{l!} \int_{t_i^0}^{t_{i+1}^0} \partial_1^{(j)} K(t_n^0, s)(s - t_i^0)^l ds \\ &+ \sum_{i=0}^{j-1} \sum_{l=0}^i \binom{i}{l} \hat{u}_{n-N_1,0}^{(l)}(t_{n-N_1}^0) [\partial_1^{(j-1-i)} K(t, t - \tau_1)]^{(i-l)}(t_n^0), \quad n \in \{N_1, \dots, N-1\}. \end{aligned}$$

Second, for x to be approximated by u_n^p ($n \in \{0, 1, \dots, N-1\}$ and $p \in \{1, 2, \dots, r-1\}$) on the interval σ_n^p , x must be approximated by u_k^j ($0 \leq k < n$ and $0 \leq j \leq p$) on each interval σ_k^j so that

$$u_n^p(t) = \sum_{j=0}^{m-1} \frac{\hat{u}_{n,p}^{(j)}(t_n^p)}{j!} (t - t_n^p)^j; \quad t \in \sigma_n^p, \quad (5)$$

where $\hat{u}_{n,p}$ is the exact solution of the integral equations

$$\begin{aligned} \hat{u}_{n,p}(t) &= g(t) + u_{N-N_1+n}^{p-1}(t - \tau_1) + u_n^{p-1}(t - \tau_2) \\ &+ \int_{t-\tau_2}^{t_{n+1}^{p-1}} K(t, s)u_n^{p-1}(s)ds + \sum_{d=n+1}^{N-N_1+n-1} \int_{t_d^{p-1}}^{t_{d+1}^{p-1}} K(t, s)u_d^{p-1}(s)ds \\ &+ \int_{t_n^p-\tau_1}^{t-\tau_1} K(t, s)u_{N-N_1+n}^{p-1}(s)ds, \quad n \in \{0, \dots, N_1 - 1\}, \end{aligned} \quad (6)$$

and

$$\begin{aligned} \hat{u}_{n,p}(t) &= g(t) + u_{n-N_1}^p(t - \tau_1) + u_n^{p-1}(t - \tau_2) + \int_{t-\tau_2}^{t_{n+1}^{p-1}} K(t, s)u_n^{p-1}(s)ds \\ &+ \sum_{d=n+1}^{N-1} \int_{t_d^{p-1}}^{t_{d+1}^{p-1}} K(t, s)u_d^{p-1}(s)ds + \sum_{i=0}^{n-N_1-1} \int_{t_i^p}^{t_{i+1}^p} K(t, s)u_i^p(s)ds \\ &+ \int_{t_n^p-\tau_1}^{t-\tau_1} K(t, s)u_{n-N_1}^p(s)ds, \quad n \in \{N_1, \dots, N-1\}. \end{aligned} \tag{7}$$

The coefficients $\hat{u}_{n,p}^{(j)}(t_n^p)$ are given by the following formulas. For $n \in \{0, \dots, N_1 - 1\}$,

$$\begin{aligned} \hat{u}_{n,p}^{(j)}(t_n^p) &= g^{(j)}(t_n^p) + \hat{u}_{N-N_1+n,p-1}^{(j)}(t_{N-N_1+n}^{p-1}) + \hat{u}_{n,p-1}^{(j)}(t_n^{p-1}) \\ &- \sum_{i=0}^{j-1} \sum_{l=0}^i \binom{i}{l} \hat{u}_{n,p-1}^{(l)}(t_n^{p-1}) [\partial_1^{(j-1-i)} K(t, t - \tau_2)]^{(i-l)}(t_n^p) \\ &+ \sum_{l=0}^{m-1} \frac{\hat{u}_{n,p-1}^{(l)}(t_n^{p-1})}{l!} \int_{t_n^p-\tau_2}^{t_{n+1}^{p-1}} \partial_1^{(j)} K(t_n^p, s)(s - t_n^{p-1})^l ds \\ &+ \sum_{d=n+1}^{N-N_1+n-1} \sum_{l=0}^{m-1} \frac{\hat{u}_{d,p-1}^{(l)}(t_d^{p-1})}{l!} \int_{t_d^{p-1}}^{t_{d+1}^{p-1}} \partial_1^{(j)} K(t_n^p, s)(s - t_d^{p-1})^l ds \\ &+ \sum_{i=0}^{j-1} \sum_{l=0}^i \binom{i}{l} \hat{u}_{N-N_1+n,p-1}^{(l)}(t_{N-N_1+n}^{p-1}) [\partial_1^{(j-1-i)} K(t, t - \tau_1)]^{(i-l)}(t_n^p), \end{aligned}$$

and for $n \in \{N_1, \dots, N - 1\}$,

$$\begin{aligned} \hat{u}_{n,p}^{(j)}(t_n^p) &= g^{(j)}(t_n^p) + \hat{u}_{n-N_1,p}^{(j)}(t_{n-N_1}^{p-1}) + \hat{u}_{n,p-1}^{(j)}(t_n^{p-1}) \\ &- \sum_{i=0}^{j-1} \sum_{l=0}^i \binom{i}{l} \hat{u}_{n,p-1}^{(l)}(t_n^{p-1}) [\partial_1^{(j-1-i)} K(t, t - \tau_2)]^{(i-l)}(t_n^p) \\ &+ \sum_{l=0}^{m-1} \frac{\hat{u}_{n,p-1}^{(l)}(t_n^{p-1})}{l!} \int_{t_n^p-\tau_2}^{t_{n+1}^{p-1}} \partial_1^{(j)} K(t_n^p, s)(s - t_n^{p-1})^l ds \\ &+ \sum_{d=n+1}^{N-1} \sum_{l=0}^{m-1} \frac{\hat{u}_{d,p-1}^{(l)}(t_d^{p-1})}{l!} \int_{t_d^{p-1}}^{t_{d+1}^{p-1}} \partial_1^{(j)} K(t_n^p, s)(s - t_d^{p-1})^l ds \\ &+ \sum_{i=0}^{n-N_1-1} \sum_{l=0}^{m-1} \frac{\hat{u}_{i,p}^{(l)}(t_i^p)}{l!} \int_{t_i^p}^{t_{i+1}^p} \partial_1^{(j)} K(t_n^p, s)(s - t_i^p)^l ds \\ &+ \sum_{i=0}^{j-1} \sum_{l=0}^i \binom{i}{l} \hat{u}_{n-N_1,p}^{(l)}(t_{n-N_1}^{p-1}) [\partial_1^{(j-1-i)} K(t, t - \tau_1)]^{(i-l)}(t_n^p). \end{aligned}$$

3 Analysis of Convergence

The following lemmas will be used in this section.

Lemma 3.1 (Discrete Gronwall-type inequality [13]) Let $\{k_j\}_{j=0}^n$ be a given nonnegative sequence, and the sequence $\{\varepsilon_n\}$ satisfy $\varepsilon_n \leq p_0 + \sum_{i=0}^{n-1} k_i \varepsilon_i$, $n \geq 0$, with $p_0 \geq 0$. Then ε_n can be bounded by $\varepsilon_n \leq p_0 \exp\left(\sum_{j=0}^{n-1} k_j\right)$, $n \geq 0$.

Lemma 3.2 Let g and K be m times continuously differentiable on their respective domains. Then there exists a positive number $\alpha(m)$ such that for all $n = 0, 1, \dots, N - 1$, $p = 0, 1, \dots, r - 1$, and $j = 0, \dots, m$, we have $\|\hat{u}_{n,p}^{(j)}\|_{L^\infty(\sigma_n^p)} \leq \alpha(m)$, where $\hat{u}_{0,0}(t) = x(t)$ for $t \in \sigma_0^0$.

Proof. The proof is split into two steps.

Claim 1. There exists a positive constant $\alpha_1(m)$ such that $\|\hat{u}_{n,0}^{(j)}\|_{L^\infty(\sigma_n^0)} \leq \alpha_1(m)$ for all $n = 0, 1, \dots, N - 1$, $j = 0, \dots, m$. Let $a_n^j = \|\hat{u}_{n,0}^{(j)}\|_{L^\infty(\sigma_n^0)}$, then, for $j = 0, \dots, m$,

$$a_0^j \leq \max \left\{ \|x^{(j)}\|_{L^\infty(\sigma_0^0)}, j = 0, \dots, m \right\} = \alpha_1^1(m). \tag{8}$$

Now, for all $n = 1, 2, \dots, N - 1$ and $j = 1, \dots, m$, by differentiating (3) and (4) j times, we obtain

$$\begin{aligned} a_n^j &\leq c + d_1^2 h \sum_{l=j}^{m-1} a_{n-N_1}^l + h d_1^1 \sum_{i=0}^{n-N_1} \sum_{l=0}^{m-1} a_i^l + m^2 h d_1^2 \sum_{l=0}^{m-1} a_{n-1-N_1}^l + h d_1^1 \sum_{l=0}^{m-1} a_{n-N_1}^l \\ &\leq c + \underbrace{(d_1^2(1+m^2) + d_1^1)}_{d_1} h \sum_{l=0}^{m-1} a_{n-N_1}^l + h d_1^1 \sum_{i=0}^{n-1} \sum_{l=0}^{m-1} a_i^l, \end{aligned} \tag{9}$$

where the constants c , d_1^1 and d_1^2 are positive and independent of N .

On the other hand, if $j = 0$, then, from (3) and (4), we have

$$a_n^0 \leq c + (d_1^1 + d_1^2) h \sum_{l=0}^{m-1} a_{n-N_1}^l + h d_1^1 \sum_{i=0}^{n-1} \sum_{l=0}^{m-1} a_i^l. \tag{10}$$

From (9) and (10), for each fixed $n \geq 1$, we consider the sequence a_n^j for $j = 0, \dots, m$,

$$a_n^j \leq c + 2h d_1 \sum_{i=0}^{n-1} \sum_{l=0}^{m-1} a_i^l. \tag{11}$$

Consider the sequence $z_n = \sum_{j=0}^m a_n^j$ for $n \geq 0$. Then, from (11), we have

$$z_n \leq \underbrace{(m+1)c}_{c_1} + h \underbrace{2(m+1)d_1}_{d_2} \sum_{i=0}^{n-1} z_i. \tag{12}$$

Moreover, from (8), we obtain

$$z_0 \leq (m+1)\alpha_1^1(m) = c_2. \tag{13}$$

Then, from (12) and (13), we have for all $n = 0, 1, \dots, N - 1$,

$$z_n \leq c_3 + h d_2 \sum_{i=0}^{n-1} z_i$$

such that $c_3 = \max(c_1, c_2)$. Using Lemma 3.1, for all $n = 0, 1, \dots, N - 1$, we obtain

$$z_n \leq \underbrace{c_3 \exp(\tau_2 d_2)}_{\alpha_1(m)}.$$

Hence, the first claim is true.

Claim 2. There exists a positive constant $\alpha_2(m)$ such that $\|\hat{u}_{n,p}^{(j)}\|_{L^\infty(\sigma_n^p)} \leq \alpha_2(m)$ for all $n = 0, 1, \dots, N - 1, j = 0, \dots, m$ and $p = 1, 2, \dots, r - 1$.

Let $a_{n,p}^{(j)} = \|\hat{u}_{n,p}^{(j)}\|_{L^\infty(\sigma_n^p)}$ and $\varepsilon_p = \max\{a_{i,p}^j, j = 0, \dots, m, i = 0, \dots, N - 1\}$ for $p = 1, \dots, r - 1$. Similarly to Claim 1, by differentiating (6) and (7) j times, we obtain for all $n = 1, \dots, N - 1$,

$$a_{n,p}^j \leq c_4 + b_1 \varepsilon_{p-1} + d_3 h \sum_{i=0}^{n-1} \sum_{l=0}^{m-1} a_{i,p}^l,$$

where c_4, b_1 , and d_3 are positive numbers. Consider the sequence $y_n = \sum_{j=0}^m a_{n,p}^j, n = 0, 1, \dots, N - 1$, using Lemma 3.1, for all $n = 0, \dots, N - 1$, we obtain

$$\begin{aligned} y_n &\leq ((m + 1)c_4 + (m + 1)b_1 \varepsilon_{p-1}) \exp \underbrace{\sum_{i=0}^{n-1} (m + 1)d_4 h}_{d_4} \\ &\leq \underbrace{(m + 1)c_4 \exp(d_4)}_{c_5} + \underbrace{(m + 1)b_1 \exp(d_4)}_{b_2} \varepsilon_{p-1} \\ &\leq \underbrace{c_6 + b_3 \alpha_1(m)}_{\alpha_2(m)}, \end{aligned}$$

where c_6 and b_3 are positive numbers.

Hence, the proof of Lemma 3.2 is completed by setting $\alpha(m) = \max\{\alpha_1(m), \alpha_2(m)\}$.

The following theorem gives the convergence of the presented method.

Theorem 3.1 *Let g and K be m times continuously differentiable on their respective domains. Then (2) and (5) define a unique approximation $u \in S_{m-1}^{(-1)}(\Pi_N)$, and the resulting error function $e = x - u$ satisfies $\|e\|_{L(I)^\infty} \leq Ch^m$, provided that h is sufficiently small, where C is a finite constant independent of h .*

Proof. The proof is split into two steps.

Claim 1. There exists a constant C_1 independent of h such that $\|e^0\|_{L^\infty(\sigma^0)} \leq C_1 h^m$, where the error $e^0 = e|_{\sigma^0}$ is defined on σ_n^0 by $e^0(t) = e_n^0(t) = |x(t) - u_n^0(t)|$ for all $n = 0, 1, \dots, N - 1$. Let $t \in \sigma_0^0$. Then we have for sufficiently small h ,

$$|e_0^0(t)| = |x(t) - u_0^0(t)| \leq \frac{\|x^m\|_{L^\infty(\sigma_0^0)}}{m!} h^m \leq \frac{\alpha(m)}{m!} h^m.$$

From (3) and (4), for $n = 1, \dots, N - 1$, we have

$$\|x - \hat{u}_{n,0}\|_{L^\infty(\sigma_n^0)} \leq hk \sum_{i=0}^{n-1} \|e_i^0\|_{L^\infty(\sigma_i^0)} + \|e_{n-N_1}^0\|_{L^\infty(\sigma_{n-N_1}^0)},$$

where $k = \|k\|_{L^\infty(I)}$, therefore, by Lemma 3.2,

$$\begin{aligned} \|e_n^0\|_{L^\infty(\sigma_n^0)} &\leq \|x - \hat{u}_{n,0}\|_{L^\infty(\sigma_n^0)} + \|\hat{u}_{n,0} - u_n^0\|_{L^\infty(\sigma_n^0)} \\ &\leq hk \sum_{i=0}^{n-1} \|e_i^0\|_{L^\infty(\sigma_i^0)} + \|e_{n-N_1}^0\|_{L^\infty(\sigma_{n-N_1}^0)} + \frac{\alpha(m)}{m!} h^m \\ &\leq hk \sum_{i=0}^{n-1} \|e_i^0\|_{L^\infty(\sigma_i^0)} + 2 \frac{\alpha(m)}{m!} h^m. \end{aligned}$$

Hence, by Lemma 3.1, for all $n = 1, \dots, N_1 - 1$,

$$\|e_n^0\|_{L^\infty(\sigma_n^0)} \leq \underbrace{\left(\frac{2\alpha(m)}{m!} \exp(\tau_2 k) \right)}_{C_1^1} h^m,$$

by taking $C_1 = \max\{\frac{\alpha(m)}{m!}, C_1^1\}$, Claim 1 is true.

Claim 2. There exists a constant C_2 independent of h such that $\|e\|_{L^\infty(I)} \leq C_2 h^m$. Define the error $e^p(t)$ on σ^p by $e^p(t) = x(t) - u^p(t)$ and on σ_n^p by $e^p(t) = e_n^p(t) = x(t) - u_n^p(t)$ for all $n = 0, \dots, N - 1$ and $p = 1, \dots, r - 1$.

Let $t \in \sigma_n^p$ for $n = 0, 2, \dots, N - 1$. Then we have from (6) and (7),

$$\begin{aligned} \|x - \hat{u}_{n,p}\|_{L^\infty(\sigma_n^p)} &\leq \|e_{N-N_1+n}^{p-1}\|_{L^\infty(\sigma_{N-N_1+n}^{p-1})} + \|e_n^{p-1}\|_{L^\infty(\sigma_n^{p-1})} + \|e_{n-N_1}^p\|_{L^\infty(\sigma_{n-N_1}^p)} \\ &\quad + 2hk \sum_{i=0}^{N-1} \|e_i^{p-1}\|_{L^\infty(\sigma_i^{p-1})} + hk \sum_{i=0}^{n-1} \|e_i^p\|_{L^\infty(\sigma_i^p)}, \end{aligned}$$

hence,

$$\begin{aligned} \|x - \hat{u}_{n,p}\|_{L^\infty(\sigma_n^p)} &\leq 2(1 + \tau_2 k) \|e^{p-1}\|_{L^\infty(\sigma^{p-1})} + \|e_{n-N_1}^p\|_{L^\infty(\sigma_{n-N_1}^p)} \\ &\quad + hk \sum_{i=0}^{n-1} \|e_i^p\|_{L^\infty(\sigma_i^p)}. \end{aligned}$$

Therefore, by Theorem 3.2, for $n = 1, 2, \dots, N - 1$,

$$\begin{aligned} \|e_n^p\|_{L^\infty(\sigma_n^p)} &\leq \|x - \hat{u}_{n,p}\|_{L^\infty(\sigma_n^p)} + \|\hat{u}_{n,p} - u_n^p\|_{L^\infty(\sigma_n^p)} \\ &\leq \|x - \hat{u}_{n,p}\|_{L^\infty(\sigma_n^p)} + \frac{\alpha(m)}{m!} h^m. \end{aligned}$$

Then we repeat the next step a times for $n = 1, 2, \dots, aN_1 - 1, a = \{1, 2, \dots, \frac{\tau_2}{\tau_1}\}$,

$$\begin{aligned} \|e_n^p\|_{L^\infty(\sigma_n^p)} &\leq 2(1 + \tau_2 k) \|e^{p-1}\|_{L^\infty(\sigma^{p-1})} + hk \sum_{i=0}^{n-1} \|e_i^p\|_{L^\infty(\sigma_i^p)} \\ &\quad + \|e_{n-N_1}^p\|_{L^\infty(\sigma_{n-N_1}^p)} + \frac{\alpha(m)}{m!} h^m, \end{aligned}$$

hence, by Lemma 3.1, for all $n = 0, 1, \dots, N - 1$,

$$\|e_n^p\|_{L^\infty(\sigma_n^p)} \leq \frac{\alpha(m)C_1 \exp(\tau_2 k)}{m!} h^m + 2(1 + \tau_2 k) \exp(\tau_2 k) \|e^{p-1}\|_{L^\infty(\sigma^{p-1})},$$

then, for all $p = 1, \dots, r - 1$, $\|e_n^p\|_{L^\infty(\sigma_n^p)} \leq C_2 h^m$.

Thus, the proof is completed by taking $C = \max\{C_1, C_2\}$.

4 Numerical Illustrations

In this section, we present numerical experiments that evaluate the effectiveness of the Taylor collocation method (TCM) in solving problems described by (1). We demonstrate convergence of order m by providing numerical examples that exhibit convergence rates of up to m when applying this method. Additionally, we record the computational time (in CPU time/s) for each example. Our numerical experiments were conducted using Maple version 17 on a personal computer equipped with an Intel Core i7-1165G7 CPU @ 2.80GHz and 16 GB of RAM, running the MS Windows 7 operating system. As the values of both n and m increase, the absolute error function decreases, thereby confirming the theoretical estimates outlined in Section 3.

Example 4.1 Consider the neutral double delay Volterra integral equation

$$x(t) = g(t) + x(t - \frac{1}{2}) + x(t - 1) + \int_{t-1}^{t-\frac{1}{2}} (ts + \cos(t + s))x(s)ds$$

for $t \in [1, 5]$, and g is chosen so that the exact solution $x(t) = \cos(t) + 1$, $x(t) = \Phi(t)$ for $t \in [0, 1]$. The absolute errors and computational time for $(N, m) = \{(2, 2), (4, 4), (6, 6), (8, 8)\}$ are presented in Table 1. The exact and approximate solutions for $N = m = 8$ are shown in Figure 1(a).

t	$N = m = 2$	$N = m = 4$	$N = m = 6$	$N = m = 8$
1.00	0.0	0.0	0.0	0.0
2.00	$1.58e - 02$	$1.02e - 5$	$1.29e - 9$	$7.08e - 11$
3.00	$1.27e - 02$	$2.89e - 6$	$2.52e - 9$	$9.70e - 10$
4.00	$4.45e - 02$	$2.53e - 4$	$1.17e - 7$	$2.53e - 08$
5.00	$1.44e - 01$	$7.31e - 3$	$3.81e - 6$	$8.50e - 07$
CPU	1.79 s	1.95 s	3.18 s	5.29 s

Table 1: Absolute errors for Example 4.1.

Example 4.2 Consider the neutral double delay Volterra integral equation

$$x(t) = g(t) + x(t - 0.4) + x(t - 0.8) + \int_{t-0.8}^{t-0.4} (t - s)e^{t-s}x(s)ds$$

for $t \in [1, 8]$, and g is chosen so that the exact solution $x(t) = e^{-t} \sin(t)$, $\Phi(t) = x(t)$ for $t \in [0, 0.8]$. The absolute errors and computational time for $(N, m) = \{(2, 6), (2, 8), (2, 10), (4, 4), (4, 6), (4, 8)\}$ are presented in Table 2. Figure 1(b) displays the exact and approximate solutions for $N = 4, m = 8$.

t	$N = 2$			$N = 4$		
	$m = 6$	$m = 8$	$m = 10$	$m = 4$	$m = 6$	$m = 8$
0.8	0	0	0	0	0	0
1.6	$5.22e - 07$	$2.26e - 09$	$2.82e - 10$	$6.28e - 06$	$9.24e - 09$	$2.81e - 10$
2.4	$1.57e - 06$	$9.66e - 09$	$1.05e - 09$	$2.59e - 05$	$2.64e - 08$	$1.08e - 09$
3.2	$5.31e - 06$	$3.57e - 08$	$3.53e - 09$	$9.19e - 05$	$8.57e - 08$	$3.75e - 09$
4.0	$1.88e - 05$	$1.30e - 07$	$1.18e - 08$	$3.21e - 04$	$2.95e - 07$	$1.29e - 08$
4.8	$6.69e - 05$	$4.67e - 07$	$3.97e - 08$	$1.12e - 03$	$1.02e - 06$	$4.46e - 08$
5.6	$3.65e - 04$	$1.66e - 06$	$1.34e - 07$	$3.91e - 03$	$3.55e - 06$	$1.54e - 07$
6.4	$8.30e - 04$	$5.86e - 06$	$4.56e - 07$	$1.35e - 02$	$1.23e - 05$	$5.32e - 07$
7.2	$2.90e - 03$	$2.06e - 05$	$1.55e - 06$	$4.71e - 02$	$4.25e - 05$	$1.83e - 06$
8.0	$1.07e - 02$	$7.81e - 05$	$4.98e - 06$	$1.65e - 01$	$1.49e - 04$	$6.28e - 06$
CPU	1.57 s	1.90 s	3.85 s	1.75 s	2.56 s	3.82 s

Table 2: Absolute errors of Example 4.2.

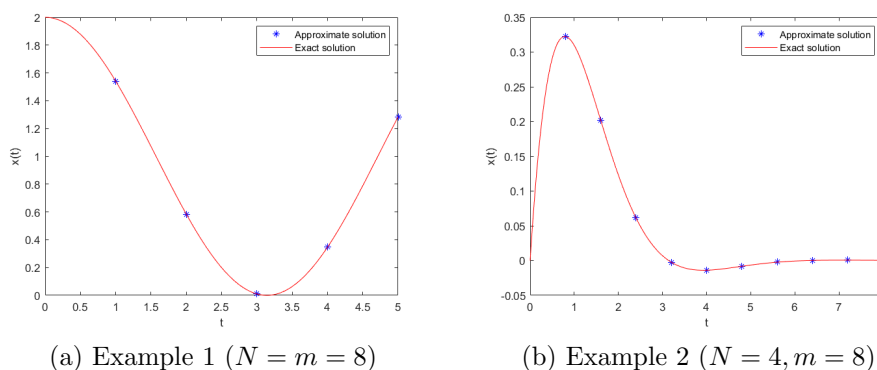


Figure 1: The exact and approximate solutions.

5 Conclusion

In the concluding remarks of our study, we have addressed the reviewer's suggestion to bolster the description of the novelty arising from our results. Our exploration of the Taylor collocation method for approximating the solution of linear DDVIEs has yielded noteworthy outcomes. Our findings underscore this method's effectiveness and ease of implementation, emphasizing its reliability in generating approximate solutions through iterative formulas without necessitating the resolution of algebraic equation systems. The numerical examples presented in this paper demonstrate the method's convergence with high accuracy. The results obtained from these examples validate our theoretical estimates and highlight the proposed approach's practical applicability. It is worth noting that the numerical outcomes consistently align with the expected convergence patterns, affirming the reliability of the Taylor collocation method in the context of linear DDVIEs. Our future research endeavors will extend beyond the scope of this paper. We plan to generalize the proposed method to tackle DDVIEs in two dimensions and a system of DDVIEs, further expanding its applicability to a broader class of problems. This

extension is anticipated to contribute to the method's versatility and potential to address complex systems exhibiting intricate temporal dependencies.

References

- [1] H. L. Smith and P. Waltman. *The Theory of the Chemostat: Dynamics of Microbial Competition*. Cambridge university press, Vol. **13**, 1995.
- [2] H. Laib, A. Bellour and A. Boulmerka. Taylor collocation method for a system of nonlinear Volterra delay integro-differential equations with application to COVID-19 epidemic. *International Journal of Computer Mathematics* **99** (4) (2022) 852–876.
- [3] S. Zhai, G. Luo, T. Huang, X. Wang, J. Tao and P. Zhou. Vaccination control of an epidemic model with time delay and its application to COVID-19. *Nonlinear Dynamics* **106** (2) (2021) 1279–1292.
- [4] X. Meng, Z. Li and J. J. Nieto. Dynamic analysis of Michaelis–Menten chemostat-type competition models with time delay and pulse in a polluted environment. *Journal of mathematical chemistry* **47** (2010) 123–144.
- [5] A. Y. Aleksandrov. Delay-Independent Stability Conditions for a Class of Nonlinear Mechanical Systems. *Nonlinear Dyn. Syst. Theory* **2221** (5) (2021) 447–456.
- [6] M. Mounni and M. Tilioua. A Neural Network Approximation for a Model of Micromagnetism. *Nonlinear Dyn. Syst. Theory* **22** (4) (2022) 432–446.
- [7] M. Iannelli, T. Kostova and F. A. Milner. A method for numerical integration of age- and size-structured population models. *Numer. Methods Partial Differ. Equ.* **25** (2009) 918–930.
- [8] D. Breda, M. Iannelli, S. Maset and R. Vermiglio. Stability analysis of the Gurtin–MacCamy model. *SIAM J. Numer. Anal.* **46** (2) (2008) 980–995.
- [9] D. Breda, C. Cusulin, M. Iannelli, S. Maset and R. Vermiglio. Stability analysis of age-structured population equations by pseudospectral differencing methods. *J. Math. Biol.* **54** (2007) 701–720.
- [10] E. Messina, E. Russo and A. Vecchio. Comparing analytical and numerical solution of a nonlinear two-delay integral equations. *Math. Comput. Simulat.* **81** (2011) 1017–1026.
- [11] H. Laib, A. Bellour and A. Boulmerka. Taylor collocation method for high-order neutral delay Volterra integro-differential equations. *Journal of Innovative Applied Mathematics and Computational Sciences* **2** (1) (2022) 53–77.
- [12] A. Bellour, E. Dads and M. Bousselsal. Existence theory and qualitative properties of solutions to double delay integral equations. *Electronic Journal of Qualitative Theory of Differential Equations* **56** (2013) 1–23.
- [13] H. Brunner. *Collocation Methods for Volterra Integral and Related Functional Differential Equations*. Cambridge university press, Vol. **15**, 2004.



Stability Analysis of a Coupled System of Two Nonlinear Differential Equations with Boundary Conditions

Besma Fadlia¹, Abdelwahab Zarour¹, Rima Faizi² and Mohamed Dalah^{1*}

¹ *University Constantine 1: Frères Mentouri, Faculty of Exact Sciences,
Department of Mathematics,
Applied Mathematics and Modeling Laboratory and Differential Equations Laboratory,
Constantine, Algeria.*

² *LAM Laboratory, University Badji Mokhtar, P.O. BOX 12, Annaba 23000, Algeria.*

Received: September 28, 2023; Revised: April 14, 2024

Abstract: We study the antiplane frictional contact models for electro-viscoelastic materials. The material is assumed to be electro-viscoelastic and is modelled by a slip rate dependent friction law and the foundation is assumed to be electrically conductive. First, we give the mathematical model of our phenomena. Second, we describe the classical formulation for the antiplane problem and we give the corresponding variational formulation which is given by a method of coupling of an evolutionary variational quality for the displacement field and a time-dependent variational equation for the electric potential field. Then we prove the existence of a unique weak solution to the model.

Keywords: *nonlinear system; electro-viscoelastic material; contact problem; weak solution; boundary condition.*

Mathematics Subject Classification (2010): 70K75, 93A30, 93C10, 49J40.

* Corresponding author: <mailto:dalah.mohamed@umc.edu.dz>

1 Introduction

Contact mechanics is the study of the deformation of solids that are in contact with each other at one or more points. Antiplane shear deformations are one of the simplest classes of deformations that solids can undergo. The antiplane shear deformation is the deformation that we expect to appear after loading a long cylinder in the direction of its generators so that the displacement field is parallel to the generators of the cylinder and independent of the axial coordinate.

The piezoelectric effect results from the coupling between electrical and mechanical properties, in which the body has the ability to produce an electrical field when a mechanical stress is present and, conversely, under the action of an electric field the body undergoes a mechanical stress. The models for piezoelectric materials can be found in [1], [2] and [3].

In this paper, we study an antiplane contact problem for electro-viscoelastic materials with the slip rate-dependent friction law, in the framework of the Mathematical Theory of Contact Mechanics, when the foundation is electrically conductive. We consider the case of antiplane shear deformation, i.e., the displacement is parallel to the generators of the cylinder and independent of the axial coordinate (see [5], [6] and the references therein). Such kind of problems was studied in a number of papers in the context of various constitutive laws and contact conditions (see, e.g. [12], [13] and [14]).

Our paper is structured as follows. In Section 2, we present the mechanical model for the quasistatic antiplane contact problem. In Section 3, we introduce the notation, list the assumption on problem's data, derive the variational formulation of the problem. Finally, in Section 4, we state our main existence and uniqueness result, i.e., Theorems 4.1-4.2. The proof of this result is carried out in several steps and is based on the arguments of evolutionary inequalities.

2 The Mathematical Model

We consider a piezoelectric body \mathcal{B} identified with a region in \mathbb{R}^3 it occupies in a fixed and undistorted reference configuration. We assume that $\mathcal{B} = \Omega \times (-\infty, +\infty)$ is a cylinder with generators parallel to the x_3 -axis with a cross-section which is a regular region Ω in the x_1, x_2 -plane, $Ox_1x_2x_3$ being a Cartesian coordinate system. The cylinder is acted upon by body forces of density \mathbf{f}_0 and has volume free electric charges of density q_0 . It is also constrained mechanically and electrically on the boundary. To describe the boundary conditions, we denote by $\partial\Omega = \Gamma$ the boundary of Ω and we assume a partition of Γ into three open disjoint parts Γ_1, Γ_2 and Γ_3 , on the one hand, and a partition of $\Gamma_1 \cup \Gamma_2$ into two open parts Γ_a and Γ_b . On the other hand, we assume that the one-dimensional measures of Γ_1 and Γ_a , denoted $\text{meas } \Gamma_1$ and $\text{meas } \Gamma_a$, are positive. Let $T > 0$ and let $[0, T]$ be the time interval of interest.

The cylinder is clamped on $\Gamma_1 \times (-\infty, +\infty)$ and therefore the displacement field vanishes there, surface tractions of density \mathbf{f}_2 act on $\Gamma_2 \times (-\infty, +\infty)$. We also assume that the electrical potential vanishes on $\Gamma_a \times (-\infty, +\infty)$ and a surface electrical charge of density q_2 is prescribed on $\Gamma_b \times (-\infty, +\infty)$. The cylinder is in contact over $\Gamma_3 \times (-\infty, +\infty)$ with a conductive obstacle, the so-called foundation. The contact is frictional and is modeled by Tresca's law.

We denote by \mathcal{S}^3 the space of the second-order symmetric tensors on \mathbb{R}^3 , and we

define the inner products and the corresponding norms on \mathbb{R}^3 and \mathcal{S}^3 by

$$\mathbf{u} \cdot \mathbf{v} = u_i v_i, \quad \|\mathbf{v}\| = (v \cdot v)^{\frac{1}{2}} \quad \text{for all } \mathbf{u} = (u_i), \mathbf{v} = (v_i) \in \mathbb{R}^3, 1 \leq i, j \leq 3,$$

$$\sigma \cdot \tau = \sigma_{i,j} \tau_{i,j}, \quad \|\tau\| = (\tau \cdot \tau)^{\frac{1}{2}} \quad \text{for all } \sigma = (\sigma_{i,j}), \tau = \tau_{i,j} \in \mathcal{S}^3, 1 \leq i, j \leq 3.$$

We assume that

$$\mathbf{f}_0 = (0, 0, f_0) \quad \text{with } f_0 = f_0(x_1, x_2, t) : \Omega \times [0, T] \longrightarrow \mathbb{R}, \quad (1)$$

and

$$\mathbf{f}_2 = (0, 0, f_2) \quad \text{with } f_2 = f_2(x_1, x_2, t) : \Gamma_2 \times [0, T] \longrightarrow \mathbb{R}. \quad (2)$$

The body forces (1) and the surface tractions (2) would be expected to give rise to a deformation of the elastic cylinder whose displacement, denoted by u , is of the form

$$\mathbf{u} = (0, 0, u), \quad \text{with } q_0 : \Omega \times [0, T] \longrightarrow \mathbb{R}. \quad (3)$$

Such kind of deformation, associated to a displacement field of the form (3), is called an antiplane shear. We assume also that

$$q_0 = q_0(x_1, x_2, t) \quad \text{with } u = u(x_1, x_2, t) : \Omega \times [0, T] \longrightarrow \mathbb{R}, \quad (4)$$

$$q_2 = q_2(x_1, x_2, t) \quad \text{with } q_2 : \Gamma_b \times [0, T] \longrightarrow \mathbb{R}. \quad (5)$$

The electric charges (4), (5) would be expected to give rise to deformations and to the electric charges of the piezoelectric cylinder corresponding to an electric potential field φ which is independent of x_3 and has the form

$$\varphi = \varphi(x_1, x_2, t) : \Omega \times [0, T] \longrightarrow \mathbb{R}. \quad (6)$$

The infinitesimal strain tensor, denoted by $\varepsilon(u) = (\varepsilon_{i,j}(u))$, is defined by

$$\varepsilon_{i,j}(u) = \frac{1}{2}(u_{i,j} + u_{j,i}), \quad 1 \leq i, j \leq 3, \quad (7)$$

where the index that follows the comma indicates a partial derivative with respect to the corresponding component of the spatial variable. Moreover, in the sequel, the convention of summation upon a repeated index is used. From (3) and (7), it follows that, in the case of the antiplane problem, the infinitesimal strain tensor becomes

$$\varepsilon(u) = \begin{pmatrix} 0 & 0 & \frac{1}{2}u_{,1} \\ 0 & 0 & \frac{1}{2}u_{,2} \\ \frac{1}{2}u_{,1} & \frac{1}{2}u_{,2} & 0 \end{pmatrix}. \quad (8)$$

We also denote by $E(\varphi) = (E_i(\varphi))$ the electric field and by $D = (D_i)$ the electric displacement field, where

$$\varepsilon_{i,j}(u) = \frac{1}{2}(u_{i,j} + u_{j,i}), \quad (9)$$

$$E_i(\varphi) = -\varphi_{,i}. \quad (10)$$

Let $\sigma = (\sigma_{i,j})$ denote the stress field. We suppose that the material's behavior is modelled by an electro-viscoelastic constitutive law of the form

$$\sigma = 2\theta\varepsilon(\dot{u}) + \zeta \text{tr}\varepsilon(\dot{u})I + 2\mu\varepsilon(u) + \lambda \text{tr}\varepsilon(u)I - \mathcal{E}^*E(\varphi), \quad (11)$$

$$D = \mathcal{E}^*\varepsilon(u) + \beta E(\varphi), \quad (12)$$

where ζ and θ are viscosity coefficients, λ and μ are the Lamé coefficients, $\text{tr } \varepsilon(u) = \varepsilon_{ii}(u)$, \mathbf{I} is the unit tensor in \mathbb{R}^3 , α is the electric permittivity constant, \mathcal{E} represents the third-order piezoelectric tensor and \mathcal{E}^* is its transpose. We assume that

$$\mathcal{E}\varepsilon = \begin{pmatrix} e(\varepsilon_{13} + \varepsilon_{31}) \\ e(\varepsilon_{23} + \varepsilon_{32}) \\ e(\varepsilon_{33}) \end{pmatrix}, \quad \forall \varepsilon = (\varepsilon_{i,j}) \in \mathcal{S}^3, \tag{13}$$

where e is a piezoelectric coefficient. We also assume that the coefficients θ, μ, β and e depend of the spatial variables x_1, x_2 , but are independent on the spatial variable x_3 . Since $\mathcal{E}\varepsilon \cdot \mathbf{v} = \varepsilon \cdot \mathcal{E}^* \mathbf{v}$ for all $\varepsilon \in \mathcal{S}^3, \mathbf{v} \in \mathbb{R}^3$, it follows from (13) that

$$\mathcal{E}^* \mathbf{v} = \begin{pmatrix} 0 & 0 & ev_1 \\ 0 & 0 & ev_2 \\ ev_1 & ev_2 & ev_3 \end{pmatrix}, \quad \forall \mathbf{v} = (v_i) \in \mathbb{R}^3. \tag{14}$$

Here and below the dot above represents the derivative with respect to the time variable. The stress field is given by the matrix

$$\sigma = \begin{pmatrix} 0 & 0 & \sigma_{13} \\ 0 & 0 & \sigma_{23} \\ \sigma_{31} & \sigma_{32} & 0 \end{pmatrix}. \tag{15}$$

In the antiplane context (3), (6), when using the constitutive equations (11)-(12) and equalities (13)-(14), it follows that the stress field and the electric displacement field are given by

$$\sigma = \begin{pmatrix} 0 & 0 & \theta \dot{u}_{,1} + \mu u_{,1} + e\varphi_{,1} \\ 0 & 0 & \theta \dot{u}_{,2} + \mu u_{,2} + e\varphi_{,2} \\ \theta \dot{u}_{,1} + \mu u_{,1} + e\varphi_{,1} & \theta \dot{u}_{,2} + \mu u_{,2} + e\varphi_{,2} & 0 \end{pmatrix}, \tag{16}$$

$$\mathbf{D} = \begin{pmatrix} eu_{,1} - \beta\varphi_{,1} \\ eu_{,2} - \beta\varphi_{,2} \\ 0 \end{pmatrix}. \tag{17}$$

We assume that the process is mechanically quasistatic and electrically static and therefore is governed by the equilibrium equations

$$\text{Div} \sigma + \mathbf{f}_0 = 0, \tag{18}$$

$$D_{i,i} - q_0 = 0 \quad \text{in } \mathcal{B} \times (0, T), \tag{19}$$

where $\text{Div} \sigma = (\sigma_{ij,j})$ represents the divergence of the tensor field σ . Thus, keeping in mind (1), (3), (4), (6), (16) and (17), the equilibrium equations above are reduced to the following scalar equations :

$$\text{div}(\theta \nabla \dot{u} + \mu \nabla u) + \text{div}(e \nabla \varphi) + f_0 = 0, \quad \text{in } \Omega \times (0, T), \tag{20}$$

$$\text{div}(e \nabla u) - \text{div}(\beta \nabla \varphi) = q_0, \quad \text{in } \Omega \times (0, T). \tag{21}$$

Here and below we use the notation

$$\text{div} \tau = \tau_{1,2} + \tau_{1,2} \quad \text{for } \tau = (\tau_1(x_1, x_2, t), \tau(x_1, x_2, t)),$$

$$\nabla v = (v_{,1}, v_{,2}), \quad \partial_\nu v = v_{,1}\nu_1 + v_{,2}\nu_2 \quad \text{for } v = v(x_1, x_2, t).$$

Recall that since the cylinder is clamped on $\Gamma_1 \times (-\infty, +\infty)$, the displacement field vanishes there. Thus (3) implies

$$u = 0 \quad \text{on } \Gamma_1 \times (0, T), \quad (22)$$

the electrical potential vanishes too on $\Gamma_a \times (-\infty, +\infty)$, thus (4) implies that

$$\varphi = 0 \quad \text{on } \Gamma_a \times (0, T). \quad (23)$$

Let ν denote the unit normal on $\Gamma \times (-\infty, +\infty)$. We have

$$\nu = (\nu_1, \nu_2, 0) \quad (24)$$

with $\nu_i = \nu_i(x_1, x_2) : \Gamma \rightarrow \mathbb{R}, i = 1, 2$. For a vector \mathbf{v} we denote by v_ν and \mathbf{v}_τ its normal and tangential components on the boundary which are given by

$$v_\nu = \mathbf{v} \cdot \nu, \quad \mathbf{v}_\tau = \mathbf{v} - v_\nu \nu, \quad (25)$$

respectively. In (25), and everywhere in this paper, " \cdot " represents the inner product on the space $\mathbb{R}^3 (d = 2, 3)$. Moreover, for a given stress field σ , we denote by σ_ν and σ_τ the normal and tangential components on the boundary, respectively, i.e.,

$$\sigma_\nu = (\sigma \nu) \cdot \nu, \quad \sigma_\tau = \sigma \nu - \sigma_\nu \nu. \quad (26)$$

From (16), (17) and (24), we deduce that the Cauchy stress vector and the normal component of the electric displacement field are given by

$$\sigma \nu = (0, 0, \theta \partial_\nu \dot{u} + \mu \partial_\nu u + \partial_\nu \varphi), \quad \mathbf{D} \cdot \nu = e \partial_\nu u - \beta \partial_\nu \varphi. \quad (27)$$

Here and subsequently we use the notations $\partial_\nu u = u_{,1}\nu_1 + u_{,2}\nu_2$ and $\partial_\nu \varphi = \varphi_{,1}\nu_1 + \varphi_{,2}\nu_2$. When keeping in mind the traction boundary condition $\sigma \nu = \mathbf{f}_2$ on $\Gamma_2 \times (-\infty, +\infty)$ and the electric condition $\mathbf{D} \cdot \nu = q_2$ on $\Gamma_b \times (-\infty, +\infty)$, it follows from (2), (5) and (27) that

$$\theta \partial_\nu \dot{u} + \mu \partial_\nu u + \partial_\nu \varphi = f_2 \quad \text{on } \Gamma_2 \times (0, T), \quad (28)$$

$$e \partial_\nu u - \beta \partial_\nu \varphi = q_2 \quad \text{on } \Gamma_b \times (0, T). \quad (29)$$

We now describe the frictional contact condition on $\Gamma_3 \times (-\infty, +\infty)$. First, we note that from (3), (24) and (25), we find $u_\nu = 0$, which shows that the contact is bilateral, that is, the contact is kept during all the process. Using now (3), (24)-(27), we conclude that

$$\mathbf{u}_\tau = (0, 0, u), \quad (30)$$

$$\sigma_\tau = (0, 0, \sigma_\tau), \quad (31)$$

where

$$\sigma_\tau = \theta \partial_\nu \dot{u} + \mu \partial_\nu u + \partial_\nu \varphi. \quad (32)$$

We assume that the friction is invariant with respect to the x_3 -axis and for all $t \in [0, T]$, it is modelled by the following conditions on Γ_3 :

$$\begin{cases} |\sigma_\tau| \leq g(|\dot{u}_\tau|) \quad \text{on } \Gamma_3 \times [0, T], \\ \sigma_\tau = -g(|\dot{u}|) \frac{\dot{u}_\tau}{|\dot{u}_\tau|}, \quad \text{on } \Gamma_3 \times [0, T]. \end{cases} \quad (33)$$

Here $g : \Gamma_3 \times \mathbb{R} \rightarrow \mathbb{R}^3$ is a given function, the friction bound, and \dot{u}_τ represents the tangential velocity on the contact boundary. In (33), the strict inequality holds in the stick zone and the equality is true in the slip zone.

Using now (30), (32), it is straightforward to see that the conditions (33) imply

$$\begin{cases} |\theta \partial_\nu \dot{u} + \mu \partial_\nu u + e \partial_\nu \varphi| \leq g(|\dot{u}|), \\ \theta \partial_\nu \dot{u} + \mu \partial_\nu u + e \partial_\nu \varphi = -g(|\dot{u}|) \frac{\dot{u}}{|\dot{u}|}, \text{ on } \Gamma_3 \times [0, T]. \end{cases} \quad (34)$$

Finally, we prescribe the initial displacement

$$u(0) = u_0, \text{ in } \Omega, \quad (35)$$

where u_0 is a given function on Ω .

Problem 2.1 Find a displacement field $u : \Omega \times [0, T] \rightarrow \mathbb{R}$ and the electric potential field $\varphi : \Omega \times [0, T] \rightarrow \mathbb{R}$ such that

$$\operatorname{div}(\theta \nabla \dot{u} + \mu \nabla u) + \operatorname{div}(e \nabla \varphi) + f_0 = 0, \text{ in } \Omega \times (0, T), \quad (36)$$

$$\operatorname{div}(e \nabla u) - \operatorname{div}(\beta \nabla \varphi) = q_0, \text{ in } \Omega \times (0, T), \quad (37)$$

$$u = 0, \text{ on } \Gamma_1 \times (0, T), \quad (38)$$

$$\theta \partial_\nu \dot{u} + \mu \partial_\nu u + e \partial_\nu \varphi = f_2, \text{ on } \Gamma_2 \times (0, T), \quad (39)$$

$$\begin{cases} |\theta \partial_\nu \dot{u} + \mu \partial_\nu u + e \partial_\nu \varphi| \leq g(|\dot{u}|), \\ \theta \partial_\nu \dot{u} + \mu \partial_\nu u + e \partial_\nu \varphi = -g(|\dot{u}|) \frac{\dot{u}}{|\dot{u}|}, \text{ on } \Gamma_3 \times (0, T), \end{cases} \quad (40)$$

$$\varphi = 0, \text{ on } \Gamma_a \times (0, T), \quad (41)$$

$$e \partial_\nu u - \beta \partial_\nu \varphi = q_2, \text{ on } \Gamma_b \times (0, T), \quad (42)$$

$$u(0) = u_0, \text{ in } \Omega \times (0, T). \quad (43)$$

3 Assumptions and Variational Formulation

To obtain a variational formulation for the mechanical problem (36)-(43), we introduce the function spaces $V = \{v \in H^1(\Omega) : v = 0 \text{ on } \Gamma_1\}$ and $W = \{\psi \in H^1(\Omega) : \psi = 0 \text{ on } \Gamma_1\}$, and here and below, we write w for the trace γw of a function $w \in H^1$ on Γ_1 .

Since $\operatorname{meas} \Gamma_1 > 0$ and $\operatorname{meas} \Gamma_a > 0$, it is well known that V and W are the real Hilbert spaces with the inner products

$$(u, v)_V = \int_\Omega \nabla u \cdot \nabla v \, dx, \forall u, v \in V,$$

and

$$(\varphi, \psi)_W = \int_\Omega \nabla \varphi \cdot \nabla \psi \, dx, \forall \varphi, \psi \in W.$$

Moreover, the associated norms

$$\|v\|_V = \|\nabla v\|_{L^2(\Omega)^2}, \forall v \in V, \quad (44)$$

$$\|\psi\|_W = \|\nabla \psi\|_{L^2(\Omega)^2}, \forall \psi \in W, \quad (45)$$

are equivalent on V and W , respectively, with the usual norm $\|\cdot\|_{H^1(\Omega)}$. By Sobolev’s trace theorem, we deduce that there exist two positive constants $c_V > 0$ and $c_W > 0$ such that

$$\|v\|_{L^2(\Gamma_3)} \leq c_V \|v\|_V, \forall v \in V, \tag{46}$$

$$\|v\|_{L^2(\Gamma_3)} \leq c_W \|\psi\|_W, \forall \psi \in W. \tag{47}$$

For a real Banach space $(X, \|\cdot\|_X)$, we use the usual notation for the spaces $L^p(0, T, X)$ and $W^{k,p}(0, T, X)$, where $1 \leq p \leq \infty, k = 1, 2, \dots$; we also denote by $C(0, T, X)$ and $C^1(0, T, X)$ the spaces of continuous and continuously differentiable functions on $[0, T]$ with values in X , with the respective norms

$$\|x\|_{C(0,T,X)} = \max_{t \in [0,T]} \|x\|_X,$$

and

$$\|x\|_{C^1(0,T,X)} = \max_{t \in [0,T]} \|x\|_X + \max_{t \in [0,T]} \|\dot{x}\|_X,$$

and we use the standard notations for the Lebesgue space $L^2(0, T, X)$ as well as the Sobolev space $W^{1,2}(0, T, X)$. In particular, recall that the norm on the space $L^2(0, T, X)$ is given by the formula

$$\|u\|_{L^2(0,T,X)}^2 = \int_0^T \|u(t)\|_X^2 dt,$$

and the norm on the space $W^{1,2}(0, T, X)$ is defined by the formula

$$\|u\|_{W^{1,2}(0,T,X)}^2 = \int_0^T \|u(t)\|_X^2 dt + \int_0^T \|\dot{u}(t)\|_X^2 dt.$$

In the study of Problem 2.1, we assume that the viscosity coefficient and the electric permittivity coefficient satisfy

$$\theta \in L^\infty(\Omega) \text{ and there } \theta^* > 0 \text{ such that } \theta(x) \geq \theta^* \text{ a.e } x \in \Omega, \tag{48}$$

$$\beta \in L^\infty(\Omega) \text{ and there } \beta^* > 0 \text{ such that } \beta(x) \geq \beta^* \text{ a.e } x \in \Omega. \tag{49}$$

We also assume that the Lamé coefficient and the piezoelectric coefficient satisfy

$$\mu \in L^\infty \text{ and } \mu(x) > 0, \text{ a.e } x \in \Omega, \tag{50}$$

$$e \in L^\infty. \tag{51}$$

The forces, tractions, volume and surface free charge densities have the regularity

$$f_0 \in W^{1,2}(0, T, L^2(\Omega)); f_2 \in W^{1,2}(0, T, L^2(\Gamma_2)), \tag{52}$$

$$q_0 \in W^{1,2}(0, T, L^2(\Omega)), \tag{53}$$

$$q_2 \in W^{1,2}(0, T, L^2(\Gamma_b)), q_2 = 0 \text{ a.e } x \in \Gamma_b. \tag{54}$$

The friction bound satisfies

$$\begin{cases} a) g : \Gamma_3 \times \mathbb{R} \longrightarrow \mathbb{R}^+ \\ b) \exists L_g > 0 \text{ such that } |g(x, r_1) - g(x, r_2)| \leq L_g |r_1 - r_2| \\ c) x \longrightarrow g(x, r) \text{ is Lebesgue measurable on } \Gamma_3 \forall r \in \mathbb{R} \\ d) \text{ the mapping } x \longrightarrow g(x, 0) \text{ belongs to } L^2(\Gamma_3), \end{cases} \tag{55}$$

the functional $j : v \times v \rightarrow \mathbb{R}$ is given by

$$j(\dot{u}, v) = \int_{\Gamma_3} g(|\dot{u}|)|v|da, \forall v \in V. \tag{56}$$

Let $\eta_1, \eta_2, v_1, v_2 \in V$, by using (55)-(56), we find that

$$|j(\eta_1, v_2) - j(\eta_1, v_1) + j(\eta_2, v_1) - j(\eta_2, v_2)| \leq L_g \|\eta_1 - \eta_2\|_{L^2(\Gamma_3)} \|v_1 - v_2\|_{L^2(\Gamma_3)},$$

and, keeping in mind (46), we obtain

$$j(\eta_1, v_2) - j(\eta_1, v_1) + j(\eta_2, v_1) - j(\eta_2, v_2) \leq c_V^2 L_g \|\eta_1 - \eta_2\|_V \|v_1 - v_2\|_V, \tag{57}$$

the initial displacement is such that

$$u_0 \in V. \tag{58}$$

We will use the functions $f : [0, T] \rightarrow V$ and $q : [0, T] \rightarrow W$ by

$$(f, v)_V = \int_{\Omega} f_0 v dx + \int_{\Gamma_2} f_2 v da, \forall v \in V, \tag{59}$$

$$(q, \psi)_V = \int_{\Gamma_b} q_2 \psi dx + \int_{\Omega} q_0 \psi da, \forall \psi \in W. \tag{60}$$

The definition of f and q are based on Riesz's representation theorem, moreover, it follows from assumptions (59)-(60) that the integrals above are well defined and

$$f \in W^{1,2}(0, T, V), \tag{61}$$

$$q \in W^{1,2}(0, T, W). \tag{62}$$

Next, we define the bilinear forms $a_\theta : V \times V \rightarrow \mathbb{R}$, $a_\mu : V \times V \rightarrow \mathbb{R}$, $a_e : V \times W \rightarrow \mathbb{R}$, $a_e : W \times V \rightarrow \mathbb{R}$, $a_\beta : W \times W \rightarrow \mathbb{R}$ by the equalities

$$a_\theta(u, v) = \int_{\Omega} \theta \nabla u \cdot \nabla v dx, \tag{63}$$

$$a_\mu(u, v) = \int_{\Omega} \mu \nabla u \cdot \nabla v dx, \tag{64}$$

$$a_e(u, \varphi) = \int_{\Omega} e \nabla \varphi \cdot \nabla v dx = a_e(\varphi, v), \tag{65}$$

$$a_\beta(\varphi, \psi) = \int_{\Omega} \beta \nabla \varphi \cdot \nabla \psi dx. \tag{66}$$

$$\tag{67}$$

Assumptions (48)-(51) imply that the integrals above are well defined and, when using (44)-(47), it follows that the forms a_θ, a_μ, a_e and a_β are continuous, moreover, the forms a_θ, a_μ and a_β are symmetric and, in addition, the form a_θ is V-elliptic since

$$a_\theta(u, v) \leq \|\theta\|_{L^\infty(\Omega)} \|u\|_V \|v\|_V \quad \forall u, v \in V, \tag{68}$$

$$a_\theta(v, v) \geq \theta^* \|v\|_V^2 \quad \forall v \in V. \tag{69}$$

The variational formulation of our problem is based on the following result.

Lemma 3.1 *If (u, φ) is a smooth solution to Problem 2.1, then $(u(t), \varphi(t)) \in X$ and*

$$a_\theta(\dot{u}(t), v - \dot{u}(t)) + a_\mu(u(t), v - \dot{u}(t)) + a_e(\varphi(t), v - \dot{u}(t)) + j(\dot{u}(t), v) - j(\dot{u}(t), \dot{u}(t)) \geq (f, v - \dot{u})_V, \forall v \in V, t \in [0, T], \quad (70)$$

$$a_\beta(\varphi, \psi) - a_e(u, \psi) = (q, \psi)_W, \forall \psi \in W, \quad (71)$$

$$u(0) = u_0. \quad (72)$$

Proof. Let (u, φ) denote a smooth solution to Problem 2.1, we have $u(t) \in V$, $\dot{u} \in V$ and $\varphi \in W$ a.e. $t \in [0, T]$ and let $v \in V$, $\psi \in W$, we multiply equations (36)-(37) by $(v - \dot{u}(t))$, ψ , integrate the result on Ω , and use Green's formula (36), and from (38)-(40), we get

$$\begin{aligned} \int_{\Omega} \theta \nabla \dot{u}(t) \cdot \nabla (v - \dot{u}(t)) dx + \int_{\Omega} \mu \nabla u(t) \cdot \nabla (v - \dot{u}(t)) dx + \int_{\Omega} e \nabla \varphi \cdot \nabla (v - \dot{u}(t)) dx + \\ \int_{\Gamma_3} g(|\dot{u}(t)|) |\dot{u}(t)| da - \int_{\Gamma_3} g(|\dot{u}(t)|) |v| da = \int_{\Omega} f_0(v - \dot{u}(t)) dx + \\ \int_{\Gamma_2} f_2(v - \dot{u}(t)) da \forall v \in V, t \in (0, T). \end{aligned} \quad (73)$$

Now, using (43), (59) and (63)-(65), we obtain (70) and (72), and from (41)-(42), we get

$$\begin{aligned} \int_{\Omega} \beta \nabla \varphi(t) \cdot \nabla \psi dx - \int_{\Omega} e \nabla u(t) \cdot \nabla \psi dx = \int_{\Omega} q_0(t) \psi dx - \\ \int_{\Gamma_b} q_2(t) \psi da, \forall \psi \in W, \forall t \in [0, T]. \end{aligned} \quad (74)$$

Using (60) and (66)-(68), we find (71). ■

Finally, the variational formulation of Problem (70)-(72) is given as follows.

Problem 3.1 Find a displacement field $u : [0, T] \rightarrow V$ and an electric potential field $\varphi : [0, T] \rightarrow W$ such that

$$a_\theta(\dot{u}(t), v - \dot{u}(t)) + a_\mu(u(t), v - \dot{u}(t)) + a_e(\varphi(t), v - \dot{u}(t)) + j(\dot{u}(t), v) - j(\dot{u}(t), \dot{u}(t)) \geq (f, v - \dot{u})_V, \forall v \in V, t \in [0, T], \quad (75)$$

$$a_\beta(\varphi, \psi) - a_e(u, \psi) = (q, \psi)_W, \forall \psi \in W, \quad (76)$$

$$u(0) = u_0. \quad (77)$$

We notice that the variational problem (75)-(77) is formulated in terms of a displacement field and electrical potential field. The existence of the unique solution to (75)-(77) is stated and proved in the next section.

4 Existence and Uniqueness of a Weak Solution

Theorem 4.1 *Assume (48)–(62), then there exists L_0 , which depends on $\Omega, \Gamma_1, \Gamma_2, \Gamma_3$, and if $L_g < L_0$, there exists a unique solution u to Problem 3.1 satisfying*

$$u \in W^{2,2}(0, T, V). \tag{78}$$

Proof of Theorem 4.1. The proof of Theorem 4.1 will be carried out in several steps.

First Step: We consider the following problem.

Problem 4.1 Find a displacement field $u : [0, T] \rightarrow V$ such that

$$a(u(t), v - \dot{u}(t)) + b(\dot{u}(t), v - \dot{u}(t)) + j(\dot{u}(t), v) - j(\dot{u}(t), \dot{u}(t)) \geq (F(t), v - \dot{u}(t))_V, \tag{79}$$

$$\forall v \in V, t \in [0, T],$$

$$u(0) = u_0. \tag{80}$$

In the study of the Cauchy problem (79)-(80), we assume that

$$\begin{cases} a : V \times V \rightarrow \mathbb{R} \text{ is a bilinear form and there exists } M > 0 \text{ such that} \\ |a(u, v)| \leq M \|u\|_V \|v\|_V, \forall u, v \in V. \end{cases} \tag{81}$$

$$\begin{cases} b : V \times V \rightarrow \mathbb{R} \text{ is a bilinear symmetric form and} \\ (a) \text{ there exists } M' > 0 \text{ such that } |b(u, v)| \leq M' \|u\|_V \|v\|_V, \forall u, v \in X, \\ (b) \text{ there exists } m' > 0 \text{ such that } b(v, v) \geq m' \|v\|_V^2 \forall v \in V, \end{cases} \tag{82}$$

$$\begin{cases} j : V \times V \rightarrow \mathbb{R} \text{ and} \\ a) \text{ for all } \eta \in V, j(\eta, \cdot) \text{ is convex and I.S.C. on } V, \\ b) \text{ there exists } \alpha \geq 0 \text{ such that} \\ |j(\eta_1, v_2) - j(\eta_1, v_1) + j(\eta_2, v_1) - j(\eta_2, v_2)| \leq \alpha \|\eta_1 - \eta_2\|_V \|v_1 - v_2\|_V, \end{cases} \tag{83}$$

$$\forall \eta_1, \eta_2, v_1, v_2 \in V, \tag{84}$$

$$u_0 \in V, \tag{84}$$

$$F \in W^{1,2}(0, T, V). \tag{85}$$

Under assumptions (81)–(85), we have the following result.

Lemma 4.1 *Assume that (81)-(85) hold, then if $m' > \alpha$, there exists a unique solution $u \in W^{1,2}(0, T, V)$ to problem (79)-(80).*

Proof. For any $t_1, t_2 \in [0, T]$, we use (79) and get

$$a(u(t_1), v - \dot{u}(t_1)) + b(\dot{u}(t_1), v - \dot{u}(t_1)) + j(\dot{u}(t_1), v) - j(\dot{u}(t_1), \dot{u}(t_1)) \geq (F(t_1), v - \dot{u}(t_1))_V, \forall v \in V, \tag{86}$$

$$a(u(t_2), v - \dot{u}(t_2)) + b(\dot{u}(t_2), v - \dot{u}(t_2)) + j(\dot{u}(t_2), v) - j(\dot{u}(t_2), \dot{u}(t_2)) \geq (F(t_2), v - \dot{u}(t_2))_V, \forall v \in V. \tag{87}$$

We take $v = \dot{u}(t_2)$ in the first inequality, and $v = \dot{u}(t_1)$ in the second one, and add the results to obtain

$$b(\dot{u}(t_1) - \dot{u}(t_2), \dot{u}(t_1) - \dot{u}(t_2)) + j(\dot{u}(t_1), \dot{u}(t_2)) - j(\dot{u}(t_1), \dot{u}(t_2)) + j(\dot{u}(t_2), \dot{u}(t_1)) - j(\dot{u}(t_2), \dot{u}(t_2)) \leq a(u(t_1) - u(t_2), \dot{u}(t_2) - \dot{u}(t_1)) + (F(t_1) - F(t_2), \dot{u}(t_2) - \dot{u}(t_1)). \quad (88)$$

We use now assumptions (81)-(83) to find

$$\|\dot{u}(t_1) - \dot{u}(t_2)\|_V \leq C(\|u(t_1) - u(t_2)\|_V + \|F(t_1) - F(t_2)\|_V), \quad (89)$$

where $C = \max\{\frac{M}{m'-\alpha}, \frac{1}{m'-\alpha}\}$. This inequality combined with the regularity $u \in C^1(0, t, V)$ shows that $\dot{u} : [0, T] \rightarrow V$ is an absolutely continuous function and, moreover,

$$\|\ddot{u}(t)\|_V \leq C(\|\dot{u}(t)\|_V + \|F(t)\|_V) \text{ a.e } t \in [0, T].$$

Finally, we conclude that $u \in W^{2,2}(0, T, V)$.

Second Step : Now, we prove the first inequality of Theorem 4.1.

Proof. From (76) we have

$$(\beta\varphi, \psi)_W - (eu, \varphi)_W = (q, \psi)_W, \quad (90)$$

the use of (90) gives that

$$\beta\varphi(t) = eu(t) + q,$$

hence

$$\varphi(t) = \frac{e}{\beta}u(t) + \frac{q}{\beta}. \quad (91)$$

Now, we take (91) and substitute in (75), we get

$$\begin{aligned} a_\theta(\dot{u}(t), v - \dot{u}(t)) + a_\mu(u(t), v - \dot{u}(t)) + a_e\left(\frac{e}{\beta}u(t), v - \dot{u}(t)\right) + j(\dot{u}(t), v) - j(\dot{u}(t), \dot{u}(t)) \\ \geq (f(t) - \beta^{-1}q, v - \dot{u})_V, \forall v \in V, t \in [0, T], \end{aligned} \quad (92)$$

$$u(0) = u_0. \quad (93)$$

Next, we define the bilinear forms $a : V \times V \rightarrow \mathbb{R}$, $b : V \times V \rightarrow \mathbb{R}$ by

$$a(u(t), v - \dot{u}(t)) = a_\mu(u(t), v - \dot{u}(t)) + a_e\left(\frac{e}{\beta}u(t), v - \dot{u}(t)\right), \quad (94)$$

$$b(\dot{u}(t), v - \dot{u}(t)) = a_\theta(\dot{u}(t), v - \dot{u}(t)), \quad (95)$$

and define the function $F : [0, T] \rightarrow V$ by

$$(F(t), v - \dot{u})_V = (f(t) - \beta^{-1}q, v - \dot{u})_V. \quad (96)$$

The bilinear form $a(\cdot, \cdot)$ and the initial data u_0 satisfy conditions (81) and (84). The regularity $f \in W^{1,2}(0, T, V)$ and $q \in W^{1,2}(0, T, W)$ combined with the definition of $F(\cdot)$

in (96), satisfy (85).

Now, for all $\eta \in V$, the functional $j(\eta, \cdot) : V \rightarrow \mathbb{R}$ is a continuous seminorm on V and therefore it satisfies condition (83)(a). Recall also that j satisfies inequality (57), which shows that condition (83)(b) holds with $\alpha = c_V L_g$.

From (68), the bilinear form b satisfies condition (83) with $m' = \theta^*$.

Choose $L_0 = \frac{\theta^*}{c_V^2}$, which depends on $\Omega, \Gamma_1, \Gamma_2, \Gamma_3$, and θ . Then, if $L_g < L_0$, we have $m' > \alpha$, and therefore the first inequality in Theorem 4.1 is a direct consequence of Lemma 3.1.

Theorem 4.2 *Assume (48)-(62) and if $L_g < L_0$, there exists a unique solution (u, φ) to Problem 3.1 satisfying*

$$\varphi \in W^{1,2}(0, T, W). \quad (97)$$

In this step, we prove the second inequality cited in Theorem 4.2.

Proof. Let $u \in W^{2,2}(0, T, V)$ be the solution of problem (77)-(97) and let $\varphi : [0, T] \rightarrow W$ be the electrical potential field defined by (91). Notice that the regularity $u \in W^{2,2}(0, T, V)$ and $q \in W^{1,2}(0, T, W)$ imply that $\varphi \in W^{1,2}(0, T, W)$.

Conclusion

We presented a model for an antiplane contact problem for electro-viscoelastic materials with two variables, i.e., a time-dependent variational equation for the potential field, where the time t is in $[0, T]$. The problem was set as a variational inequality for the displacements and a variational equality for the electric potential. The existence of a unique weak solution for the problem was established by using arguments from the theory of evolutionary variational inequalities and a fixed-point theorem.

Acknowledgment

We would like to thank Reviewers for taking the necessary time and effort to review the manuscript. We sincerely appreciate all your valuable comments and suggestions, which helped us in improving the quality of the manuscript. Finally, I wanted to express my gratitude to Dr. A. ZAROOR and Dr. R. FAIZI for their help and support. Thank you for taking the time to carefully edit my work to make it enjoyable to read.

References

- [1] R. C. Batra and J. S. Yang. Saint-Venant's principle in linear piezoelectricity. *J. Elasticity* **38** (2009) 209–218.
- [2] T. Ikeda. *Fundamentals of Piezoelectricity*. Oxford Univ. Press, Oxford, 1990.
- [3] V. Z. Patron and B. A. Kudryavtsev. *Electromagnetoelasticity, Piezoelectrics and Electrically Conductive Solids*. Gordon Breach, London, 1988.
- [4] W. Han and M. Sofonea. *Quasistatic Contact Problems in Viscoelasticity and Viscoplasticity*. Studies in Advanced Mathematics, Americal Mathematical Society, Providence, RI–International Press, Somerville, MA, **30**, 2002.

- [5] A. Matei, V. V. Motreanu and M. Sofonea. A quasistatic antiplane contact problem with slip dependent friction. *Adv. Nonlinear Var. Inequal.* **4** (2001) 1–21.
- [6] M. Sofonea and A. Mate. *Variational Inequalities with Applications, A Study of Antiplane Frictional Contact Problems*. Springer Macmillan, New York, 2009.
- [7] A. Borrelli, C. O. Horgan and M. C. Patria. Saint-Venant’s principle for antiplane shear deformations of linear piezoelectric materials. *SIAM J. Appl. Math.* **62** (2002) 2027–2044.
- [8] C. O. Horgan. Anti-plane shear deformation in linear and nonlinear solid mechanics. *SIAM Rev.* **37** (1995) 53–81.
- [9] C. O. Horgan. Recent developments concerning Saint-Venant’s principle: a second update. *Appl. Mech. Rev.* **49** (1996) 101–111.
- [10] C. O. Horgan and K. L. Miller. Anti-plane shear deformation for homogeneous and inhomogeneous anisotropic linearly elastic solids. *J. Appl. Mech.* **61** (1994) 23–29.
- [11] C. O. Horgan and G. Saccomandi. Superposition of generalized plane strain on antiplane shear deformation in isotropic incompressible hyperelastic materials. *J. Elast.* **73** (2003) 221–235.
- [12] M. Dalah. Analysis of elctro-viscelstic antiplane contact probleme with total slip rate dependent friction. *Electronic Journal of Differential Equations* **118** (2009) 1–15.
- [13] M. Sofonea and M. Dalah. Antiplane Frictional Contact of Electro-Viscoelastic Cylinders. *Electronic Journal of Differential Equations* **161** (2027) 1–14.
- [14] M. Sofonea, M. Dalah and A. Ayadi. Analysis of an antiplane electro-elastic contact problem. *Adv. Math. Sci. Appl.* **17** (2007) 385–400.



Trajectory Estimation of Amphibious Aircraft Using H -Infinity and Ensemble Kalman Filter Methods

T. Herlambang¹, S. Syamsuar², F. Yudianto³, A. Basuki³,
G. Wijiatmoko³, A. Roschyntawati², H. Hendrato², K. Oktafianto⁴
and R. S. Marjianto^{5*}

¹ *Department of Information Systems, Universitas Nahdlatul Ulama Surabaya, Indonesia.*

² *Transportation Technology Research Center, Energy and Manufacturing Research Organization, National Research and Innovation Agency, Indonesia.*

³ *Laboratory of Aerodynamics, Aeroelastics and Aeroacoustics, National Research and Innovation Agency, Indonesia.*

⁴ *Department of Mathematics, University of PGRI Ronggolawe, Indonesia.*

⁵ *Departement of Engineering, Faculty of Vocational Studies, Universitas Airlangga, Indonesia.*

Received: August 19, 2023; Revised: April 20, 2024

Abstract: An amphibious aircraft is an aircraft that has the ability to operate from a runway like a conventional aircraft or from shallow water. Such type of aircraft is widely used for tourist transportation, taking tourists to areas only reachable by water. It is not uncommon for amphibious aircraft to be used as rescue and forest fire fighting tools. The need for amphibious aircraft is in line with the development of navigation and guidance systems required by such amphibious aircraft. Navigation and motion control systems for amphibious aircraft refer to technologies and systems allowing aircraft to operate in the air and also sail on the water surface. Amphibious aircrafts are designed to have capabilities that allow them to take off and land on conventional runways and to operate to and from water area. Several navigation guidance methods in the field of robotics can also be used, one of which is for amphibious aircraft position estimation. The accuracy of aircraft position estimation is very important to ensure that the amphibious aircraft follows the specified trajectory accurately. The estimation methods used in this paper are the H -infinity and Ensemble Kalman Filter (EnKF). This study compared the numerical simulation results of the two methods, EnKF and H -infinity, aiming to estimate the position of the amphibious aircraft by generating 300 and 600 ensembles, and the simulation results with 800 ensembles had the best accuracy of about 95-98%.

Keywords: *amphibious aircraft; trajectory estimation; H -infinity and Ensemble Kalman Filter methods.*

Mathematics Subject Classification (2010): 93E10, 62F10.

* Corresponding author: <mailto:rachmansinatriya@vokasi.unair.ac.id>

1 Introduction

An amphibious aircraft is a fixed-wing aircraft able to take off and land on solid ground and water. Its history dates back to World War II when, especially in the Pacific, the Allies needed search and rescue aircrafts to rescue airmen adrift at sea after their aircrafts were shot down by the enemy. An amphibious aircraft is an aircraft able to operate from a runway like a conventional aircraft or from shallow water [1]. Such type of aircraft is widely used for tourist transportation, taking tourists to areas only reachable by water [2].

In addition, that type of aircraft is needed for logistics transportation in remote areas having no airstrips. In fact, in the past, it could also be used as a naval reconnaissance aircraft due to its range. At that time the most famous amphibious aircrafts were the PBY Catalina and the Grumman HU 16 Albatross. After the end of WWII, these aircrafts were still widely used until around the 1960s, in both civilian and military environments. Some of them with excellent maintenance and modifications are still widely used in the United States, especially as a forest firefighting fleet.

An amphibious aircraft requires a technology of navigation and guidance systems, of which the navigation system is a system that directs the position of the amphibious aircraft to follow a predetermined trajectory and as much as possible has a fairly high accuracy [3]. Navigation and motion control systems for amphibious aircraft refer to technologies and systems allowing an aircraft to operate in the air and also sail on the water surface [4]. Amphibious aircrafts are designed to have amphibious capabilities that allow them to take off and land on conventional runways and operate to and from water areas. Several navigation guidance methods in the field of robotics can also be used, one of which is for amphibious aircraft position estimation. The accuracy of aircraft position estimation is very important to ensure that the amphibious aircraft follows the specified trajectory accurately.

One of the estimation methods having a small error is the Ensemble Kalman Filter method, which is very reliable for a nonlinear model. The EnKF method is often used for motion and position estimation of AUVs [5], [6], [7], mobile robots [8], and missiles [9]. Given that the EnKF method is a reliable estimation method, in this study, two methods are applied, that is, the EnKF method and the H -infinity method. This study compared the numerical simulation results of the two methods, the EnKF and H -infinity, with the aim of estimating the position of the amphibious aircraft by generating 300 and 600 ensembles.

2 Amphibious Aircraft Model

The forces working on an unmanned amphibious aircraft can be categorized into the aircraft mass, hydrodynamic forces, aerodynamic forces and engine thrust as shown in Fig 1. The nonlinear longitudinal dynamic motion model of the unmanned amphibious aircraft is represented by the following equations.

In the earth coordinate system $X_e; Y_e; Z_e$, then the aircraft body coordinate system $X_b; Y_b; Z_b$ and the steady-translation coordinate system $X_s; Y_s; Z_s$:

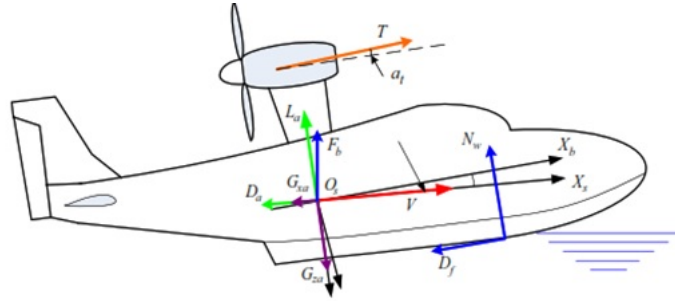


Figure 1: Forces working on amphibious aircraft [4].

$$\begin{aligned}
 m\dot{V} &= T \cos(\alpha + \alpha_t) - D_a - N_w \sin \alpha - D_f \cos \alpha + G_{xa}, \\
 mV\dot{\alpha} &= mVq - T \sin(\alpha + \alpha_t) - L_a - N_w \cos \alpha + D_f \sin \alpha + G_{za}, \\
 I_y\dot{q} &= M_a + M_w + M_T, \\
 \dot{\theta} &= q, \\
 \dot{x}_g &= u \cos \theta + w \sin \theta, \\
 \dot{z}_g &= -u \sin \theta + w \cos \theta.
 \end{aligned}$$

3 Ensemble Kalman Filter Algorithm

Below is the algorithm flow of the Ensemble Kalman Filter method.

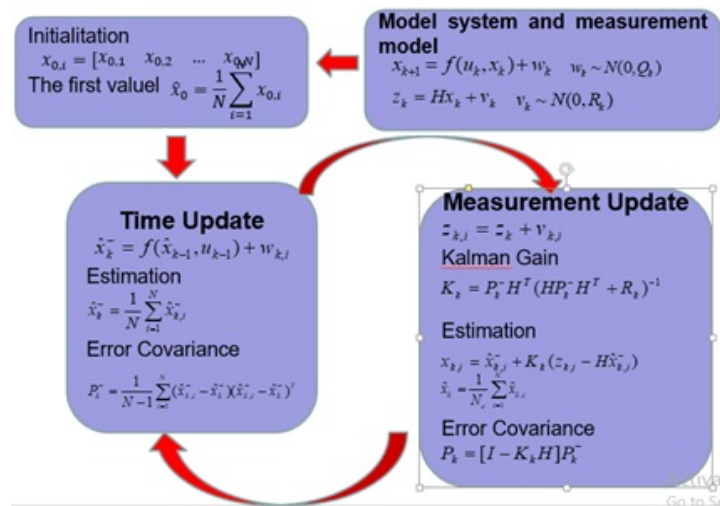


Figure 2: Ensemble Kalman Filter Algorithm [9], [10], [11].

α	Angle of attack	m	Amphibious aircraft mass
θ	Angle of pitch	D_a	Aerodynamic drag force
V	Velocity	G_{xa}	gravity along X_s
α_t	Angle between engine force and X_b	G_{za}	gravity along Z_s
M_a	Total pitching moment of Air	X_g	aircraft position along X_e
M_w	Total pitching moment of Air	Z_g	aircraft position along Z_e
M_T	Total pitching moment of Engine	u	velocity component of aircraft velocity along X_b
T	Engine thrust	w	velocity component of aircraft along Z_b
N_w	Normal directional water pressure at the bottom of the aircraft	q	Pitch angular rate
D_f	Frictional force of water along the bottom of the aircraft	I_y	moment of Inertia of amphibious aircraft against Y_b
L_a	Aerodynamic lifting force	$\dot{\theta}$	Increase/decrease in angle of pitch
\dot{V}	Increase/decrease in velocity	$\dot{\alpha}$	Increase/decrease in angle of attack

Table 1: Description of amphibious aircraft model [4].

4 H -Infinity Algorithm

Below is the algorithm flow of the H -infinity method.

5 Simulation Results

In this paper, we compared the accuracy of simulation results, the resulted accuracy of the H -infinity method to that of the EnKF method by generating 300 and 600 ensembles. The simulation results are as shown in Figures 4-6, each figure represents the simulation results by the H -infinity and EnKF methods with 300 and 600 ensembles generated. And the errors of the simulation results are as compared in Table 2. In each figure, there are two images, that is, a and b, the image a means the simulation result by using 600 ensembles, and the image b means that by using 300 ensembles.

As seen in Figure 4, the red line is the real value of the horizontal position determined for a flight at a certain distance from the initial position of the amphibious aircraft so that the amphibious aircraft flies as high as 1400 m from the surface and advances about 2250 meters from the original place, so the position will always advance to 2250 m at the 100th iteration either by the H -Infinity method or by EnKF method. The horizontal position is closely related to the altitude at which when the horizontal position advances (does not turn), the altitude will follow the horizontal position to get the maximum flight

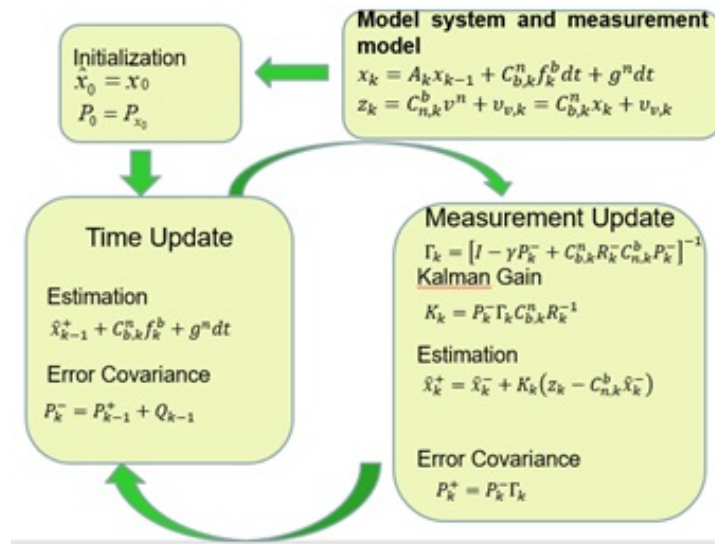


Figure 3: *H*-Infinity Algorithm [12], [11], [14].

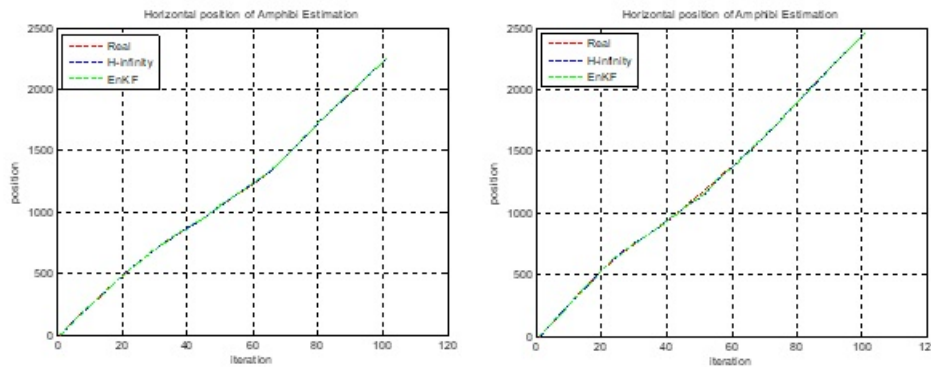


Figure 4: Horizontal position estimation of amphibious aircraft by the *H*-Infinity and EnKF methods, a) with 600 ensembles and b) with 300 ensembles.

altitude. In Figures 4 and 5, it can also be seen that the difference between the distance by *H*-infinity and that by EnKF is almost the same as the real value and the RMSE value is quite large, this can be seen in Table 2.

In Figure 5, it can be seen that the red line is the real value of the flight altitude determined for the amphibious aircraft in order to follow the predetermined trajectory. In this case, the height of the amphibious aircraft represents the maximum height the amphibious aircraft can pass, and the simulation is made for the amphibious aircraft to fly only and not to land again.

In Figure 6, it can be seen that the red line is the real horizontal position and the specified altitude that the amphibious aircraft will pass through while flying at a certain

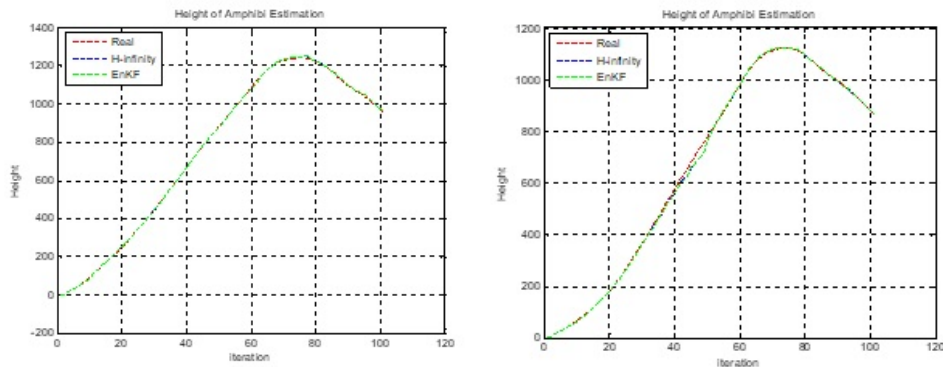


Figure 5: Height estimation of amphibious aircraft by the H -Infinity and EnKF methods, a) with 600 ensembles and b) with 300 ensembles.

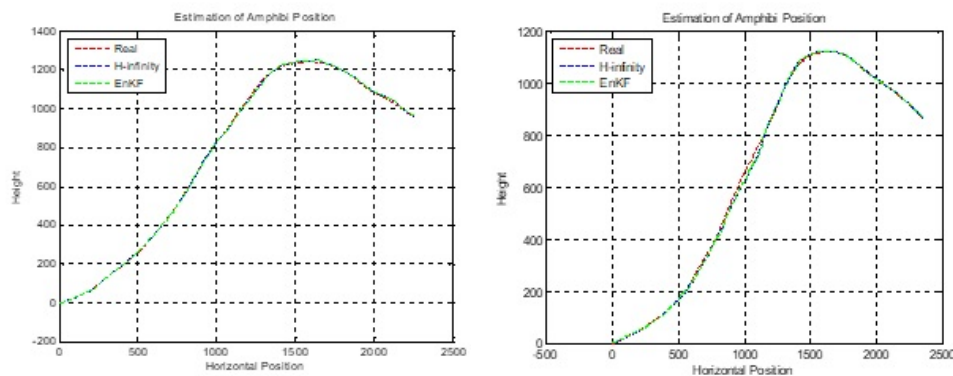


Figure 6: Position estimation of the amphibious aircraft on the predetermined trajectory by the H -Infinity and EnKF methods, a) with 600 ensembles and b) with 300 ensembles.

altitude and distance, of which Figure 6a has better accuracy than Figure 6b using 300 ensembles. Figure 6 shows that the amphibious aircraft follows the predetermined trajectory from the beginning of takeoff up to flying at a certain altitude. Table 2 also shows that the EnKF method has a smaller error than the H -infinity method.

	EnKF with 300 ensembles	H -infinity	EnKF with 600 ensembles	H -infinity
XY Motion	3.57%	4.79%	2.14%	4.56%
Time Simulation	8.45 s	7.5 s	14.73 s	12.89 s

Table 2: Comparison of the position estimation error of amphibious aircraft by the H -infinity and EnKF methods.

As shown in Table 2, these simulation results can be compared each other. If we look at the comparison based on the accuracy of the methods, then the EnKF method

has higher accuracy than the H -infinity, but it has a longer simulation time. If we look at the comparison based on the number of ensembles, then the generation of 600 ensembles indicates better accuracy than that of 300 ensembles. Overall, the EnKF method by generating 600 ensembles has the highest accuracy. In this case, both estimation methods, namely H -infinity and EnKF, have an accuracy of above 95%, so the estimation methods can be effectively used to estimate the motion of the amphibious aircraft.

6 Conclusion

Based on the results of the analysis of the two simulations above, it can be concluded that the EnKF method by generating 600 ensembles has the highest level of accuracy. If we look at the comparison based on the number of ensembles, then that with 600 ensembles has a better accuracy than that with 300 ensembles. Thus, both estimation methods, namely H -infinity and EnKF, have an accuracy of above 95%, so that the estimation methods can be effectively used to estimate the motion of amphibious aircraft.

Acknowledgment

High appreciation to the BRIN for the very fund support for the research conducted in the year of 2022 with contract number B-802/II.7.5/FR/6/2022, B-9106/III-3/KS.00.00/9/2022 and B-4563/III-3/KU.07.01/7/2022.

References

- [1] K. Ito, T. Dhaene, Y. Hirakawa, T. Hirayama and T. Sakurai. Longitudinal Stability Augmentation of Seaplanes in Planing. *Journal of Aircraft* (2016) 1–19.
- [2] L. Wang, H. Yin, K. Yang, H. Liu and J. Zhu. Water take off performance calculation method for amphibious aircraft based on digital virtual flight. *Chinese Journal of Aeronautics* **33** (12) (2020) 3082–3091.
- [3] X. Li, X. Wei, Y. Wang, and Q. Yin. Tracking deviation correction control for landing taxiing of amphibious unmanned aerial vehicles. *Aerospace Science and Technology* **116** (2021) 106863.
- [4] H. Du, G. Fan, and J. Yi. Autonomous takeoff control system design for unmanned seaplanes. *Ocean Engineering* **85** (2014) 21–31.
- [5] S. Subchan, T. Herlambang and H. Nurhadi. UNUSAITs AUV Navigation and Guidance System with Nonlinear Modeling Motion Using Ensemble Kalman Filter. In: *Proc. International Conference on Advanced Mechatronics, Intelligent Manufacture, and Industrial Automation (ICAMIMIA)* Malang, Indonesia, 2019.
- [6] T. Herlambang, S. Subchan and H. Nurhadi. Navigation and Guidance Control System of UNUSAITs AUV Based on Dynamical System Using Ensemble Kalman Filter Square Root. In: *Proc. The Third International Conference on Combinatorics, Graph Theory and Network Topology* Jember, Indonesia, 2019.
- [7] H. Nurhadi, T. Herlambang and D. Adzkiya. Design of Sliding Mode Control for Surge, Heave and Pitch Motion Control of UNUSAITs AUV. In: *Proc. International Conference on Mechanical Engineering*, 2019.
- [8] T. Herlambang, F. A. Susanto, D. Adzkiya, A. Suryowinoto and K. Oktafianto. Design of Navigation and Guidance Control System of Mobile Robot with Position Estimation Using Ensemble Kalman Filter (EnKF) and Square Root Ensemble Kalman Filter (SR-EnKF). *Nonlinear Dynamics and Systems Theory* **22** (4) (2022) 390–399.

- [9] T. Herlambang. Design of a Navigation and Guidance System of Missile with Trajectory Estimation Using Ensemble Kalman Filter Square Root (EnKF-SR). In: *Proc. International Conference on Computer Applications and Information Processing Technology (CAIPT)* Bali, Indonesia, 2019, 8–10.
- [10] A. Muhith, T. Herlambang, D. Rahmalia, I. Irhamah and M. Y. Anshori. Estimation of Fresh Frozen Plasma Blood in PMI Gresik using Ensemble and Extended Kalman Filter. In: *Proc. 1st International Conference on Neuroscience and Learning Technology (ICON-SATIN)* Jember, Indonesia, 2021.
- [11] T. Herlambang, A. Muhith, D. Rahmalia and H. Nurhadi. Motion Optimization using Modified Kalman Filter for Invers-Kinematics based Multi DOF Arm Robot. *International Journal of Control and Automation* **13** (2s) (2020) 66–71.
- [12] T. Herlambang, H. Nurhadi, A. Muhith, A. Suryowinoto and K. Oktafianto. Estimation of Forefinger Motion with Multi-DOF Using Advanced Kalman Filter. *Nonlinear Dynamics and Systems Theory* **23** (1) (2023) 24–33.
- [13] T. Herlambang, A. Muhith, I. Irhamah, M. Y. Anshori, D. Rahmalia, and D. F. Karya. Implementation of H -infinity and Ensemble Kalman Filter for Whole Blood (WB) Estimation in PMI Bojonegoro. In: *AIP Conference Proceedings 2577, 020019; Proceedings of the 6th National Conference on Mathematics and Mathematics Education*, 2022.
- [14] M. Y. Anshori, T. Herlambang, P. Katias, F. A. Susanto, and R. R. Rasyid. Profitability estimation of XYZ company using H -infinity and Ensemble Kalman Filter. In: *The 5th International Conference of Combinatorics, Graph Theory, and Network Topology (ICCGANT)* Jember, Indonesia, 2021.



Numerical Solution for Benjamin-Bona-Mahony-Burgers Equation Using Septic B-Spline Galerkin Method

Ali M. Jasim¹, Adham A. Ali^{2*}, Isam H. Halil¹, Fatima Z. Ahmed¹
and Muhannad A. Shallal¹

¹ *Department of Mathematics, College of Science, University of Kirkuk, Kirkuk, Iraq.*

² *Department of Software, College of Computer Science and Information Technology,
University of Kirkuk, Kirkuk, Iraq.*

Received: August 31, 2023; Revised: April 25, 2024

Abstract: In this research, a numerical solution to the Benjamin-Bona-Mahony-Burger (BBMB) equation utilizing septic B-spline Galerkin method has been proposed. The accuracy of the method has been tested by evaluating L_2 and L_∞ error norms. Furthermore, the obtained numerical results are compared with those available in the literature. Finally, some graphical representations have been presented to show the method efficiency.

Keywords: *partial differential equations (PDEs); Benjamin-Bona-Mahony-Burger (BBMB) equation; B-spline Galerkin method.*

Mathematics Subject Classification (2010): 70K25, 70K40, 93Axx.

1 Introduction

Many phenomena in applied sciences such as engineering, physics, and chemistry can be described through mathematical models. Partial differential equations (PDEs) can be considered one of the most important of these models [1], [2]. The Benjamin-Bona-Mahoney-Burger (BBMB) equation is one of the fundamental types of nonlinear dispersive equations that has occurred in various areas of applied mathematics [3], [4]. The BBMB equation is a mathematical model proposed in [5] to study the unidirectional long wave motion with small amplitudes. The BBMB equation represents the mathematical

* Corresponding author: <mailto:adham.ali@uokirkuk.edu.iq>

model of propagation of small amplitude long waves in the nonlinear dispersive media along with the dissipation, which is alternate to the Korteweg-de Vries equation [6]. This equation incorporates nonlinearity as well as the dispersive and the dissipative effects. The terms u_{xx} and u_{xxt} represent the dissipative and the dispersive effects of the equation, respectively. This equation is used in a number of branches of science and engineering. Many studies have been conducted to find the exact solution to the BBMB equation, such as, the homotopy analysis method [7], the exp-function method [8], the multipliers method [9], (see also [10], [11], [12], [13], [14]). In this research paper, the septic B-spline Galerkin method is used to solve the one-dimensional BBMB equation numerically. Several authors have investigated the numerical solution of the BBMB equation, for example, finite difference method [15, 16], domain decomposition technique [17], [18], [19], cubic spline collocation method [20], finite element method [21], [22], [23], Crank–Nicolson-type finite difference methods [24], [25], [26], [27], and B-spline quadratic finite element method [28]. In this research paper, in Section 2, the septic B-spline Galerkin method has been applied to the BBMB equation. In Section 3, two examples are solved using the proposed method, and the accuracy of the method has been tested by comparing the obtained numerical solutions with the exact solutions and with the methods existing in the literature. Finally, a summary of the main conclusions is presented in Section 4.

2 Septic B-spline Galerkin Method

The BBMB equation is defined as

$$v_t - v_{xxt} - \alpha v_{xx} + \beta v_x + vv_x = 0, \quad c \leq x \leq d, \quad t > 0. \quad (1)$$

The boundary conditions are given as

$$\begin{aligned} v(c, t) = v(d, t) = 0, \quad v_x(c, t) = v_x(d, t) = 0, \\ v_{xx}(c, t) = v_{xx}(d, t) = 0, \quad v_{xxx}(c, t) = v_{xxx}(d, t) = 0, \quad t > 0. \end{aligned} \quad (2)$$

and the initial condition is

$$v(x, 0) = f(x), \quad x \in [c, d]. \quad (3)$$

Applying the Galerkin technique to (1) with the test functions ψ yields

$$\int_0^h \psi (u_t - u_{xxt} - \alpha u_{xx} + \beta u_x + uu_x) dx = 0. \quad (4)$$

Therefore, we have

$$\int_0^h (\psi u_t + \psi_x u_{xt} + \alpha \psi_x u_x + \beta \psi u_x + \psi uu_x) dx = 0. \quad (5)$$

The approximating solution is defined as follows:

$$\begin{aligned} u_n(x, t) &= \sum_{p=-3}^{n+3} \delta_p(t) H_p(x), \\ \psi(x) &= H_p(x), \quad p = -3, \dots, n+3, \end{aligned} \quad (6)$$

where H_p is the septic B-spline function:

$$H_p(z) = \frac{1}{h^7} \begin{cases} (z - z_{p-4})^7 & z \in [z_{p-4}, z_{p-3}] \\ (z - z_{p-4})^7 - 8(z - z_{p-3})^7 & z \in [z_{p-3}, z_{p-2}] \\ (z - z_{p-4})^7 - 8(z - z_{p-3})^7 + 28(z - z_{p-2})^7 & z \in [z_{p-2}, z_{p-1}] \\ (z - z_{p-4})^7 - 8(z - z_{p-3})^7 + 28(z - z_{p-2})^7 - 56(z - z_{p-1})^7 & z \in [z_{p-1}, z_p] \\ (z_{p+4} - z)^7 - 8(z_{p+3} - z)^7 + 28(z_{p+2} - z)^7 - 56(z_{p+1} - z)^7 & z \in [z_p, z_{p+1}] \\ (z_{p+4} - z)^7 - 8(z_{p+3} - z)^7 + 28(z_{p+2} - z)^7 & z \in [z_{p+1}, z_{p+2}] \\ (z_{p+4} - z)^7 - 8(z_{p+3} - z)^7 & z \in [z_{p+2}, z_{p+3}] \\ (z_{p+4} - z)^7 & z \in [z_{p+2}, z_{p+3}] \\ 0 & otherwise. \end{cases} \tag{7}$$

When using the equation as $h\mu = z - z_p$, the septic B-splines (7) in terms of the variable μ over $[0, 1]$ can be given as follows:

$$\begin{aligned} H_{p-3}(z) &= 1 - 7\mu + 21\mu^2 - 35\mu^3 + 35\mu^4 - 21\mu^5 + 7\mu^6 - \mu^7, \\ H_{p-2}(z) &= 120 - 392\mu + 504\mu^2 - 280\mu^3 + 84\mu^5 - 42\mu^6 + 7\mu^7, \\ H_{p-1}(z) &= 1191 - 1715\mu + 315\mu^2 + 665\mu^3 - 315\mu^4 - 105\mu^5 + 105\mu^6 - 21\mu^7, \\ H_p(z) &= 2416 - 1680\mu + 560\mu^4 - 140\mu^6 + 35\mu^7, \\ H_{p+1}(z) &= 1191 + 1715\mu + 315\mu^2 - 665\mu^3 - 315\mu^4 + 105\mu^5 + 105\mu^6 - 35\mu^7, \\ H_{p+2}(z) &= 120 + 392\mu + 504\mu^2 + 280\mu^3 - 84\mu^5 - 42\mu^6 + 21\mu^7, \\ H_{p+3}(z) &= 1 + 7\mu + 21\mu^2 + 35\mu^3 + 35\mu^4 + 21\mu^5 + 7\mu^6 - 7\mu^7, \\ H_{p+4}(z) &= \mu^7. \end{aligned} \tag{8}$$

Therefore, the approximate solution (6) is reduced over the element $[x_p, x_{p+1}]$ to the following form:

$$v_n^e = \sum_{i=p-3}^{p+4} \delta_i(t) H_i(x). \tag{9}$$

Substituting Eq.(9) into (5), we obtain

$$\begin{aligned} \sum_{j=p-3}^{p+4} \int_0^1 H_i H_j \dot{\delta}_j d\mu + \sum_{j=p-3}^{p+4} \int_0^1 H_i H_j' \dot{\delta}_j d\mu + \alpha \sum_{j=p-3}^{p+4} \int_0^1 H_i H_j' \delta_j d\mu + \\ \beta \sum_{j=p-3}^{p+4} \int_0^1 H_i H_j' \delta_j d\mu + \sum_{j=p-3}^{p+4} \sum_{k=p-3}^{p+4} \int_0^1 H_i H_j H_k' \delta_k \delta_j d\mu = 0, \quad p = 0, 1, \dots, n - 1. \end{aligned} \tag{10}$$

Here, "•" refers to the derivative with respect to time. Rewrite (10) in a matrix form

$$A^e \dot{\delta}^e + B^e \dot{\delta}^e + \alpha B^e \delta^e + \beta C^e \delta^e + D^e (\delta^e)^T \delta^e = 0, \tag{11}$$

where

$$A_{i,j}^e = \int_0^1 H_i H_j d\mu, \quad B_{i,j}^e = \int_0^1 H_i H_j' d\mu, \quad C_{i,j}^e = \int_0^1 H_i H_j' d\mu, \quad D_{i,j,k}^e = \int_0^1 H_i H_j H_k' d\mu.$$

The matrices $A_{ij}^e, B_{ij}^e, C_{ij}^e$ are matrices of 8×8 , and the matrix D is $8 \times 8 \times 8$. The matrix D is designed to be in the form of 8×8 as

$$E_{i,j}^e = \sum_{k=p-3}^{p+4} D_{ijk} \delta_k. \tag{12}$$

Thus Eq.(11) becomes

$$(A^e + B^e) \dot{\delta}^e + (\alpha B^e + \beta C^e + E^e) \delta^e = 0. \tag{13}$$

Assembling the element matrix (13), we get

$$(A + B) \dot{\delta} + (\alpha B + \beta C + E) \delta = 0, \tag{14}$$

where A, B, C, E are obtained from the element matrices A^e, B^e, C^e, E^e , respectively. Applying the forward finite difference formula, $\delta = \frac{\delta^{n+1} - \delta^n}{\Delta t}$, with the Crank-Nicolson scheme $\delta = \frac{\delta^{n+1} + \delta^n}{2}$ to Eq.(14), we obtain

$$[2A + (2 + \alpha\Delta t)B + \Delta t(\beta C + E)] \delta^{n+1} = [2A + (2 - \alpha\Delta t)B - \Delta t(\beta C + E)] \delta^n. \quad (15)$$

3 Numerical Examples

In this section, we explain the effectiveness of the proposed method through two examples. The results have been tested using the error norms

$$L_2 = \|v^{exact} - v^{num}\|_2 = \sqrt{h \sum_{j=0}^N |v_j^{exact} - v_j^{num}|^2}, \quad L_\infty = \max_j |v_j^{exact} - v_j^{num}|.$$

Example 1

Take equation (1) at $\alpha = \beta = 1$, with the following initial condition:

$$v(x, 0) = \sin(x).$$

The exact solution is given by

$$v(x, t) = e^{-t} \sin(x).$$

The boundary conditions are chosen from the exact solution. The obtained results are compared with the exact solution by evaluating L_2 and L_∞ error norms at different values of time. Moreover, the results are compared with the results in [15] [23], which are shown in Table 1. In Figures 1 and 2, we plotted the exact and numerical solutions of Example 1, and it turns out that the two plots are very close to each other.

	T	L_2	L_∞
The proposed method	1	3.02235×10^{-7}	1.811223×10^{-10}
	2	5.9976×10^{-7}	4.55663×10^{-10}
	5	9.5589×10^{-7}	2.996753×10^{-9}
	10	1.86532×10^{-6}	8.76521×10^{-9}
[15]	1	2.976712×10^{-6}	1.906127×10^{-9}
	2	4.675453×10^{-6}	3.745931×10^{-9}
	5	1.876409×10^{-5}	2.996753×10^{-8}
	10	2.318245×10^{-5}	4.906127×10^{-8}
[23]	1	4.238861×10^{-3}	8.732152×10^{-4}
	2	2.74893×10^{-3}	4.720312×10^{-4}
	5	1.009326×10^{-2}	3.258217×10^{-3}
	10	3.112871×10^{-2}	2.531897×10^{-3}

Table 1: Errors between the numerical and exact solutions in Example 1, at different times.

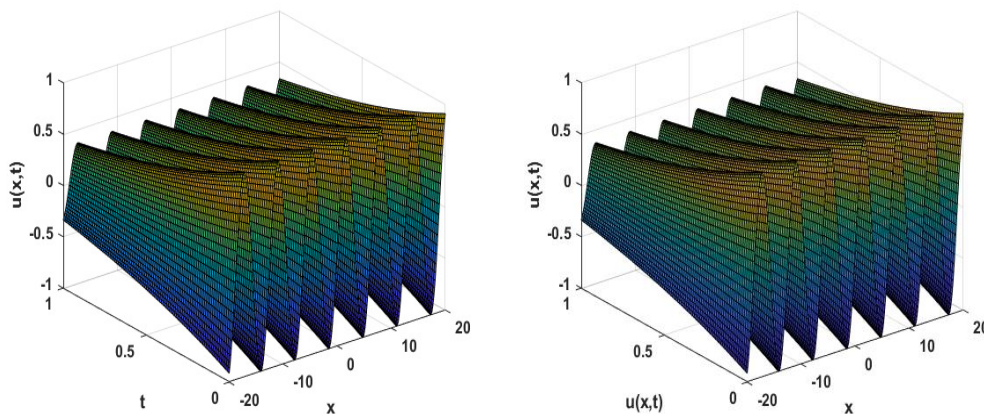


Figure 1: Numerical and exact solutions in Example 1 at $-20 \leq x \leq 20$, and $0 \leq t \leq 1$. Left: Exact solution; right: Numerical solution.

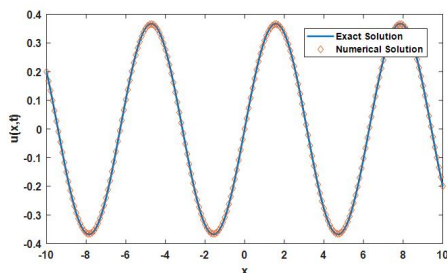


Figure 2: Comparison between the exact and approximate solution in Example 1 at $t = 1$.

Example 2

Take equation (1) at $\alpha = 0$, $\beta = 1$, the initial condition is given by

$$v(x, 0) = \sec h^2\left(\frac{x}{4}\right).$$

The exact solution is

$$v(x, t) = e^{-t} \sin\left(\frac{x}{4} - \frac{t}{3}\right).$$

In Figure 3, the numerical and exact solutions are plotted. The obtained numerical results for Example 2 are compared with the exact solution at different values of h, k and t and are presented in Table 2. Again, it turns out that the results obtained using the proposed method are more accurate when compared with the results in [13], [15], [22].

	h	k	t	Absolute error
The proposed method	0.1	0.1	1	3.78786×10^{-9}
	0.1	0.1	5	9.746302×10^{-9}
	0.05	0.1	1	3.911113×10^{-11}
	0.05	0.1	5	7.55322×10^{-10}
[15]	0.1	0.1	1	1.906512×10^{-8}
	0.1	0.1	5	6.746302×10^{-8}
	0.05	0.1	1	5.650921×10^{-10}
	0.05	0.1	5	1.0774219×10^{-9}
[22]	0.1	0.1	1	6.479231×10^{-2}
	0.1	0.1	5	4.209547×10^{-2}
	0.05	0.1	1	1.226197×10^{-3}
	0.05	0.1	5	2.626195×10^{-3}
[13]	0.1	0.1	1	4.783312×10^{-4}
	0.1	0.1	5	1.622166×10^{-4}
	0.05	0.1	1	2.040573×10^{-6}
	0.05	0.1	5	1.192831×10^{-6}

Table 2: Absolute errors between the numerical and exact solutions in Example 2 at different values for h, k and t.

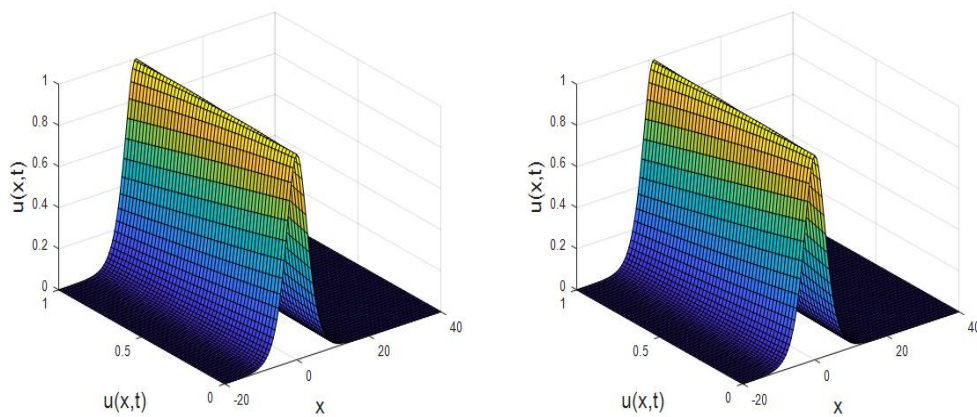


Figure 3: Numerical and exact solutions in Example 2 at $-20 \leq x \leq 40$, and $0 \leq t \leq 1$. Left: Exact solution; right: Numerical solution.

4 Conclusions

In this research paper, the BBMB equation has been solved successfully by using the septic B -spline Galerkin method. From Tables 1 and 2, the obtained numerical results show that the results are more accurate and close to the exact solutions. The results achieved from the numerical approach show that proposed technique is better than the methods used in [13], [15], [22], [23]. Thus, the results illustrated that the proposed method is novel, powerful and efficient. So, we advise to utilize the method to solve several types of partial differential equations.

References

- [1] M. A. Shallal, A. A. Ali and A. M. Jasim. Finite Element Solution to the Strongly Reaction-Diffusion System. *Nonlinear Dynamics and Systems Theory* **22** (1) (2022) 97–104.
- [2] A. A. Ali and F. Z. Ahmed. Decay in Systems with Neutral Short-Wavelength Stability: The Presence of a Zero Mode. *Discontinuity, Nonlinearity and Complexity* **10** (2) (2021) 195–205.
- [3] D. Lannes. *The water waves problem: Mathematical analysis and asymptotics, in Mathematical surveys and monographs*. AMS, New York, 2013.
- [4] D. H. Peregrine. J. Calculations of the development of an undular bore. *Journal of Fluid Mechanics* **25** (2) (1966) 321–330.
- [5] T. B. Benjamin, J. L. Bona and J. J. Mahony. Model equations for long waves in nonlinear dispersive systems. *Philosophical Transactions of the Royal Society of London. Series A, Mathematical and Physical Sciences* **272** (1220) (1972) 47–78.
- [6] V. K. Kukreja. Numerical treatment of Benjamin-Bona-Mahony-Burgers equation with fourth-order improvised B-spline collocation method. *Journal of Ocean Engineering and Science* **7** (2) (2022) 99–111.
- [7] A. Fakhari, G. Domairry and Ebrahimpour. Physics Letters A. *Approximate explicit solutions of nonlinear BBMB equations by homotopy analysis method and comparison with the exact solution* **368** (1–2) (2007) 64–68.
- [8] Z. Z. Ganji, D. D. Ganji and H. Bararnia. Approximate general and explicit solutions of nonlinear BBMB equations by Exp-Function method. *Applied Mathematical Modelling* **33** (4) (2009) 1836–1841.
- [9] M. S. Bruzón, T. M. Garrido and R. delaRosa. Conservation laws and exact solutions of a Generalized Benjamin–Bona–Mahony–Burgers equation. *Chaos, Solitons & Fractals* **89** (2016) 578–583.
- [10] K. Al-Khaled, S. Momani and A. Alawneh. Approximate wave solutions for generalized Benjamin–Bona–Mahony–Burgers equations. *Applied Mathematics and Computation* **171** (1) (2005) 281–292.
- [11] H. Tari and D. D. Ganji. Approximate explicit solutions of nonlinear BBMB equations by He’s methods and comparison with the exact solution. *Physics Letters A* **367** (1–2) (2007) 95–101.
- [12] A. C. Gomez, A. H. Salas and B. A. Frias. New periodic and soliton solutions for the generalized BBM and BBM–Burgers equations. *Applied Mathematics and Computation* **217** (2010) 1430–1434.
- [13] S. Abbasbandy and A. Shirzadi. The first integral method for modified Benjamin–Bona–Mahony equation. *Communications in Nonlinear Science and Numerical Simulation* **15**, (7) (2010) 1759–1764.

- [14] A. Mohebbi and Z. Faraz. Solitary wave solution of nonlinear Benjamin–Bona–Mahony–Burgers equation using a high-order difference scheme. *Computational and Applied Mathematics* **36** (2) (2017) 915–927.
- [15] Kh. Omrani and M. Ayadi. Finite difference discretization of the Benjamin–Bona–Mahony–Burgers equation. *Numerical Methods for Partial Differential Equations: An International Journal* **24**, (1) (2008) 239–248.
- [16] Z. Mahboob Dana, H. Saberi Najafi and A. H. Refahi Sheikhan. An efficient numerical method for solving Benjamin–Bona–Mahony–Burgers equation using difference scheme. *Journal of Difference Equations and Applications* **26** (4) (2020) 574–585.
- [17] K. Al-Khaled, S. Momani and A. Alawneh. Approximate wave solutions for generalized Benjamin–Bona–Mahony–Burgers equations. *Applied Mathematics and Computation* **171** (1) (2005) 281–292.
- [18] D. Kaya. A numerical simulation of solitary-wave solutions of the generalized regularized long-wave equation. *Applied Mathematics and Computation* **149** (3) (2004) 833–841.
- [19] D. Kaya and I.E. Inan. Exact and numerical traveling wave solutions for nonlinear coupled equations using symbolic computation. *Applied Mathematics and Computation* **151**, (3) (2004) 775–787.
- [20] S.A.V. Manickam, A. K. Pani and S. K. Chang. A second-order splitting combined with orthogonal cubic spline collocation method for the Rosenau equation. *Numerical Methods for Partial Differential Equations: An International Journal* **14** (6) (1998) 695–716.
- [21] K. Omrani. The convergence of fully discrete Galerkin approximations for the Benjamin–Bona–Mahony (BBM) equation. *Applied Mathematics and Computation* **180** (2) (2006) 614–621.
- [22] S. Kundu, A. K. Pani, and M. Khebchareon. Asymptotic Analysis and Optimal Error estimates for Benjamin–Bona–Mahony–Burgers’ Type Equations. *Numerical Methods for Partial Differential Equations* **34** (3) (2018) 1053–1092.
- [23] T. Kadri, N. Khiari and F. Abidi. *Methods for the Numerical Solution of the Benjamin–Bona–Mahony–Burgers Equation*. Wiley InterScience, (2008).
- [24] K. Omrani and M. Ayadi. Finite difference discretization of the Benjamin–Bona–Mahony–Burgers equation. *Numerical Methods for Partial Differential Equations: An International Journal* **24** (1) (2008) 239–248.
- [25] T. Kadri, N. Khiari, F. Abidi and K. Omrani. Methods for the numerical solution of the Benjamin–Bona–Mahony–Burgers equation. *Numerical Methods for Partial Differential Equations: An International Journal* **24** (6) (2008) 1501–1516.
- [26] G. Berikelashvili and M. Mirianashvili. On the convergence of difference schemes for generalized Benjamin–Bona–Mahony equation. *Numerical Methods for Partial Differential Equations* **30** (1) (2014) 301–320.
- [27] G. Berikelashvili and M. Mirianashvili. A one-parameter family of difference schemes for the regularized long-wave equation. *Georgian Mathematical Journal* **18** (2011) 639–667.
- [28] G. Arora, R. C. Mittal and B. K. Singh. Numerical solution of BBM–Burger equation with quartic B-spline collocation method. *Journal of Engineering Science and Technology* **9** (2014) 104–116.



A New Chaotic Supply Chain Model, Its Bifurcation Analysis, Multi-Stability and Synchronization Using Backstepping Control

M. D. Johansyah¹, A. Sambas^{2,3}, S. Vaidyanathan⁴, S. S. Abas²,
H. Hassan², M. Makhtar², S. Purnama⁵ and B. Foster⁵

¹ *Department of Mathematics, Universitas Padjadjaran, Jatinangor, Kabupaten Sumedang 45363, Indonesia.*

² *Faculty of Informatics and Computing, Universiti Sultan Zainal Abidin, Besut Campus 22200, Terengganu, Malaysia.*

³ *Department of Mechanical Engineering, Universitas Muhammadiyah Tasikmalaya, Tasikmalaya 46196, Indonesia.*

⁴ *Centre for Control Systems, Vel Tech University, Avadi, Chennai-600062, Tamil Nadu, India.*

⁵ *Faculty of Economics and Business, Universitas Informatika dan Bisnis Indonesia, Bandung 40285, Indonesia.*

Received: October 13, 2023; Revised: April 8, 2014

Abstract: A supply chain is a network of interconnected organizations, people, activities, information, and resources involved in the creation and distribution of products or services from the raw material stage to the end consumer. It encompasses the entire process of transforming raw materials into finished products and delivering them to customers. In this paper, we have proposed a new mathematical model for the chaotic supply chain with one absolute nonlinearity and one quadratic function. Furthermore, we have validated stability analysis and dynamical analysis using numerical MATLAB simulation. Our finding system exhibits the index-1 spiral saddle and index-2 spiral saddle. We show that the new chaotic supply chain model exhibits multistability with coexisting chaotic attractors for different initial states. Finally, as a control application, active backstepping control has been applied to achieve complete synchronization of a pair of new chaotic supply chain models taken as the master and slave systems. The Lyapunov stability theory has been used to achieve the control result using active backstepping control.

Keywords: *chaos; dynamical system; supply chain management.*

Mathematics Subject Classification (2010): 34D20, 34H10, 34H20, 65P20, 90B06.

* Corresponding author: <mailto:muhamad.deni@unpad.ac.id>

1 Introduction

The development of chaotic systems in supply chain management related to the study and application of chaos theory to understand and manage the complex and unpredictable behaviors that can emerge within supply chains [1]. Chaos theory is a branch of mathematics that deals with complex, non-linear systems that exhibit sensitive dependence on initial conditions [2]. In the context of supply chain management, chaotic behavior can lead to unexpected fluctuations, delays, and disruptions, which can significantly impact the efficiency and effectiveness of the supply chain [3].

Supply chains are inherently complex systems involving various interconnected entities such as suppliers, manufacturers, distributors, retailers, and customers [4–6]. The interactions among these entities can lead to non-linear and unpredictable behaviors [7]. Furthermore, chaotic behavior challenges traditional demand forecasting methods that assume linear relationships and steady-state conditions [8]. Instead, chaotic systems require more sophisticated approaches that account for sudden shifts and fluctuations in demand patterns [9, 10].

Chaos theory has also found applications in the field of economics, particularly in understanding complex and non-linear dynamics within economic systems such as financial markets [11] and bitcoin market [12], business cycles [13], decision making [14] and policy analysis [15]. Yingjin et al. [16] conducted research on the intricacies of the bullwhip effect within supply chains. The Bullwhip Effect, characterized by internal non-linearity, was explored to comprehend its intricacies in the context of order processing under demand signals. Their aim was to establish a mathematical correlation connecting the bullwhip effect in the supply chain network with fractal and chaotic dynamics. Lei et al. [17] constructed a three-tier network for a supply chain using the dynamic and chaotic Lorenz model. They examined a nonlinear model for a three-level supply chain, which, under specific circumstances, can manifest as a set of chaotic Lorenz equations. They introduced the concept of synchronizing a chaotic supply chain network through the application of the RBF neural network technique. Additionally, the influence of external perturbations on this model was explored. Xu et al. [18] proposed an adaptive super-twisting (STW) sliding mode control (SMC) algorithm to manage the chaotic supply chain system, they demonstrated that the provided control creation combined with dynamic analysis is crucial for strategic decision-makers in contemporary supply chain management.

The main contribution of this work is assessing the stability and dynamic behavior of a new chaotic supply chain model featuring an absolute nonlinearity and a quadratic function. This analysis encompassed the use of phase portraits, Poincaré maps, Lyapunov exponents, and bifurcation diagrams.

Multistability is a complex phenomenon typically observed for chaotic nonlinear dynamical systems with the coexistence of different periodic or chaotic attractors for the same set of system parameters but different values of the initial states [19, 20]. In this research work, we also show that the new chaotic supply chain model exhibits multistability with coexisting chaotic attractors for different initial states.

Finally, as a control application, active backstepping control has been applied to achieve the complete synchronization of a pair of new chaotic supply chain models taken as the master and slave systems. The Lyapunov stability theory has been used to achieve the control result using active backstepping control. MATLAB simulations have been shown to illustrate the results presented in this research work.

2 A New Chaotic Supply Chain Model

In 2022, Hamidzadeh et al. [21] defined a chaotic supply chain model as follows:

$$\begin{cases} \dot{y}_1 = y_2, \\ \dot{y}_2 = y_3, \\ \dot{y}_3 = ay_1 - by_2 - y_3 - y_1^2, \end{cases} \quad (1)$$

where y_1 is retailers, y_2 is distributors, and y_3 is manufacturers, system (1) exhibits chaotic behavior with the parameter $a = 7.5; b = 3.8$ and the initial conditions are $y_1(0) = 1, y_2(0) = 1, y_3(0) = 1$.

In this work, we propose a chaotic supply chain with an absolute nonlinearity and a quadratic function, which is modelled as follows:

$$\begin{cases} \dot{y}_1 = y_2, \\ \dot{y}_2 = y_3, \\ \dot{y}_3 = ay_1 - by_2 - y_3 - |y_1| - y_1^2. \end{cases} \quad (2)$$

System (2) exhibits chaotic behavior with the parameter $a = 8.5; b = 3.8$ and the initial conditions are $y_1(0) = 0.1, y_2(0) = 0.1, y_3(0) = 0.1$. Using the Wolf algorithm, the Lyapunov characteristic exponents of the model (2) are $LE_1 = 0.18109, LE_2 = 0.11839$ and $LE_3 = -1.1929$. The Kaplan-Yorke dimension of the model (2) is derived as

$$D_{KY} = 2 + \frac{LE_1 + LE_2}{|LE_3|} = 2.251. \quad (3)$$

Subsequently, we compute the equilibrium positions of the recently introduced chaotic supply chain model (2). To achieve this, we address the resolution of the subsequent system of equations

$$\begin{cases} 0 = y_2, \\ 0 = y_3, \\ 0 = ay_1 - by_2 - y_3 - |y_1| - y_1^2. \end{cases} \quad (4)$$

It is a simple calculation to verify that the revised system of the chaotic supply chain model (2) is found to possess a pair of equilibrium points, specifically determined by

$$E_0 = \begin{bmatrix} 0 \\ 0 \\ 0 \end{bmatrix} = \begin{bmatrix} 7.5 \\ 0 \\ 0 \end{bmatrix}. \quad (5)$$

The matrix provided below represents the Jacobian matrix associated with the chaotic supply chain model (2):

$$JE_i = \begin{bmatrix} 0 & 0 & 0 \\ 0 & 0 & 1 \\ 8.5 - \text{sign}(x) - 2x & -3.8 & -1 \end{bmatrix}. \quad (6)$$

We find that

$$E_0 = \begin{bmatrix} 0 & 0 & 0 \\ 0 & 0 & 1 \\ 7.5 & -3.8 & -1 \end{bmatrix}, \quad (7)$$

which has the characteristics equation as follows:

$$\lambda^3 + \lambda^2 + 3.8\lambda - 7.5. \quad (8)$$

The Jacobian matrix JE_0 has the eigenvalues 1.1781, $-1.0891 \pm 2.2759i$. The system (2) exhibits the Index-1 spiral saddle point, which is unstable. The Jacobian matrix of the system (2) at $E_1 = (7.5, 0, 0)$ is obtained as follows:

$$E_0 = \begin{bmatrix} 0 & 1 & 0 \\ 0 & 0 & 1 \\ -7.5 & -3.8 & -1 \end{bmatrix}, \quad (9)$$

which has the characteristics equation as follows

$$\lambda^3 + \lambda^2 + 3.8\lambda + 7.5 = 0. \quad (10)$$

The Jacobian matrix JE_1 has the eigenvalues $-1.5858, 0.2929 \pm 2.1548i$. The system (2) exhibits the Index-2 spiral saddle point, which is unstable.

The Runge-Kutta 4th-order method is a type of the numerical integration technique that allows one to approximate the solution of an ODE by iteratively stepping through the independent variable [22]. It is particularly useful when there is no analytical solution available or when the ODE is too complex to solve directly. By using this method, in Figure 1, the MATLAB plots are displayed for the chaotic supply chain (2) with $(a, b) = (8.5, 3.8)$, with the initial conditions $Y(0) = (0.1, 0.1, 0.1)$.

3 Dynamical Analysis of the New Chaotic Supply Chain Model

A bifurcation diagram is a graphical representation used in the field of dynamical systems and nonlinear mathematics to visualize the behavior of a system as a parameter changes [23]. It helps to illustrate how the qualitative behavior of a system changes as a parameter varies, particularly when the system undergoes bifurcations. Meanwhile, the Lyapunov exponent is a concept from the field of chaos theory and dynamical systems that quantifies the rate of exponential divergence or convergence of nearby trajectories in a nonlinear system [24]. It is used to characterize the sensitivity of a system to initial conditions, which is a fundamental aspect of chaotic behavior.

The behavior of the supply chain system (2) was explored by varying the bifurcation parameter a within the range of 6 to 9.5. The bifurcation diagram and Lyapunov exponent diagram of the chaotic supply chain system model (2) are presented in Figures 2(a) and 2(b), respectively. It is evident from these figures that the system (2) showcases both limit cycles and demonstrates chaotic patterns. Meanwhile, confirming the existence of a path to chaos through period doubling is straightforward when the parameter a is increased.

By altering the parameter b within the range of [3.8, 4.8], the behavior of the supply chain system (2) is explored. Figure 3(a) exhibits the bifurcation diagram, while Figure 3(b) presents the associated Lyapunov exponent spectrum of system (2). These figures illustrate the system's capacity to transition from chaotic to periodic behavior. The presence of a route from chaos to period doubling becomes apparent upon increasing the value of the parameter b .

A Poincaré map, also known as a Poincaré section or Poincaré surface of section, is a graphical tool used to study the behavior of chaotic systems and to analyze the dynamics of a system in a reduced-dimensional space. In addition, the Poincaré map of supply chain system (2) in Figure 4 exhibits chaotic characteristics.

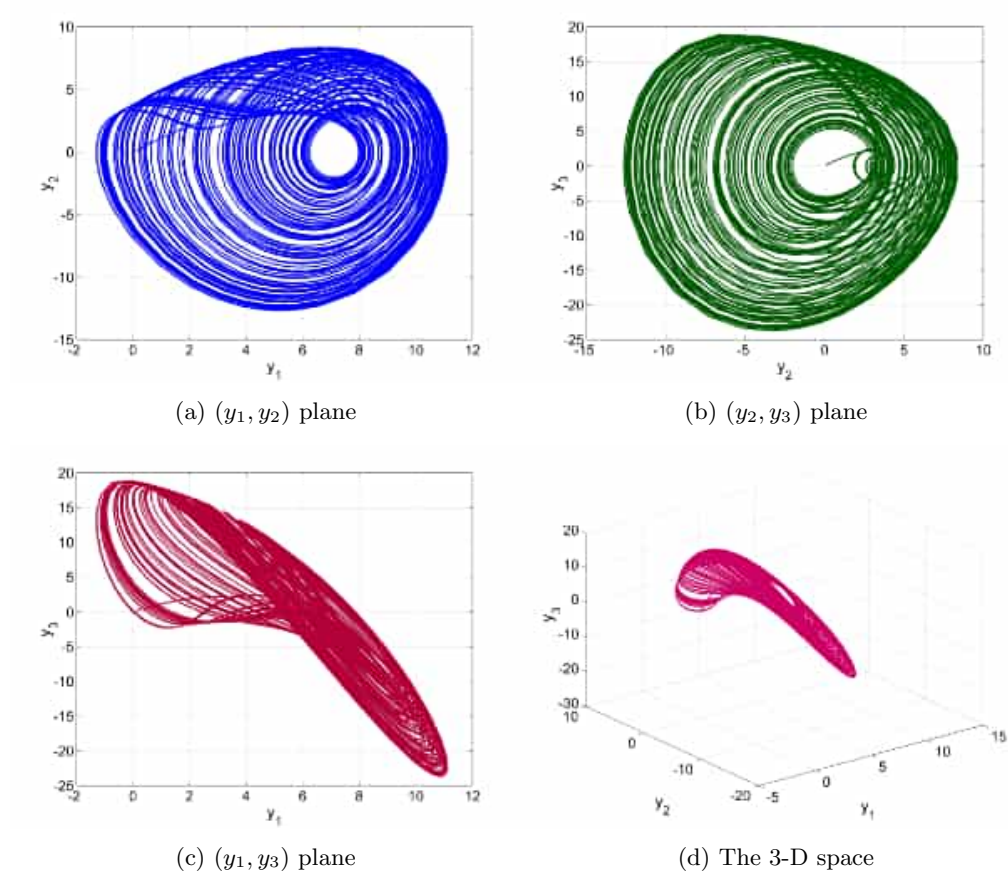


Figure 1: Chaotic attractors supply chain model (2) using MATLAB in (a) $y_1 - y_2$ plane (b) $y_2 - y_3$ plane, (c) $y_1 - y_3$ plane and (d) 3D plane.

4 Multistability of the New Chaotic Supply Chain Model

Multistability is a complex phenomenon typically observed for chaotic nonlinear dynamical systems with the coexistence of different periodic or chaotic attractors for the same set of system parameters but different values of the initial states [19,20]. In this research work, we also exhibit that the new chaotic supply chain model (2) exhibits multistability with coexisting chaotic attractors for different initial states.

We fix the parametric values as in the chaotic case, *viz.* $a = 8.5$ and $b = 3.8$. We choose two initial states as $Y_0 = (0.1, 0.1, 0.1)$ and $Z_0 = (0.5, 0.2, 0.5)$, and we denote the corresponding state flows of the new chaotic supply chain model (2) as $Y(t)$ (in blue color) and $Z(t)$ (in red color), respectively.

Figure 5 shows the multistability with coexisting chaotic attractors of the new chaotic supply chain model (2), where the blue orbit corresponds to the chaotic attractor for $Y_0 = (0.1, 0.1, 0.1)$ and the red orbit corresponds to the chaotic attractor for $Z_0 = (0.5, 0.2, 0.5)$. In this figure, the parametric values are kept fixed at $a = 8.5$ and $b = 3.8$.

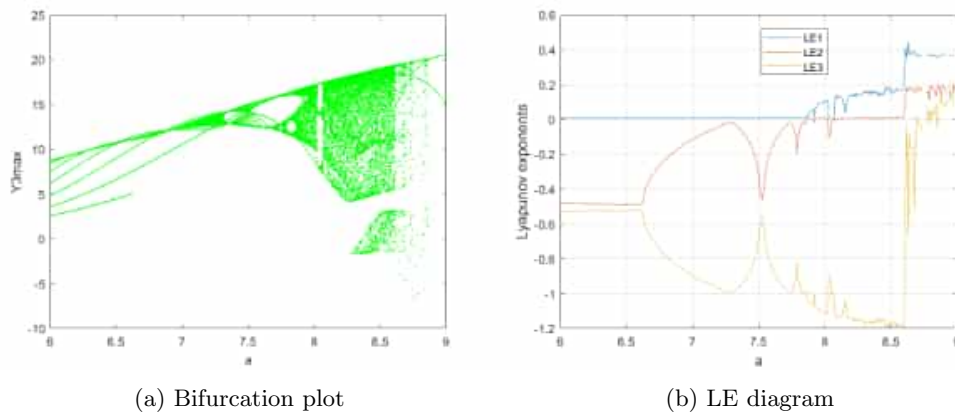


Figure 2: (a) Bifurcation plot and (b) Lyapunov exponents diagram of supply chain model (2) with variation of the parameter a .

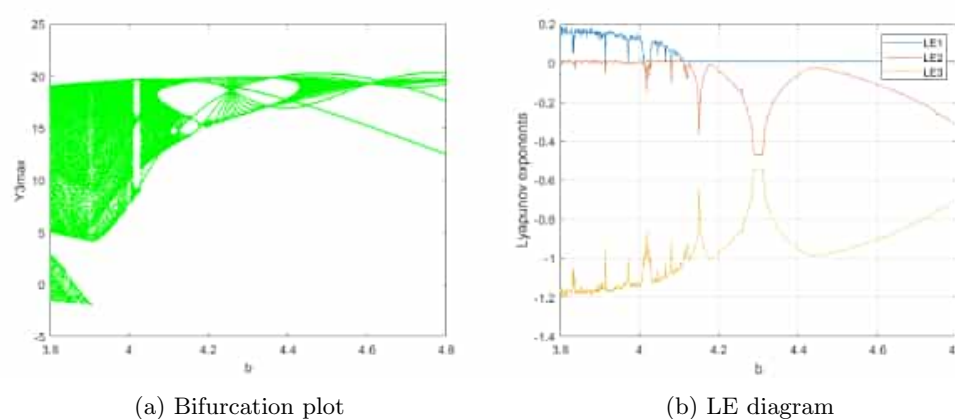


Figure 3: (a) Bifurcation plot and (b) Lyapunov exponents diagram of supply chain model (2) with variation of the parameter b .

5 Complete Synchronization of the New Chaotic Supply Chain Models

In this section, we use the active backstepping control method [25] to solve the design problem of achieving the complete chaos synchronization of a pair of new chaotic supply chain models taken as the master and slave systems.

As the master system, we take the new chaotic supply chain model given by the jerk dynamics

$$\begin{aligned} \dot{y}_1 &= y_2, \\ \dot{y}_2 &= y_3, \\ \dot{y}_3 &= ay_1 - by_2 - y_3 - |y_1| - y_1^2. \end{aligned} \quad (11)$$

As the slave system, we consider the new chaotic supply chain model given by the

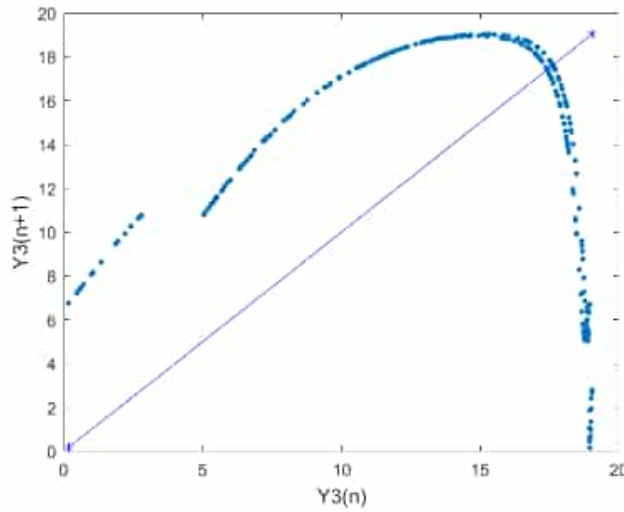


Figure 4: Poincaré section of the chaotic supply chain model (2).

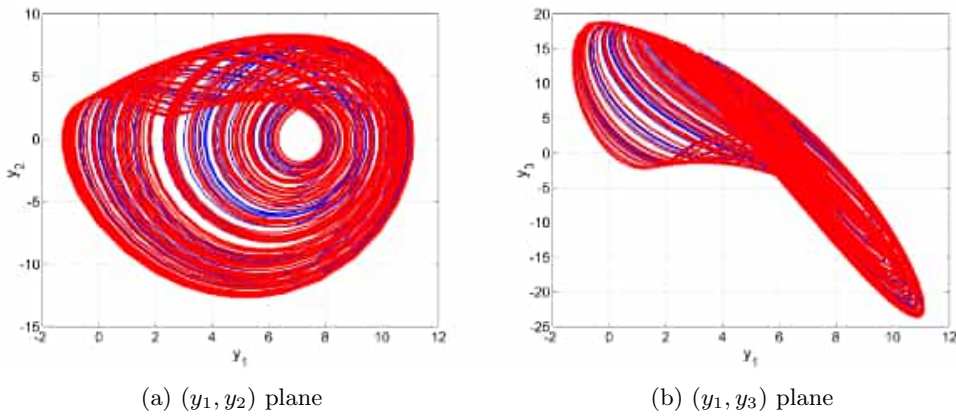


Figure 5: Multistability of the new chaotic supply chain model (2).

jerk dynamics

$$\begin{aligned} \dot{z}_1 &= z_2, \\ \dot{z}_2 &= z_3, \\ \dot{z}_3 &= az_1 - bz_2 - z_3 - |z_1| - z_1^2 + v. \end{aligned} \tag{12}$$

In Eq.(12), v is an active backstepping control, which is to be designed in this section.

The error between the chaotic supply chain models (11) and (12) can be defined as follows:

$$\begin{aligned} \mu_1 &= z_1 - y_1, \\ \mu_2 &= z_2 - y_2, \\ \mu_3 &= z_3 - y_3. \end{aligned} \tag{13}$$

Using the dynamics of the systems (11) and (12), we can compute the error dynamics as follows:

$$\begin{aligned}\dot{\mu}_1 &= \mu_2, \\ \dot{\mu}_2 &= \mu_3, \\ \dot{\mu}_3 &= a\mu_1 - b\mu_2 - \mu_3 - |z_1| + |y_1| - z_1^2 + y_1^2 + v.\end{aligned}\tag{14}$$

Theorem 5.1 *The new chaotic supply chain models (11) and (12) are completely synchronized for all initial values and in R^3 when the active control law v is chosen as*

$$v = -(3+a)\mu_1 - (5-b)\mu_2 - 2\mu_3 + |z_1| - |y_1| + z_1^2 - y_1^2 - kw_3,\tag{15}$$

where $k > 0$ is a gain constant and $w_3 = 2\mu_1 + 2\mu_2 + \mu_3$.

Proof. We use the active backstepping control method [26] to establish the result in Theorem 5.1. First, we begin with the Lyapunov function given by

$$P_1(w_1) = \frac{1}{2}w_1^2,\tag{16}$$

where

$$w_1 = \mu_1.\tag{17}$$

Then we get

$$\dot{P}_1 = \mu_1\dot{\mu}_1 = \mu_1\mu_2 = -w_1^2 + w_1(\mu_1 + \mu_2).\tag{18}$$

In order to simplify our calculations, we define

$$w_2 = \mu_1 + \mu_2.\tag{19}$$

Using (19), we can simplify Eq.(18) as follows:

$$\dot{P}_1 = -w_1^2 + w_1w_2.\tag{20}$$

Next, we define the Lyapunov function given by

$$P_2(w_1, w_2) = P_1(w_1) + \frac{1}{2}w_2^2 = \frac{1}{2}w_1^2 + \frac{1}{2}w_2^2.\tag{21}$$

Then it is easy to show that

$$\dot{P}_2 = -w_1^2 - w_2^2 + w_2(2\mu_1 + 2\mu_2 + \mu_3).\tag{22}$$

In order to simplify our calculations, we define

$$w_3 = 2\mu_1 + 2\mu_2 + \mu_3.\tag{23}$$

Using (23), we can simplify Eq.(22) as follows:

$$\dot{P}_2 = -w_1^2 - w_2^2 + w_2w_3.\tag{24}$$

Finally, we define the Lyapunov function given by

$$P(w_1, w_2, w_3) = P_2(w_1, w_2) + \frac{1}{2}w_3^2 = \frac{1}{2}w_1^2 + \frac{1}{2}w_2^2 + \frac{1}{2}w_3^2.\tag{25}$$

Then we calculate the derivative of P along the error dynamics (14) as follows:

$$\dot{P} = -w_1^2 - w_2^2 + w_2w_3 + w_3\dot{w}_3 = -w_1^2 - w_2^2 - w_3^2 + w_3Z. \tag{26}$$

A standard calculation yields the following:

$$Z = (3 + a)\mu_1 + (5 - b)\mu_2 + 2\mu_3 - |z_1| + |y_1| - z_1^2 + y_1^2 + v. \tag{27}$$

Substituting the formula given in Eq.(15) for v into Eq.(28), we get $Z = -kw_3$. Then Eq.(26) can be simplified as follows:

$$\dot{P} = -w_1^2 - w_2^2 - (1 + k)w_3^2. \tag{28}$$

Hence, we have shown that \dot{P} is a quadratic and negative definite function on R^3 .

Using the Lyapunov stability theory, we conclude that the error dynamics (14) is globally asymptotically stable.

Hence, the error variables $\mu_1(t)$, $\mu_2(t)$, and $\mu_3(t)$ converge to zero asymptotically as $t \rightarrow \infty$ for all initial error conditions. This completes the proof.

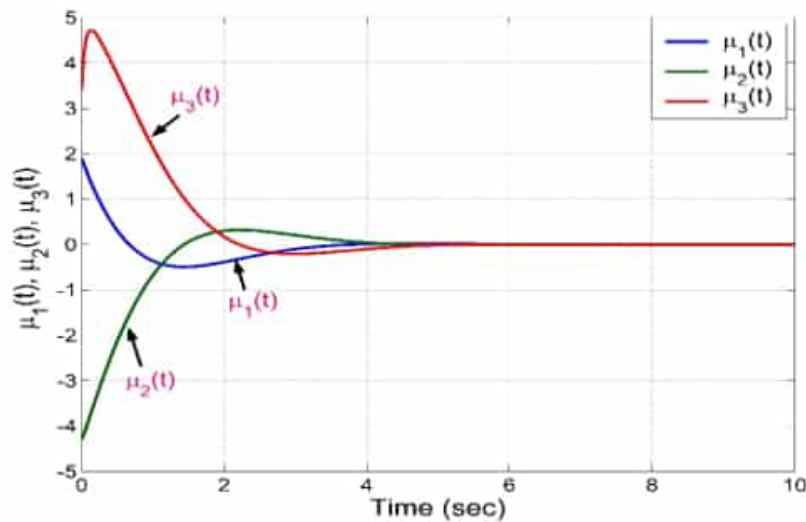


Figure 6: Convergence of the synchronization errors $\mu_1(t)$, $\mu_2(t)$, $\mu_3(t)$.

For MATLAB values, we take the values of a and b as in the chaotic case studied in Section 2, viz. $a = 7.5$ and $b = 3.8$. We pick the control gain constant k as $k = 20$.

The initial values of the master and slave chaotic supply chain systems given in the equations (11) and (12) are taken as $y(0) = (1.7, 5.4, 2.8)$ and $z(0) = (3.6, 1.1, 6.2)$, respectively.

Figure 6 shows the convergence of the synchronization errors between the master and slave chaotic supply chain systems given in the equations (11) and (12), respectively.

6 Conclusions

This study presents a new chaotic supply chain system featuring two unstable equilibrium points, which are saddle points. The main contribution of this work is assessed stability

and dynamic behavior for a new chaotic supply chain model featuring an absolute non-linearity and a quadratic function. The fundamental dynamic properties of the system are explored using phase portraits, equilibrium analysis, the Kaplan–Yorke dimension, Lyapunov exponents, and bifurcation analysis. Our investigations reveal that the new chaotic supply chain system demonstrates both periodic and chaotic behaviors. Using the active backstepping control method, we derived a new control law for achieving the complete synchronization between the new chaotic supply chain models taken as the master and slave chaotic systems. In the future research, we will investigate the robustness of the proposed control method under various disturbances and uncertainties in the supply chain system. This could involve analyzing the performance of the control method in the presence of external factors that may affect the stability and synchronization.

Acknowledgment

Muhamad Deni Johansyah would like to thank the Rector of Universitas Padjadjaran for the financial support through Research of Universitas Padjadjaran 2023.

References

- [1] D. Stapleton, J. B. Hanna and J. R. Ross. Enhancing supply chain solutions with the application of chaos theory. *Supply Chain Management: An International Journal* **11** (2) (2006) 108–114.
- [2] A. Sambas, W. S. M. Sanjaya, M. Mamat and Halimatussaiyah. Design and analysis bidirectional chaotic synchronization of Rossler circuit and its application for secure communication. *Applied Mathematical Sciences* **7** (1-4)(2013) 11–21.
- [3] S. E. Fawcett and M. A. Waller. Making sense out of chaos: Why theory is relevant to supply chain research. *Journal of Business Logistics* **32** (2011) 1–5.
- [4] M. Akin Ateş, R. Suurmond, D. Luzzini and D. Krause. Order from chaos: a meta-analysis of supply chain complexity and firm performance. *Journal of Supply Chain Management* **58** (2022) 3–30.
- [5] H. B. Hwang and X. Yuan. Interpreting supply chain dynamics: A quasi-chaos perspective. *European Journal of Operational Research* **233** (2014) 566–579.
- [6] X. Chen and J. Zhou. The complexity analysis and chaos control in omni-channel supply chain with consumer migration and advertising cost sharing. *Chaos, Solitons and Fractals* **146** (2021) 110884.
- [7] J. Ma, H. Ren, M. Yu and M. Zhu. Research on the complexity and chaos control about a closed-loop supply chain with dual-channel recycling and uncertain consumer perception. *Complexity* **2018** (2018) 1–13.
- [8] N. Mishra, A. K. Choudhary and M. K. Tiwari. Modeling the planning and scheduling across the outsourcing supply chain: a Chaos-based fast Tabu–SA approach. *International Journal of Production Research* **46** (2008) 3683–3715.
- [9] N. Açıkgöz, G. Çağıl and Y. Uyaroglu. The experimental analysis on safety stock effect of chaotic supply chain attractor. *Computers and Industrial Engineering* **150** (2020) 106881.
- [10] T. Li and J. Ma. Complexity analysis of the dual-channel supply chain model with delay decision. *Nonlinear Dynamics* **78** (2014) 2617–2626.
- [11] L. Inglada-Perez. A comprehensive framework for uncovering non-linearity and Chaos in financial markets: Empirical evidence for four major stock market indices. *Entropy* **22** (2020) 1435.

- [12] S. Lahmiri, S. Bekiros and S. Chaos, randomness and multi-fractality in Bitcoin market. *Chaos, solitons and fractals* **106** (2018) 28–34.
- [13] A. C. L. Chian, F. A. Borotto, E. L. Rempel, and C. Rogers, Attractor merging crisis in chaotic business cycles. *Chaos, Solitons and Fractals* **24** (3) (2005) 869–875.
- [14] J. G. Du, T. Huang and Z. Sheng. Analysis of decision-making in economic chaos control. *Nonlinear analysis: real world applications* **10** (4) (2009) 2493–2501.
- [15] H. Yoshida and T. Asada. Dynamic analysis of policy lag in a Keynes–Goodwin model: stability, instability, cycles and chaos. *Journal of Economic Behavior and Organization* **62** (3) (2007) 441–469.
- [16] L. U. Yingjin, T. A. N. G. Yong and T. Xiaowo. Study on the complexity of the bullwhip effect. *Journal of electronic science and technology* **2004** (2) 86–91.
- [17] Z. Lei, Y. J. Li and Y. Q. Xu. Chaos synchronization of bullwhip effect in a supply chain. In: *2006 international conference on management science and engineering* (2006, October) 557–560. IEEE.
- [18] X. Xu, S. D. Lee, H. S. Kim and S. S. You. Management and optimisation of chaotic supply chain system using adaptive sliding mode control algorithm. *International journal of production research* **59** (9) (2021) 2571–2587.
- [19] F. Hannachi and R. Amira. On the Dynamics and FSHP Synchronization of a New Chaotic 3-D System with Three Nonlinearities. *Nonlinear Dynamics and Systems Theory* **23** (3) (2023) 283–294.
- [20] K. A. Alattas, J. Mostafae, A. Sambas, A. K. Alanazi, S. Mobayen, M. T. Vu and A. A. Zhilenkov. Nonsingular integral-type dynamic finite-time synchronization for hyper-chaotic systems. *Mathematics* **10** (1) (2021) 115.
- [21] S. M. Hamidzadeh, M. Rezaei and M. Ranjbar-Bourani. Chaos synchronization for a class of uncertain chaotic supply chain and its control by ANFIS. *International Journal of Production Management and Engineering* (2023) 103–116.
- [22] R. Rameshbabu, K. Kavitha, P. S. Gomathi and K. Kalaichelvi. A New Hidden Attractor Hyperchaotic System and Its Circuit Implementation, Adaptive Synchronization and FPGA Implementation. *Nonlinear Dynamics and Systems Theory* **23** (2) (2023) 214–226.
- [23] M. H. Rafiq, A. Jhangeer and N. Raza. The analysis of solitonic, supernonlinear, periodic, quasiperiodic, bifurcation and chaotic patterns of perturbed Gerdjikov–Ivanov model with full nonlinearity. *Communications in Nonlinear Science and Numerical Simulation* **116** (2023) 106818.
- [24] B. Kharabian and H. Mirinejad. Fuzzy Lyapunov exponents placement for chaos stabilization. *Physica D: Nonlinear Phenomena* **445** (2023) 133648.
- [25] S. Yan, J. Wang, E. Wang, Q. Wang, X. Sun and L. Li. A four-dimensional chaotic system with coexisting attractors and its backstepping control and synchronization. *Integration* **91** (2023) 67–78.
- [26] Z. Bai, S. Li, H. Liu and X. Zhang. Adaptive fuzzy backstepping control of fractional-order chaotic system synchronization using event-triggered mechanism and disturbance observer. *Fractal and Fractional* **6** (12) (2022) 714.



On Unique Solvability and a Generalized Newton Method for Solving New General Absolute Value Equations

M. Khaldi* and M. Achache

Fondamental and Numerical Mathematics Laboratory, Ferhat Abbas University Sétif 1, Sétif 19000, Algeria.

Received: October 11, 2023; Revised: April 15, 2024

Abstract: In this paper, we consider some sufficient conditions to guarantee the unique solvability of the new general absolute value equations (NGAVE), $Ax - |Bx| = b$, ($A, B \in \mathbb{R}^{n \times n}$, $b \in \mathbb{R}^n$). Besides Picard's iterative method for solving the NGAVE, a generalized Newton method is also proposed for solving the NGAVE. Moreover, under suitable assumptions, we show that the proposed methods are globally linearly convergent. We also report some numerical results of the proposed method for solving the NGAVE, which show the efficiency of our proposed methods.

Keywords: *absolute value equations; Picard's iterative method; generalized Newton method; global convergence.*

Mathematics Subject Classification (2010): 65F08, 90C33, 93C05.

1 Introduction

In this paper, we consider new general absolute value equations (abbreviated as NGAVE) of the type

$$Ax - |Bx| = b, \quad (1)$$

where $A, B \in \mathbb{R}^{n \times n}$ are given matrices, $b \in \mathbb{R}^n$, and $|Bx|$ is a vector whose i -th entry is the absolute value of the i -th entry of Bx . If $B = I$ is the identity matrix, then the NGAVE (1) can be reduced to the type

$$Ax - |x| = b. \quad (2)$$

* Corresponding author: mailto:Khaldi_m2007@yahoo.fr

Moreover, the system (2) is a special case of the generalized absolute value equation (GAVE) of the following form:

$$Ax - B|x| = b, \quad (3)$$

where $B \in \mathbb{R}^{n \times n}$, the last one was introduced by Rohn [14] and investigated in a more general context by Mangasarian and Meyer (see [9]). Other studies for the AVE can be found in [1, 5, 6, 11, 13, 16]. The AVE (2), GAVE (3) and NGAVE (1) have received much attention from the optimization community. It is currently an active research topic due to its broad application in many areas of scientific computing and engineering. For instance, linear complementarity, linear programming, convex quadratic programming and bi-matrix games can be equivalent to the NGAVE(1). The research effort can be summarized to the following two aspects. One is purely theoretical analysis. Authors focus on the reformulations of AVE (2), GAVE (3) and NGAVE (1) as different equivalent problems because determining the existence and uniqueness of a solution of the NGAVE (1) is an NP-hard problem because of the nonlinear and non-differentiable term $|Bx|$ in the NGAVE (1). For the unique solution of NGAVE (1), some necessary and sufficient conditions were presented in [17]. The other one is the numerical solvability of AVEs. Recently, several algorithms have been designed to solve the AVE and GAVE, see e.g., [4, 7, 12] and the references therein. For example, Mangasarian in [10] proposed a semi-smooth Newton method for solving the AVE, and under suitable conditions, he showed the finite and linear convergence to a solution of the AVE. However, other numerical approaches focus on reformulating the AVE as a horizontal linear complementarity problems (HLCP) (see Achache [3]), where they introduce an infeasible path-following interior-point method for solving the AVE by using equivalent reformulations as an HLCP. Recently, Achache and Anane [2] have presented Picard's iterative fixed point method for getting the solution of the uniquely solvable GAVE. Under some suitable conditions, they showed that the proposed method is globally linearly convergent.

The goal of this paper is twofold. First, we present some weaker sufficient conditions that guarantee the unique solvability of the NGAVE (1). Second, for its numerical solution, we propose a generalized Newton method. In particular, under a mild assumption, we show that this method is always well-defined and the generated sequence converges globally and linearly to the unique solution of the NGAVE from any starting initial point. Finally, numerical results are provided to illustrate the efficiency of our proposed algorithm for solving the NGAVE. In addition, a numerical comparison is made with an available method.

The outline of this paper is as follows. The main results of the unique solvability of the NGAVE are stated in Section 2. In Section 3, Picard's iterative method for solving the NGAVE is presented. In Section 4, a generalized Newton method is proposed for solving the NGAVE. Moreover, under suitable conditions, the global convergence to the unique solution is proved. In Section 5, some numerical results are provided to show the efficiency of the proposed algorithm. Finally, a conclusion and some remarks are drawn in the last section of the paper.

At the end of this section, some notations are presented. Let $\mathbb{R}^{n \times n}$ be the set of all $n \times n$ real matrices. The scalar product and the Euclidean norm are denoted, respectively, by $x^T y$, $x, y \in \mathbb{R}^n$ and $\|x\| = \sqrt{x^T x}$. Recall that a subordinate matrix norm for $A \in \mathbb{R}^{n \times n}$ is defined as follows: $\|A\| := \max \{\|Ax\| : x \in \mathbb{R}^n, \|x\| = 1\}$, this definition implies

$$\|Ax\| \leq \|A\| \|x\|, \|AB\| \leq \|A\| \|B\|, \forall A, B \in \mathbb{R}^{n \times n} \text{ and } x \in \mathbb{R}^n.$$

The $\text{sign}(x)$ denotes a vector with the components equal to -1, 0 or 1 depending on

whether the corresponding component is negative, zero or positive. In addition, $D(x) := \text{Diag}(\text{sign}(x))$ will denote a diagonal matrix corresponding to $\text{sign}(x)$. The absolute value of a matrix $A = (a_{ij}) \in \mathbb{R}^{n \times n}$ and the vector of all ones are denoted by $|A| = (|a_{ij}|) \in \mathbb{R}^{n \times n}$ and $e \in \mathbb{R}^n$, respectively. $\sigma_{\min}(A)$, $\sigma_{\max}(A)$ represent, respectively, the smallest and the largest singular value of the matrix A . As is well known, $\sigma_{\min}^2(A) = \min_{\|x\|=1} x^T A^T A x$, and $\sigma_{\max}^2(A) = \max_{\|x\|=1} x^T A^T A x$. Finally, a matrix $A \in \mathbb{R}^{n \times n}$ is positive definite if for a nonzero vector x , $x^T A x > 0$, and the inverse of a non singular matrix A is denoted by A^{-1} .

2 The Main Results

In this section, some conditions to guarantee the unique solution of the NGAVE (1) are presented. First, for given matrices $A, B \in \mathbb{R}^{n \times n}$ and for any diagonal matrix $D \in \mathbb{R}^{n \times n}$ whose diagonal elements are ± 1 and 0, we define the matrix $(A - DB) \in \mathbb{R}^{n \times n}$. Then to achieve our main results, the following lemma is required.

Lemma 2.1 *Each of three conditions below implies the non singularity of $(A - DB)$.*

1. $\sigma_{\min}(A) > \sigma_{\max}(B)$,
2. $\|A^{-1}\| \|B\| < 1$, provided A is non singular,
3. the matrix $A^T A - \|B\|^2 I$ is positive definite.

Proof. For the first claim, assume that $(A - DB)$ is singular, then

$$(A - DB)x = 0, \text{ for some } x \neq 0.$$

We then have

$$\begin{aligned} \sigma_{\min}^2(A) &= \min_{\|y\|=1} y^T A^T A y \leq x^T A^T A x = x^T B^T D D B x \\ &\leq \max_{\|z\|=1} z^T B^T D D B z = \|DB\|^2 \\ &\leq \|D\|^2 \|B\|^2 \leq \|B\|^2 = \max_{\|z\|=1} z^T B^T B z \\ &= \sigma_{\max}^2(B), \end{aligned}$$

which contradicts the first condition. Hence $(A - DB)$ is non singular. Next, by the same argument, assume that A is non singular and let a nonzero vector x with $\|x\| = 1$ be such that

$$(A - DB)x = 0.$$

Next, because $x = A^{-1}DBx$, we then have

$$\begin{aligned} 1 &= \|x\| = \|A^{-1}DBx\| \\ &\leq \|A^{-1}\| \|D\| \|B\| \|x\| \\ &\leq \|A^{-1}\| \|B\|, \end{aligned}$$

which leads to a contradiction and hence $(A - DB)$ is non singular. For the last claim, assume on the contrary that $(A - DB)$ is singular, then for a nonzero vector x with $\|x\| = 1$, we have

$$(A - DB)x = 0.$$

As $Ax = DBx$, we then have

$$\begin{aligned} x^T A^T A x - \|B\|^2 x^T x &= x^T (DB)^T DBx - \|B\|^2 x^T x \\ &= \|DBx\|^2 - \|B\|^2 x^T x \\ &\leq \|D\|^2 \|B\|^2 \|x\|^2 - \|B\|^2 x^T x \\ &\leq \|B\|^2 - \|B\|^2 = 0, \end{aligned}$$

and consequently,

$$x^T A^T A x - \|B\|^2 x^T x \leq 0.$$

This contradicts the fact that the matrix $A^T A - \|B\|^2 I$ is positive definite. Hence $(A - DB)$ is non singular for any diagonal matrix D whose elements are ± 1 and 0 . This completes the proof.

The following result guarantees the unique solvability of the NGAVE.

Theorem 2.1 *The matrices A and B satisfy*

1. $\sigma_{\min}(A) > \sigma_{\max}(B)$,
2. $\|A^{-1}\| \|B\| < 1$, provided A is non singular,
3. *The matrix $A^T A - \|B\|^2 I$ is positive definite, then the NGAVE (1) is uniquely solvable for any b .*

Proof. Let $y = Bx$, then the equation NGAVE (1) is equivalent to

$$\begin{cases} Ax + |y| = b, \\ -Bx + y = 0. \end{cases} \tag{4}$$

The latter system can be expressed as

$$\begin{pmatrix} A & -D(y) \\ -B & I \end{pmatrix} \begin{pmatrix} x \\ y \end{pmatrix} = \begin{pmatrix} b \\ 0 \end{pmatrix}, \tag{5}$$

where $D(y) := \text{diag}(\text{sign}(y))$, $y \in \mathbb{R}^n$. Once we find the unique solution of the two-by-two linear Eq.(5), naturally, the unique solution of NGAVE (1) is obtained as well. To show that the equation admits a unique solution, it suffices to show that the application of

$$F(x, y) = \begin{pmatrix} A & -D \\ -B & I \end{pmatrix} \begin{pmatrix} x \\ y \end{pmatrix}$$

is one-to-one for any diagonal matrix D whose elements are ± 1 and 0 . To do so, we prove only that the Null $F = \{0\}$. For that, let $(u^T, v^T)^T \in \mathbb{R}^{2n}$, we have

$$\begin{aligned} F(u, v) = 0 &\Rightarrow \begin{pmatrix} A & D \\ -B & I \end{pmatrix} \begin{pmatrix} u \\ v \end{pmatrix} = \begin{pmatrix} 0 \\ 0 \end{pmatrix} \\ &\Rightarrow \begin{cases} Au - Dv = 0, \\ v = Bu, \end{cases} \\ &\Rightarrow \begin{cases} (A - DB)u = 0, \\ v = Bu. \end{cases} \end{aligned}$$

Based on Lemma 2.1, the matrix $(A - DB)$ is non singular for any diagonal matrix D whose elements are ± 1 and 0 , then $u = 0$, and consequently, $v = 0$. Thus, Null $F = \{0\}$

and so F is one-to-one. Hence, the NGAVE (1) is uniquely solvable for any b . This completes the proof.

Then it is clear that the NGAVE (1) is uniquely solvable for any b if the matrix of coefficients $(A - DB)$ is non singular for any diagonal matrix D whose elements are ± 1 or 0 .

3 Picard's Fixed Point Method of NGAVE

In this section, we provide Picard's fixed point iteration method for computing an approximated solution of the uniquely solvable NGAVE. The principal feature of the method is the use of the following equivalent scheme for NGAVE (1):

$$x_{k+1} = A^{-1}|Bx_k| + A^{-1}b, k = 0, 1, 2, \dots$$

to find an approximated solution. The details of Picard's iterative algorithm for solving the NGAVE (1) are described in Figure 1.

Algorithm 3.1

Input
 An accuracy parameter $\epsilon > 0$;
 an initial starting point $x_0 \in \mathbb{R}^n$;
 two matrices A and B and a vector b ;
 set $k:=0$;
while $\|Ax_k - |Bx_k| - b\| > \epsilon$ **do**
begin
 compute x_{k+1} from the linear system $x_{k+1} = A^{-1}(|Bx_k| + b)$;
 $k := k + 1$;
end;
end.

Figure 1: Picard's algorithm for the NGAVE.

The convergence of Picard's fixed point scheme is based on the Banach fixed point theorem (see [8]).

Theorem 3.1 *Let A be a non singular matrix and if*

$$\|A^{-1}\| \|B\| < 1,$$

then the sequence $\{x_k\}$ converges to the unique solution x^ of the NGAVE (1) for any arbitrary $x_0 \in \mathbb{R}^n$. In this case, the error bound is given by*

$$\|x_{k+1} - x^*\| \leq \frac{\|A^{-1}\| \|B\|}{1 - \|A^{-1}\| \|B\|} \|x_{k+1} - x_k\|, k = 0, 1, 2, \dots$$

Moreover, the sequence $\{x_k\}$ converges to the unique solution x^ as follows:*

$$\|x_{k+1} - x^*\| \leq \|A^{-1}\| \|B\| \|x_k - x^*\|, k = 0, 1, 2, \dots$$

Proof. The proof is similar to the one given in [2].

4 The Proposed Generalized Newton Method for the NGAVE

In this section, we propose a generalized Newton method for solving the NGAVE (1) and we show its convergence.

Let the function $F : \mathbb{R}^n \rightarrow \mathbb{R}^n$ be defined as

$$F(x) = Ax + |Bx| - b. \tag{6}$$

The generalized Jacobian $\partial F(x)$ of $F(x)$ is given by

$$\partial F(x) = A - D(Bx)B, \tag{7}$$

where $D(Bx) := \text{diag}(\text{sign}(Bx))$, $x \in \mathbb{R}^n$. The generalized Newton method for finding a zero of the equation $F(x) = 0$ after some simplifications consists then of the following iteration:

$$(A - D(Bx_k)B)x_{k+1} = b, k = 0, 1, \dots$$

The details of the algorithm for solving the NGAVE (1) are described in Figure 2.

Algorithm 4.1

Input
 An accuracy parameter $\epsilon > 0$;
 an initial starting point $x_0 \in \mathbb{R}^n$;
 two matrices A and B and a vector b ;
 set $k:=0$;
while $\|Ax_k - |Bx_k| - b\| > \epsilon$ **do**
begin
 compute x_k from the linear system $(A - D(Bx_k)B)x_{k+1} = b$;
 $k := k + 1$;
end;
end.

Figure 2: A generalized Newton algorithm for the NGAVE.

Next, following Achache [1, 10], we will study the global convergence of the generalized Newton method, first, we give the following lemma.

Lemma 4.1 *For all $x \in \mathbb{R}^n$ and $y \in \mathbb{R}^n$, we obtain the following results:*

$$\| |x| - |y| \| \leq \|x - y\|.$$

Proof. For a detailed proof, see Lemma 5 [10].

Lemma 4.2 *Suppose that $\|(A - DB)^{-1}\| \leq \frac{1}{2\|B\|}$, when $\|B\| \neq 0$, for any diagonal matrix D with diagonal elements of ± 1 or 0 . Then the generalized Newton iteration converges linearly from any starting point to a solution x^* of the NGAVE (1).*

Proof. Let x^* be a solution of the NGAVE (1), then $(A - D(Bx^*)B)x^* = b$. Note that $|Bx^*| = D(Bx^*)Bx^*$ and $|Bx_k| = D(Bx_k)Bx_k$. Now, subtracting

$(A - D(Bx^*)B)x^* = b$ from $(A - D(Bx_k)B)x_k = b$, we obtain

$$\begin{aligned} A(x_{k+1} - x^*) &= D(Bx_k)Bx_{k+1} - D(Bx^*)Bx^* = 0 \\ &= D(Bx_k)(x_{k+1} + x_k - x_k) - D(Bx^*)Bx^* \\ &= |Bx_k| - |Bx^*| + D(Bx_k)B(x_{k+1} - x^* + x^* - x_k) \\ &= |Bx_k| - |Bx^*| - D(Bx_k)B(x_k - x^*) + D(Bx_k)B(x_{k+1} - x^*). \end{aligned}$$

Hence

$$(A - D(Bx_k)B)(x_{k+1} - x^*) = |Bx_k| - |Bx^*| - D(Bx_k)B(x_k - x^*).$$

Consequently,

$$(x_{k+1} - x^*) = (A - D(Bx_k)B)^{-1}(|Bx_k| - |Bx^*| - D(Bx_k)B(x_k - x^*)).$$

By Lemma 4.1, we have

$$\|x_{k+1} - x^*\| = \|(A - D(Bx_k)B)\|^{-1} \|B\| \|(x_k - x^*)\| - \|B\| \|(x_k - x^*)\|.$$

Hence,

$$\|x_{k+1} - x^*\| \leq 2\|A - D(Bx_k)B\|^{-1} \|B\| \|(x_k - x^*)\|.$$

So by the condition

$$\|(A - DB)^{-1}\| \leq \frac{1}{2\|B\|},$$

it follows that $\|x_{k+1} - x^*\| < \|x_k - x^*\|$. Hence the sequence $\{x^k\}$ converges linearly to x^* . This completes the proof.

We are now ready to prove our main result of the global convergence. We quote first the following lemma.

Lemma 4.3 *If assumption $\|A^{-1}\| \leq \frac{1}{\|B\|}$, when $\|B\| \neq 0$, holds, then $(A - DB)$ is nonsingular and*

$$\|(A - DB)^{-1}\| \leq \frac{\|A^{-1}\|}{1 - \|A^{-1}B\|}.$$

Proof. The first part follows directly from Lemma 2.1. For the proof of the second part, we have $(A - DB)^{-1}$ can be written in the form

$$(A - DB)^{-1} = (I - A^{-1}DB)^{-1}A^{-1}.$$

But since $(I - A^{-1}DB)^{-1}(I - A^{-1}DB) = I$, it follows that

$$(I - A^{-1}DB)^{-1} = I + (I - A^{-1}DB)^{-1}A^{-1}DB.$$

By introducing an induced matrix norm, we get

$$\|(I - A^{-1}DB)^{-1}\| \leq \frac{1}{1 - \|A^{-1}\|\|D\|\|B\|} \leq \frac{1}{1 - \|A^{-1}\|\|B\|}.$$

Because

$$\|(A - DB)^{-1}\| = \|(I - A^{-1}DB)^{-1}A^{-1}\|,$$

it follows that

$$\|(A - DB)^{-1}\| \leq \frac{\|A^{-1}\|}{1 - \|A^{-1}\|\|B\|}.$$

This completes the proof.

and

$$B = 1/2 \begin{bmatrix} -51 & -5 & 1 & 1 & 1 & 1 & 1 & 1 & 1 & 1 \\ -5 & -51 & -5 & 1 & 1 & 1 & 1 & 1 & 1 & 1 \\ 1 & -5 & -51 & -5 & 1 & 1 & 1 & 1 & 1 & 1 \\ 1 & 1 & -5 & -51 & -5 & 1 & 1 & 1 & 1 & 1 \\ 1 & 1 & 1 & -5 & -51 & -5 & 1 & 1 & 1 & 1 \\ 1 & 1 & 1 & 1 & -5 & -51 & -5 & 1 & 1 & 1 \\ 1 & 1 & 1 & 1 & 1 & -5 & -51 & -5 & 1 & 1 \\ 1 & 1 & 1 & 1 & 1 & 1 & -5 & -51 & -5 & 1 \\ 1 & 1 & 1 & 1 & 1 & 1 & 1 & -5 & -51 & -5 \\ 1 & 1 & 1 & 1 & 1 & 1 & 1 & 1 & -5 & -51 \end{bmatrix}.$$

Applying Theorem 2.1, we have $\|A^{-1}\| \|B\| = 0.9166 < 1$, then this problem is uniquely solvable for any b . For this example, we take

$$b = [54, 54, 54, 54, 54, 54, 54, 54, 54, 54]^T.$$

Our starting point for this example is taken as

$$x_0 = [0.5, 0.5, 0.5, 0.5, 0.5, 0.5, 0.5, 0.5, 0.5, 0.5]^T.$$

The exact unique solution of this problem is given by

$$x^* = [3.653, 3.008, 3.154, 2.9412, 2.8306, 2.692, 2.567, 2.4604, 2.2705, 2.5987]^T.$$

The obtained numerical results are stated in Table 1.

Algorithms→	Picard's Algorithm	GN Algorithm
Iter	5	2
CPU	0.032344	0.014184
RSD	$5.9765e - 007$	0

Table 1: Numerical results for Example 5.1.

Example 5.2 The hydrodynamic equations (equilibrium problem) are modeled as the following non-differentiable algebraic equations:

$$Cx + \max(0, x) = c,$$

where $C \in \mathbb{R}^{n \times n}$, $c \in \mathbb{R}^n$ are given. By using the identity

$$\max(a, b) = \frac{1}{2}(a + b + |a - b|),$$

the hydrodynamic equation can be reformulated as an AVE (2). We have

$$Cx + \frac{1}{2}(x + |x|) = c \Leftrightarrow Ax - |x| - b = 0,$$

where $A = -(2C + I)$, $B = I$ and $b = -2c$.

Consider now a random hydrodynamic equation, where $C \in \mathbb{R}^{n \times n}$ and c are given by

$$C = (c_{ij}) = \begin{bmatrix} -25.5 & -2.5 & 0 & \dots & 0 & 0 \\ -2.5 & -25.5 & -2.5 & \dots & 0 & 0 \\ 0 & -2.5 & -25.5 & \dots & 0 & \vdots \\ \vdots & \vdots & \ddots & \ddots & -2.5 & 0 \\ 0 & 0 & 0 & \dots & -25.5 & -2.5 \\ 0 & 0 & \dots & 0 & -2.5 & -25.5 \end{bmatrix},$$

and

$$c = [-27, -29.5, \dots, -29.5, -27]^T.$$

For this example, we have taken two initial points such as

$$x_1^0 = [0.5, \dots, 0.5]^T \text{ and } x_2^0 = [0.9, \dots, 0.9]^T.$$

The computational results with different size of n are summarized in Table 2.

Algorithms→		Picard’s Algorithm		GN Algorithm	
Size n	x^0	Iter	CPU	Iter	CPU
100	x_1^0	11	0.064263	2	0.042966
	x_2^0	12	0.487104	3	0.051011
1000	x_1^0	88	26.133205	3	5.022345
	x_2^0	89	2.149593	3	5.884994
2000	x_1^0	335	54.093104	3	45.347198
	x_2^0	333	54.651662	3	45.064239

Table 2: Numerical results for Example 5.2.

Example 5.3 The matrices A and B are given by

$$A = \begin{bmatrix} 4 & -1 & 0 & \dots & 0 & 1 & 0 & 0 & \dots & 0 \\ -1 & 4 & \ddots & \ddots & \vdots & 0 & 1 & \ddots & \ddots & \vdots \\ 0 & \ddots & \ddots & \ddots & 0 & 0 & \ddots & \ddots & \ddots & 0 \\ \vdots & \ddots & \ddots & 4 & -1 & \vdots & \ddots & \ddots & 1 & 0 \\ 0 & \dots & 0 & -1 & 4 & 0 & \dots & 0 & 0 & 1 \\ 0.3 & 0 & 0 & \dots & 0 & 1/5 & -2 & -1/3 & \dots & 0 \\ 0 & 0.3 & \ddots & \ddots & \vdots & -2 & 1/5 & \ddots & \ddots & \vdots \\ 0 & \ddots & \ddots & \ddots & 0 & 1/4 & \ddots & \ddots & \ddots & -1/3 \\ \vdots & \ddots & \ddots & 0.3 & 0 & \vdots & \ddots & \ddots & 1/5 & -2 \\ 0 & \dots & 0 & 0 & 0.3 & 0 & \dots & 1/4 & -2 & 1/5 \end{bmatrix}.$$

$$B = (1/n) \begin{bmatrix} -2 & -1 & 1/5 & \cdots & 1/5 & -1 & 0 & 0 & \cdots & 0 \\ 0.4 & -2 & \ddots & \ddots & \vdots & 0 & -1 & \ddots & \ddots & \vdots \\ 3 & \ddots & \ddots & \ddots & 1/5 & 0 & \ddots & \ddots & \ddots & 0 \\ \vdots & \ddots & \ddots & -2 & -1 & \vdots & \ddots & \ddots & -1 & 0 \\ 3 & \cdots & 3 & 0.4 & -2 & 0 & \cdots & 0 & 0 & -1 \\ -12 & 0 & 5 & \cdots & 0 & -2 & -1 & 1/5 & \cdots & 0 \\ 0 & -12 & \ddots & \ddots & \vdots & 0.4 & -2 & \ddots & \ddots & \vdots \\ 1/5 & \ddots & \ddots & \ddots & 5 & 3 & \ddots & \ddots & \ddots & 1/5 \\ \vdots & \ddots & \ddots & -12 & 0 & \vdots & \ddots & \ddots & -2 & -1 \\ 0 & \cdots & 1/5 & 0 & -12 & 3 & \cdots & 3 & 0.4 & -2 \end{bmatrix}.$$

$$b = [5, -2, \dots, 5, -2]^T.$$

The obtained numerical results for different size of n , are summarized in Table 3.

Algorithms→	Picard's Algorithm		GN Algorithm	
Size n	Iter	CPU	Iter	CPU
4	40	0.025384	2	0.040067
8	23	0.028198	2	0.028242
40	26	0.060005	3	0.032638
80	22	0.113059	2	0.056422
200	25	0.560619	3	0.210737
400	30	5.126521	2	1.211867
1000	*	*	3	21.045136

Table 3: Numerical results for Example 5.3.

6 Conclusion

This paper presents a theoretical analysis and numerical study for solving new general absolute value equations (NGAVE). In the first part, we have presented some weaker sufficient conditions for the unique solvability of the NGAVE. For solving this NGAVE, we applied the generalized Newton method. In particular, the sufficient conditions for the convergence of our algorithm are studied. The obtained numerical results deduced from the testing examples illustrate that the suggested algorithms are efficient and valid to solve the NGAVE problems. Finally, an interesting topic of research in the future is solving the NGAVEs by introducing the Splitting method.

References

- [1] M. Achache, On the unique solvability and numerical study of absolute value equations. *J. Numer. Anal. Approx. Theory* **48** (2019) 112–121.
- [2] M. Achache and N. Anane. On the unique solvability and Picard's iterative method for absolute value equations. *Bulletin of Transilvania. Series III: Mathematics and Computer Sciences* **1** (63) (2021) 13–26.

- [3] M. Achache and N. Hazzam. Solving absolute value equations via linear complementarity and interior-point methods. *Journal of Nonlinear Functional Analysis*. Article. ID **39** (2018) 1–10.
- [4] N. Anane, Z. Kebaili and M. Achache. A DC Algorithm for Solving non-Uniquely Solvable Absolute Value Equations. *Nonlinear Dynamics and Systems Theory* **21** (2) (2023) 119–128.
- [5] M. Hladick. Bounds for the solution of absolute value equations. *Computational Optimization and Applications* **69** (1) (2018) 243–266.
- [6] S. Ketabchi and H. Moosaei. An efficient method for optimal correcting of absolute value equations by minimal changes in the right hand side. *Comput. Math. Appl.* **64** (2012) 1882–1885.
- [7] Y. Ke. The new iteration algorithm for absolute value equation. *Applied Mathematics Letters* **99** (2020).
- [8] E. Kreyszig. *Introductory Functional Analysis with Applications*. John Wiley Sons. New-York, London, Sydney. 1978.
- [9] O. L. Mangasarian and R. R. Meyer. Absolute value equations. *Linear Algebra and its Applications* **419** (2006) 359–367.
- [10] O. L. Mangasarian. A generalized Newton method for absolute value equations. *Optimization Letters* **3** (2009) 101–108.
- [11] F. Mezzardi. On the solution of general Absolute value equations. *Appl. Math. Lett* **117** (2020).
- [12] M. A. Noor, J. Iqbal and E. Al-Said, Residual iterative method for solving absolute value equations. *Abst. Appl. Anal.* 2012, Article. ID (2012) 1–9.
- [13] J. Rohn. On unique solvability of the absolute value equations. *Optimization Letters* **4**(2) (2010) 287–292.
- [14] J. Rohn. A theorem of the alternatives for the equations $Ax - B|x| = b$. *Linear and Multilinear Algebra* **52** (6)(2004) 421–426.
- [15] J. Rohn. A theorem of the alternatives for the equations $Ax - |B||x| = b$. *Optimization Letters* **6** (2012) 585–591.
- [16] S. L. Wang and C. X. Li. A note on unique solvability of the absolute value equation. *Optimization Letters* (2019).
- [17] S. L. Wu. The unique solution of a class of the new generalized absolute value equation. *Appl. Math. Lett.* **116** (2021).
- [18] A. Yu. Aleksandrov. Delay-Independent Stability Conditions for a Class of Nonlinear Mechanical Systems. *Nonlinear Dynamics and Systems Theory* **21** (5) (2021) 447–456.



Adaptive Control for the Stabilization, Synchronization and Anti-Synchronization of New Chaotic System with a Line Equilibrium

K. Mesbah^{1*} and N. E. Hamri²

¹ *Departement of Mathematics, University of Constantine 1, Constantine 25000, Algeria.*

² *Laboratory of Mathematics and Their Interactions,
Departement of Mathematics and Computer Science, University Center of Mila, 43000,
Algeria.*

Received: October 11, 2023; Revised: May 4, 2024

Abstract: This paper derives new results on the adaptive control, synchronization and anti-synchronization for the new chaotic system with a line equilibrium when the system's parameters are unknown. Firstly, we construct an adaptive controller to stabilize the new chaotic system to its unstable equilibrium at the origin. Then, we construct an adaptive controller to synchronize the new identical chaotic systems with unknown parameters. Finally, the corresponding adaptive controller to realize the anti-synchronization is also constructed for the same new identical chaotic systems. The Lyapunov stability theory and adaptive control theory have been applied to prove all the control, synchronization and anti-synchronization results derived in this paper. Numerical simulations have been presented to illustrate the main results for the new chaotic system with a line equilibrium.

Keywords: *chaos control; adaptive control; synchronization and anti-synchronization; Lyapunov stability theory.*

Mathematics Subject Classification (2010): 34H10, 37N35, 93C95, 93C40, 34D08, 34D06.

* Corresponding author: <mailto:kaouther.mesbah@umc.edu.dz>

1 Introduction

Over the last decades, there has been a great interest in the study of the chaotic behavior in deterministic systems. There are two leading applications in the chaos theory: chaos control and chaos synchronization. The emergence of these two areas in the study of nonlinear systems is due to the classical chaos control theory by Ott, Grebogi and Yorke [3] and chaos synchronization by Pecora and Carroll [7], followed by several types of synchronization that have been studied, namely generalized synchronization [9], projective synchronization [4], phase synchronization [14], anti-synchronization [8], etc.

Chaos, control and synchronization have received much attention due to their applications in many areas such as secure communication [11], biomedical engineering [2], ecological systems [1] and some other fields.

Lots of literature have studied the control, synchronization and anti-synchronization between two identical systems via classical control techniques, including PC and OGY methods, nonlinear optimal control [5], active control [15], adaptive control [12, 13], etc.

In this paper, the first case obtained after a systematic computer search from the Sprott case A with a line equilibrium is chosen to illustrate the proposed techniques. We design state control laws to stabilize the new chaotic system around the unstable periodic solutions or unstable equilibrium points. On the other hand, we use the adaptive control method to synchronize two new identical systems with a line equilibrium. Chaos synchronization investigates the linking of the trajectory of one system to the other system with the same parameter values, the two coupled chaotic systems are called synchronized if the error system converges to zero as time goes to infinity. Similarly, two coupled chaotic systems are called anti-synchronized if the sum system converges to zero as time goes to infinity, we demonstrate the effectiveness and validity of the proposed adaptive stabilization, synchronization and anti-synchronization schemes for the new chaotic system with a line equilibrium.

The paper is organized as follows. In Section 2, a system description is given. In Section 3, we apply the adaptive control for stabilizing the chaotic orbits to the equilibrium point of the system. In Section 4, we use the adaptive control method to synchronize two identical systems with unknown parameters. In Section 5, we also build a new adaptive controller to anti-synchronize the same new identical chaotic systems. Finally, some conclusions are given in Section 6.

2 System Description

We consider a general parametric form of the Sprott case A system [6] with quadratic nonlinearities of the form

$$\begin{cases} \dot{x} = y, \\ \dot{y}_2 = a_1x + a_2yz, \\ \dot{z}_2 = a_3x + a_4y + a_5y^2 + a_7xy + a_8xz + a_9yz. \end{cases} \quad (1)$$

This system has a line equilibrium in $(0, 0, z)$ with no other equilibria.

In 2013, after a systematic computer search, six simple chaotic cases $LE_1 - LE_6$ were founded [10] with only six terms and all these cases were dissipative. The typical example (LE_1) is given by

$$\begin{cases} \dot{x} = y, \\ \dot{y} = -x + yz, \\ \dot{z} = -x - axy - bxz, \end{cases} \quad (2)$$

where $(a, b) \in \mathbb{R}^2$.

For $(x_0, y_0, z_0) = (0., 0.5, 0.5)$, the chaotic attractor is shown in Figure 1.

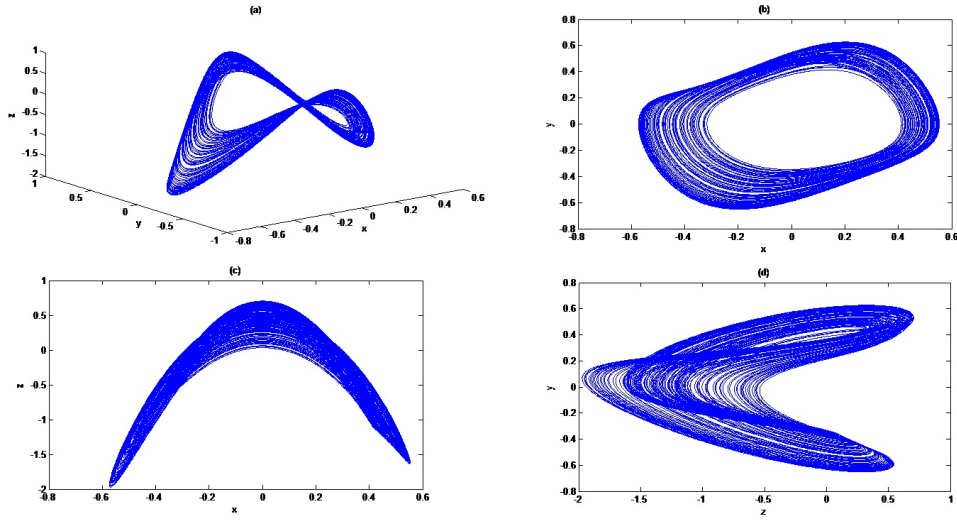


Figure 1: New chaotic system (2) with $a = 15$ and $b = 1$. (a) The strange attractor. (b) Projection on the x-y plane, (c) Projection on the x-z plane and (d) Projection on the z-y plane.

3 Adaptive Control of the New Chaotic System with a Line Equilibrium

3.1 Theoretical results

In this section, we design an adaptive control law for stabilizing the new chaotic system with a line equilibrium when the parameter values are unknown.

We add controllers to the system (2), then the controlled system is given by

$$\begin{cases} \dot{x} = y + u_1, \\ \dot{y} = -x + yz + u_2, \\ \dot{z} = -x - axy - bxz + u_3, \end{cases} \quad (3)$$

where u_1 , u_2 and u_3 are the function controllers to be designed using the variables x , y and z .

In order to ensure that the controlled system (3) converges to the zero equilibrium asymptotically, we consider the following adaptive control functions:

$$\begin{cases} u_1(t) = -y - x, \\ u_2(t) = x - yz - y, \\ u_3(t) = x + \hat{a}xy + \hat{b}xz - z, \end{cases} \quad (4)$$

where \hat{a} and \hat{b} are the estimates of the unknown parameters a and b .

Substituting the control law (4) into the controlled system (3), we obtain

$$\begin{cases} \dot{x} = -x, \\ \dot{y} = -y, \\ \dot{z} = (\hat{a} - a)xy + (\hat{b} - b)xz - z. \end{cases} \quad (5)$$

Let us now define the parameter errors as follows:

$$\begin{aligned} e_a &= a - \hat{a}, \\ e_b &= b - \hat{b}. \end{aligned}$$

For the derivation of the update law in order to adjust the parameter estimates \hat{a} and \hat{b} , the Lyapunov approach is used.

Consider the quadratic Lyapunov function

$$V = \frac{1}{2}(x^2 + y^2 + z^2 + e_a^2 + e_b^2),$$

which is a positive definite function on \mathbb{R}^5 .

By deriving V , we get

$$\dot{V} = -x^2 - y^2 + z(-e_a xy - e_b xz - z) + e_a(-\dot{\hat{a}}) + e_b(-\dot{\hat{b}}). \quad (6)$$

In view of Eq.(6), the estimated parameters are updated by the following law:

$$\begin{cases} \dot{\hat{a}} = -zxy + e_a, \\ \dot{\hat{b}} = -z^2x + e_b. \end{cases} \quad (7)$$

Substituting (7) into (6), we get

$$\dot{V} = -x^2 - y^2 - z^2 - e_a^2 - e_b^2 < 0. \quad (8)$$

Next, we prove the following result

Theorem 3.1 *The new controlled system (3) with unknown parameters is exponentially stabilized by the adaptive control law (4), where the parameter update law is given by (7).*

3.2 Numerical results

For the numerical simulations, the fourth-order Runge-Kutta method with the time step $\Delta t = 0.001$ is used to solve the system (3) with the adaptive control law (4) and parameter update law (7). The parameters of the system (3) are selected as: $a = 15$ and $b = 1$. Suppose that the initial values of the estimated parameters are $\hat{a}(0) = 0$ and $\hat{b}(0) = 4$. The initial states of the controlled system (3) are taken as: $x(0) = 0.5$, $y(0) = -0.5$ and $z(0) = 1.5$. When the adaptive control law (4) and the parameter update law (7) are used, the controlled system converges to the origin exponentially as shown in Figure 2. The time evolution of the parameter estimates is shown in Figure 3.

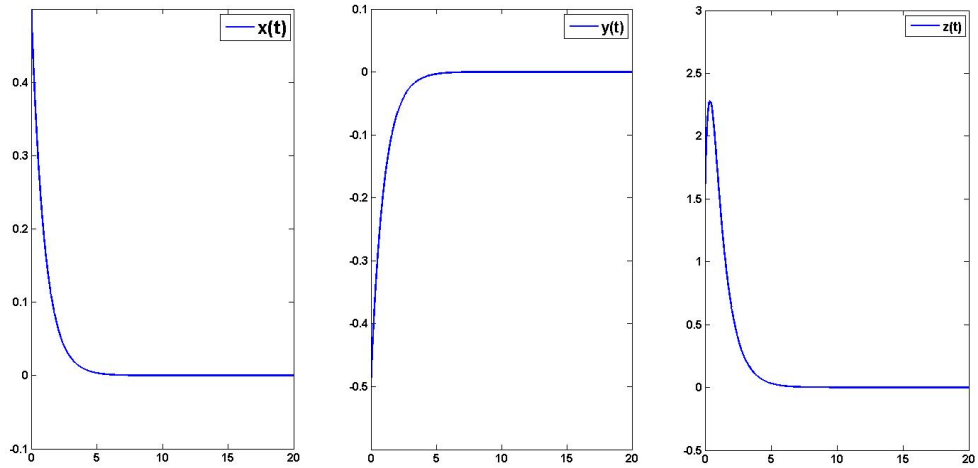


Figure 2: Time responses of the controlled system (3).

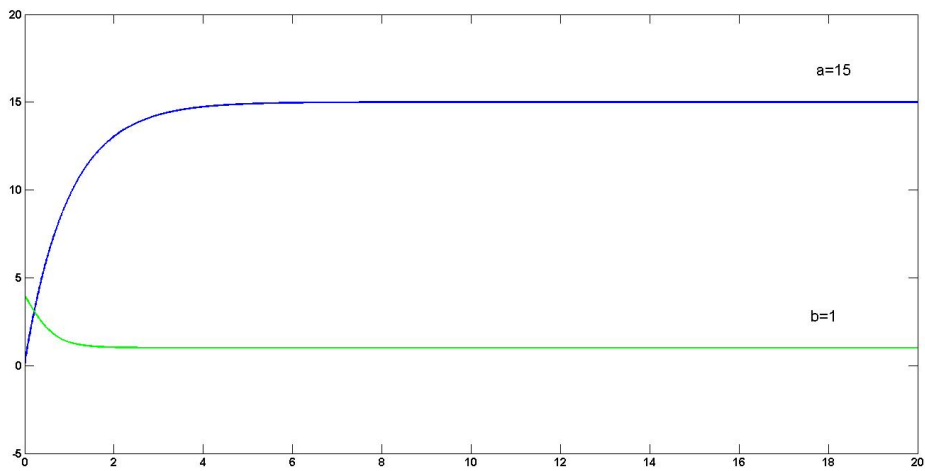


Figure 3: Time evolution of the parameter estimates $\hat{a}(t)$ and $\hat{b}(t)$.

4 Adaptive Synchronization of New Identical Chaotic Systems with a Line Equilibrium

4.1 Theoretical results

In this section, we design a control law for achieving synchronization between two new chaotic systems with two unknown parameters a and b .

The master system is given by

$$\begin{cases} \dot{x}_1 = y_1, \\ \dot{y}_1 = -x_1 + y_1 z_1, \\ \dot{z}_1 = -x_1 - ax_1 y_1 - bx_1 z_1. \end{cases} \quad (9)$$

The slave system is given by

$$\begin{cases} \dot{x}_2 = y_2 + u_1, \\ \dot{y}_2 = -x_2 + y_2 z_2 + u_2, \\ \dot{z}_2 = -x_2 - ax_2 y_2 - bx_2 z_2 + u_3, \end{cases} \quad (10)$$

where $u_i (i = 1, 2, 3)$ are the adaptive control functions to be designed.

It is said that synchronization occurs between master system (9) and slave system (10) if

$$\lim_{t \rightarrow \infty} \| X_2(t) - X_1(t) \| = 0,$$

where

$$\begin{aligned} X_1 &= (x_1, y_1, z_1), \\ X_2 &= (x_2, y_2, z_2). \end{aligned}$$

Now, for our synchronization scheme, let us define error signals between system (9) and system (10) as

$$\begin{cases} e_x(t) = x_2(t) - x_1(t), \\ e_y(t) = y_2(t) - y_1(t), \\ e_z(t) = z_2(t) - z_1(t). \end{cases}$$

The time derivative of the error signal is

$$\begin{cases} \dot{e}_x(t) = e_y + u_1(t), \\ \dot{e}_y(t) = -e_x + y_2 z_2 - y_1 z_1 + u_2(t), \\ \dot{e}_z(t) = -e_x - a(x_2 y_2 - x_1 y_1) - b(x_2 z_2 - x_1 z_1) + u_3(t). \end{cases} \quad (11)$$

New chaotic systems (9) and (10) can be synchronized asymptotically for any different initial conditions with the following adaptive controller:

$$\begin{cases} u_1(t) = -e_y - e_x, \\ u_2(t) = e_x - y_2 z_2 + y_1 z_1 - e_y, \\ u_3(t) = e_x + \hat{a}(x_2 y_2 - x_1 y_1) + \hat{b}(x_2 z_2 - x_1 z_1) - e_z. \end{cases} \quad (12)$$

Let us now define the parameter errors as

$$\begin{aligned} e_a &= a - \hat{a}, \\ e_b &= b - \hat{b}. \end{aligned}$$

Then

$$\begin{cases} \dot{e}_x(t) = -e_x, \\ \dot{e}_y(t) = -e_y, \\ \dot{e}_z(t) = -e_a(x_2 y_2 - x_1 y_1) - e_b(x_2 z_2 - x_1 z_1) - e_z. \end{cases} \quad (13)$$

For the derivation of the update law for adjusting the parameter estimates \hat{a} and \hat{b} , let us take the following Lyapunov function candidate:

$$V = \frac{1}{2}(e_x^2 + e_y^2 + e_z^2 + e_a^2 + e_b^2),$$

which is a positive definite function on \mathbb{R}^5 .

By deriving V , we get

$$\dot{V} = -e_x^2 - e_y^2 + e_z(-e_a(x_2y_2 - x_1y_1) - e_b(x_2z_2 - x_1z_1) - e_z) + e_a(-\dot{\hat{a}}) + e_b(-\dot{\hat{b}}). \quad (14)$$

In view of Eq.(14), the estimated parameter is updated by the following law:

$$\begin{cases} \dot{\hat{a}} = e_z(x_2y_2 - x_1y_1) + e_a, \\ \dot{\hat{b}} = e_z(x_2z_2 - x_1z_1) + e_b. \end{cases} \quad (15)$$

Substituting (15) into (14), we get

$$\dot{V} = -e_x^2 - e_y^2 - e_z^2 - e_a^2 - e_b^2 < 0. \quad (16)$$

Next, we prove the following result

Theorem 4.1 *The new identical chaotic systems (9) and (10) are exponentially synchronized by the adaptive control law (12), where the parameter update law is given by (15).*

4.2 Numerical results

Numerical simulations are performed to verify the efficiency and feasibility of the controller (12). The Runge-Kutta method is employed with the time step $\Delta t = 0.001$. The parameters of the system (9) are selected as $a = 15$ and $b = 1$. Suppose that the initial values of the estimated parameters are: $\hat{a}(0) = 0$ and $\hat{b}(0) = 4$. We take the initial values of the master system (9) as: $x_1(0) = 0$, $y_1(0) = 0.5$ and $z_1(0) = 0.5$. We take the initial values of the slave system (10) as: $x_2(0) = 0.5$, $y_2(0) = -1$ and $z_2(0) = 1$. Figure 4 shows the complete synchronization of the identical systems (9) and (10). Figure 5 shows the time evolution of the parameter estimates $\hat{a}(t)$ and $\hat{b}(t)$.

5 Adaptive Anti-Synchronization of New Identical Chaotic Systems with a Line Equilibrium

5.1 Theoretical results

In this section, we design an adaptive control law for achieving the anti-synchronization of new identical chaotic systems with two unknown parameters.

The master system is given by

$$\begin{cases} \dot{x}_1 = y_1, \\ \dot{y}_1 = -x_1 + y_1z_1, \\ \dot{z}_1 = -x_1 - ax_1y_1 - bx_1z_1. \end{cases} \quad (17)$$

The slave system is given by

$$\begin{cases} \dot{x}_2 = y_2 + u_1, \\ \dot{y}_2 = -x_2 + y_2z_2 + u_2, \\ \dot{z}_2 = -x_2 - ax_2y_2 - bx_2z_2 + u_3, \end{cases} \quad (18)$$

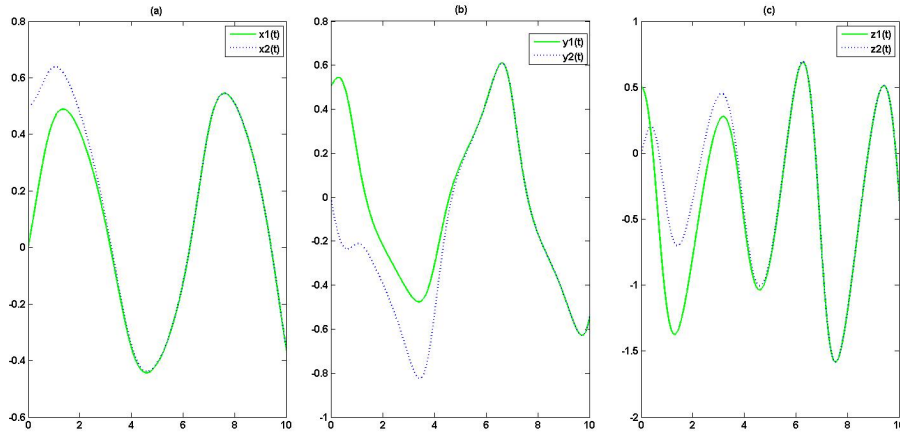


Figure 4: Time series of systems (9) and (10). (a) $x_1(t)$ and $x_2(t)$. (b) $y_1(t)$ and $y_2(t)$. (c) $z_1(t)$ and $z_2(t)$.

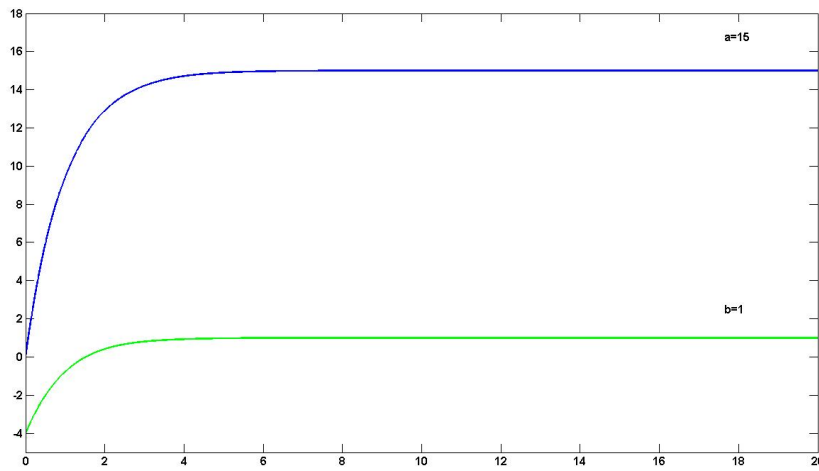


Figure 5: Time evolution of the parameter estimates $\hat{a}(t)$ and $\hat{b}(t)$.

where u_i ($i = 1, 2, 3$) are the adaptive control functions to be designed. The anti-synchronization error between system (17) and system (18) is defined by

$$\lim_{t \rightarrow \infty} \| X_2(t) + X_1(t) \| = 0,$$

where

$$\begin{aligned} X_1 &= (x_1, y_1, z_1) \\ X_2 &= (x_2, y_2, z_2). \end{aligned}$$

Then

$$\begin{cases} e_x(t) = x_2(t) + x_1(t), \\ e_y(t) = y_2(t) + y_1(t), \\ e_z(t) = z_2(t) + z_1(t). \end{cases}$$

The time derivative of the error signal is

$$\begin{cases} \dot{e}_x(t) = e_y + u_1(t), \\ \dot{e}_y(t) = -e_x + y_2z_2 + y_1z_1 + u_2(t), \\ \dot{e}_z(t) = -e_x - a(x_2y_2 + x_1y_1) - b(x_2z_2 + x_1z_1) + u_3(t). \end{cases} \quad (19)$$

New chaotic systems (17) and (18) can be anti-synchronized asymptotically for any different initial conditions with the following adaptive controller:

$$\begin{cases} u_1(t) = -e_y - e_x, \\ u_2(t) = e_x - y_2z_2 - y_1z_1 - e_y, \\ u_3(t) = e_x + \hat{a}(x_2y_2 + x_1y_1) + \hat{b}(x_2z_2 + x_1z_1) - e_z. \end{cases} \quad (20)$$

Let us now define the parameter errors as

$$\begin{aligned} e_a &= a - \hat{a}, \\ e_b &= b - \hat{b}. \end{aligned}$$

Then

$$\begin{cases} \dot{e}_x(t) = -e_x, \\ \dot{e}_y(t) = -e_y, \\ \dot{e}_z(t) = -e_a(x_2y_2 + x_1y_1) - e_b(x_2z_2 + x_1z_1) - e_z. \end{cases} \quad (21)$$

For the derivation of the update law for adjusting the parameter estimates \hat{a} and \hat{b} , let us take the following Lyapunov function candidate:

$$V = \frac{1}{2}(e_x^2 + e_y^2 + e_z^2 + e_a^2 + e_b^2),$$

which is a positive definite function on \mathbb{R}^5 .

By deriving V , we get

$$\dot{V} = -e_x^2 - e_y^2 - e_z(-e_a(x_2y_2 + x_1y_1) - e_b(x_2z_2 + x_1z_1) - e_z) + e_a(-\dot{\hat{a}}) + e_b(-\dot{\hat{b}}). \quad (22)$$

In view of Eq.(22), the estimated parameter is updated by the following law:

$$\begin{cases} \dot{\hat{a}} = -e_z(x_2y_2 + x_1y_1) + e_a, \\ \dot{\hat{b}} = -e_z(x_2z_2 + x_1z_1) + e_b. \end{cases} \quad (23)$$

Substituting (23) into (22), we get

$$\dot{V} = -e_x^2 - e_y^2 - e_z^2 - e_a^2 - e_b^2 < 0. \quad (24)$$

Next, we prove the following result.

Theorem 5.1 *The new identical chaotic systems are exponentially anti-synchronized by the adaptive control law (20), where the parameter update law is given by (23).*

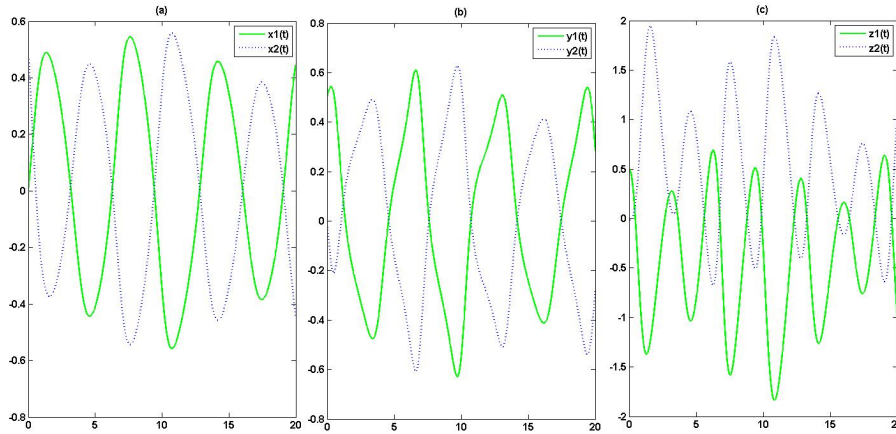


Figure 6: Time series of systems (18) and (19). (a) $x_1(t)$ and $x_2(t)$. (b) $y_1(t)$ and $y_2(t)$. (c) $z_1(t)$ and $z_2(t)$.

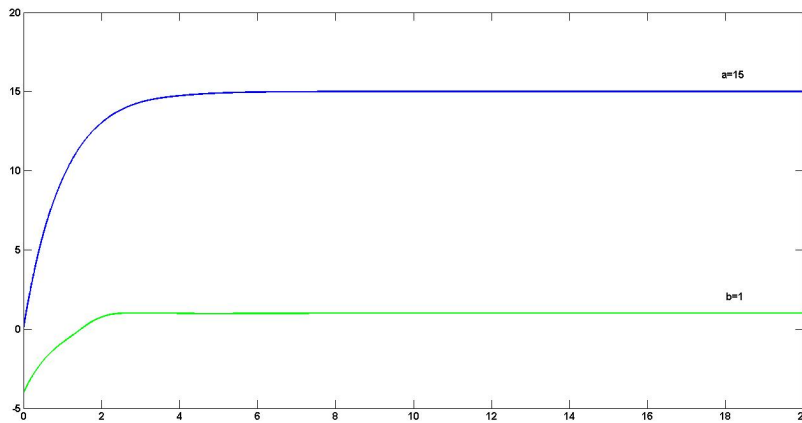


Figure 7: Time evolution of the parameter estimates $\hat{a}(t)$ and $\hat{b}(t)$.

5.2 Numerical results

The Runge-Kutta method is employed with the time step $\Delta t = 0.001$. The parameters of system (17) are selected as: $a = 15$ and $b = 1$. The initial values of the estimated parameters are $\hat{a}(0) = 0$ and $\hat{b}(0) = -4$. We take the initial values of the master system (17) as: $x_1(0) = 0$, $y_1(0) = 0.5$ and $z_1(0) = 0.5$. We take the initial values of the slave system (18) as: $x_2(0) = 0.5$, $y_2(0) = 0$ and $z_2(0) = 0$. Figure 6 shows the anti-synchronization of the identical systems (17) and (18). Figure 7 shows the time evolution of the parameter estimates $\hat{a}(t)$ and $\hat{b}(t)$.

6 Conclusion

In this paper, based on the Lyapunov stability theory and adaptive control theory, new results of stabilization, synchronization and anti-synchronization of the new chaotic system with a line equilibrium obtained from the Sprott case A are demonstrated. First, we designed adaptive control laws to stabilize the new chaotic system with unknown parameters to its unstable equilibrium point at the origin. Then, the synchronization and anti-synchronization of the new identical chaotic systems with unknown parameters are also realized. The proposed adaptive control method is very effective to achieve chaos control, synchronization and anti-synchronization. Numerical simulations are shown to demonstrate the effectiveness of the controllers in this paper.

References

- [1] B. Blasius, A. Huppert and L. Stone. Complex dynamics and phase synchronization in spatially extended ecological system. *Nature* **399** (1999) 354–359.
- [2] B. Zsolt. Chaos theory and power spectrum analysis in computerized cardiocography. *European Journal of Obstetrics & Gynecology and Reproductive Biology* **71** (2) (1997) 163–168.
- [3] E. Ott, C. Grebogi and J. A. Yorke. Controlling chaos. *Physical Review Letters* **64** (1990) 1196–1199.
- [4] F. Wang and Z. Zheng. Quasi-projective synchronization of fractional order chaotic systems under input saturation. *Physica A: Statistical Mechanics and Its Applications* **534** (2019) 122132.
- [5] G. Rigatos and M. Abbaszadeh. Nonlinear optimal control and synchronization for chaotic electronic circuits. *Journal of Computational Electronics* **20** (2) (2021) 1050–1063.
- [6] J. C. Sprott. Some simple chaotic flows. *Phys. Rev. E* **50** (1994) R647(R).
- [7] L. M. Pecora and T. L. Carroll. Synchronization in chaotic systems. *Physical Review Letters* **64** (1990) 821–824.
- [8] M. Labid and N. Hamri. Chaos Synchronization and Anti-Synchronization of two Fractional-Order Systems via Global Synchronization and Active Control. *Nonlinear Dynamics and Systems Theory* **19** (3) (2019) 416–426.
- [9] O. Martinez-Fuentes, J. Javier Montesinos-Garcia and J. Francisco Gomez-Aguilar. Generalized synchronization of commensurate fractional-order chaotic systems: Applications in secure information transmission. *Digital Signal Processing* **126** (2022) 103494.
- [10] S. Jafari and J. C. Sprott. Simple chaotic flows with a line equilibrium. *Chaos, Solitons and Fractals* **57** (2013) 79–84.
- [11] T. L. Liao and S. H. Tsai. Adaptive synchronization of chaotic systems and its applications to secure communications. *Chaos, Solitons and Fractals* **11** (2000) 1387–1396.
- [12] V. Sundarapandian. Adaptive control and synchronization of hyperchaotic Chen system. *International Journal of Information Technology Convergence and Services* **1** (3) (2011) 22–33.
- [13] X. Wang and Y. Wang. Adaptive control for synchronization of a four-dimensional chaotic system via a single variable. *Nonlinear Dynamics*. **65** (2011) 311–316.
- [14] Y. C. Hung and T. F. Hsu. Measuring phase synchronization in periodically driven Lu oscillator with a phase-incoherent attractor. *Nonlinear Dynamics* **86** (2016) 227–234.
- [15] Y. Lei, W. Xu and H. Zheng. Synchronization of two chaotic nonlinear gyros using active control. *Physics Letters A* **343** (1) (2005) 153–158.



Properties of MDTM and RDTM for Nonlinear Two-Dimensional Lane-Emden Equations

N. Teyar *

Department of Mathematics, Faculty of Exact Sciences, Brothers Mentouri University, Constantine-Algeria.

Received: September 30, 2023; Revised: April 25, 2024

Abstract: In this paper, we study the linear and the nonlinear forms of two-dimensional Lane-Emden type equations by proving and applying new product and quotient properties for different differential transform methods (RDTM and MDTM), in order to minimize computation to the maximum. We will obtain exact analytic solutions without linearization, discretization or perturbation, even with less computation.

Keywords: *two-dimensional Lane-Emden equation; two-dimensional Lane-Emden system of equations; reduced differential transform method; modified differential transform method; initial value problems.*

Mathematics Subject Classification (2010): 35J15, 35J47, 70F15, 35J75, 70K99.

1 Introduction

The linear and nonlinear two-dimensional Lane-Emden type equations are first introduced by Wazwaz, Rach and Duan in [8], as follows:

$$u_{xx} + \frac{\alpha}{x}u_x + u_{yy} + \frac{\beta}{y}u_y + g(x, y)f(u) = 0, \quad (1)$$

$$x > 0, y > 0, \alpha > 0, \beta > 0,$$

$$u(x, 0) = h(x), u_y(x, 0) = 0, \quad (2)$$

where $g(x, y)f(u)$ is a linear or nonlinear term.

* Corresponding author: <mailto:teyarnadir@gmail.com>

In this paper, we apply reduced and modified differential transform methods for solving this kind of elliptic problems, with singularities in both x and y , for obtaining exact solutions, not by multiplying singular equation by xyu^n , $n \in \mathbb{N}$, as we have done in other paper, but by proving new product and quotient properties for the RDTM and MDTM, which implies a minimum of computation.

L. Maia, G. Nornberg and F. Pacella in [7], introduce a dynamical system approach for second-order Lane–Emden type problems by defining some new variables that allow us to transform the radial fully nonlinear Lane-Emden equations into a quadratic dynamical system. For the one-dimension Lane-Emden equation, the original formal conservation of specific entropy along streamlines was given by a PDE in the function of t (time) and r (radius).

2 Definition and Properties of Reduced Differential Transform Method (RDTM)

We introduce the basic definitions of the reduced differential transform method as follows.

Definition 2.1 If the function $u(x, y)$ is analytic and differentiated continuously with respect to x and y , in the domain of interest, then let

$$U_k(x) = \frac{1}{k!} \left(\frac{\partial^k}{\partial y^k} u(x, y) \right)_{y=0}, \quad k \in \mathbb{N}, \quad (3)$$

where the y -dimensional spectrum function $U_k(x)$ is the reduced transformed function. In this paper, the lowercase $u(x, y)$ represents the original function, while the uppercase $U_k(x)$ stands for the transformed function.

Definition 2.2 The reduced differential inverse transform $U_k(x)$ of $u(x, y)$ is defined as follows:

$$u(x, y) = \sum_{k=0}^{\infty} U_k(x) y^k. \quad (4)$$

Then, combining equation (3) and (4), we write

$$u(x, y) = \sum_{k=0}^{\infty} \frac{1}{k!} \left(\frac{\partial^k}{\partial y^k} u(x, y) \right)_{y=0} y^k.$$

Some important properties of RDTM used in this paper, can be readily obtained and are listed in Table 1.

3 Definition and Properties of Modified Differential Transform Method (MDTM)

We introduce the basic definitions of the modified differential transform method as follows

Definition 3.1 The modified differential transform of $u(x, y)$ with respect to the variable y at y_0 is defined as

$$U(x, h) = \frac{1}{h!} \left(\frac{\partial^h}{\partial x^h} u(x, y) \right)_{y=y_0}, \quad k \in \mathbb{N}, \quad (5)$$

where $u(x, y)$ is the original function and $U(x, h)$ is the transformed function.

Original functions	Transformed functions
$w(x, y) = \alpha u(x, y) \pm \beta v(x, y)$	$W_k(x) = \alpha U_k(x) \pm \beta V_k(x)$
$w(x, y) = x^m y^n$	$W_k(x) = x^m \delta(k - n)$
$w(x, y) = x^m y^n u(x, y)$	$W_k(x) = x^m U_{k-n}(x)$
$w(x, y) = u(x, y)v(x, y)$	$W_k(x) = \sum_{r=0}^k U_r(x)U_{k-r}(x)$
$w(x, y) = [u(x, y)]^3$	$W_k(x) = \sum_{r=0}^k \sum_{s=0}^r U_{k-r}(x)U_s(x)U_{r-s}(x)$
$w(x, y) = \frac{\partial u(x, y)}{\partial x}$	$W_k(x) = \frac{\partial}{\partial x} U_k(x)$
$w(x, y) = \frac{\partial^2 u(x, y)}{\partial x^2}$	$W_k(x) = \frac{\partial^2}{\partial x^2} U_k(x)$
$w(x, y) = \frac{\partial^r u(x, y)}{\partial y^r}$	$W_k(x) = \frac{(k+r)!}{k!} U_{k+r}(x)$
$w(x, y) = e^{au(x, y)}$	$W_k(x) = \begin{cases} e^{aU_0(x)} & k = 0 \\ a \sum_{r=0}^{k-1} \frac{r+1}{k} U_{r+1}(x)W_{k-r-1}(x) & k \geq 1 \end{cases}$

Table 1: Fundamental properties of the RDTM.

Definition 3.2 The modified inverse differential transform $U(x, h)$ of $u(x, y)$ is defined as

$$u(x, y) = \sum_{h=0}^{\infty} U(x, h)(y - y_0)^h. \tag{6}$$

Then, combining equations (5) and (7), we write

$$u(x, y) = \sum_{h=0}^{\infty} \frac{1}{h!} \left(\frac{\partial^h}{\partial x^h} u(x, y) \right)_{y=y_0} (y - y_0)^h. \tag{7}$$

When (x, y_0) is taken as $(x, 0)$, then (6) can be expressed as

$$u(x, y) = \sum_{h=0}^{\infty} U(x, h)y^h.$$

Some important properties of MDTM used in this paper, are listed in Table 2.

4 Theorems and Corollaries

Theorem 4.1

$$w(x, y) = \frac{u(x, y)}{v(x, y)}$$

and $V(x, 0) \neq 0$, then the modified differential transform version is

$$W(x, h) = \begin{cases} \frac{U(x, 0)}{V(x, 0)}, & h = 0, \\ \frac{U(x, h) - \sum_{i=0}^{h-1} W(x, i)V(x, h-i)}{V(x, 0)} & h \geq 1. \end{cases}$$

Original functions	Transformed functions
$w(x, y) = \alpha u(x, y) \pm \beta v(x, y)$	$W(x, h) = \alpha U(x, h) + \beta V(x, h)$
$w(x, y) = x^m y^n$	$W(x, h) = x^m \delta(h - n)$
$w(x, y) = x^m y^n u(x, y)$	$W(x, h) = x^m U(x, h - n)$
$w(x, y) = u(x, y)v(x, y)$	$W(x, h) = \sum_{s=0}^k U(x, s)V(x, h - s)$
$w(x, y) = [u(x, y)]^3$	$W(x, h) = \sum_{r=0}^h \sum_{s=0}^r U(x, h - r)U(x, s)U(x, r - s)$
$w(x, y) = \frac{\partial u(x, y)}{\partial x}$	$W(x, h) = \frac{\partial U(x, h)}{\partial x}$
$w(x, y) = \frac{\partial^2 u(x, y)}{\partial x^2}$	$W(x, h) = \frac{\partial^2 U(x, h)}{\partial x^2}$
$w(x, y) = \frac{\partial u(x, y)}{\partial y}$	$W(x, h) = (h + 1)U(x, h + 1)$
$w(x, y) = \frac{\partial^2 u(x, y)}{\partial y^2}$	$W(x, h) = (h + 1)(h + 2)U(x, h + 2)$
$w(x, y) = e^{au(x, y)}$	$W(x, h) = \begin{cases} e^{aU(x, 0)} & h = 0 \\ a \sum_{s=0}^{h-1} \frac{s+1}{h} U(x, s+1)W(x, h-s-1), & h \geq 1 \end{cases}$

Table 2: Fundamental properties of the MDTM.

Proof.

$$v(x, y)w(x, y) = u(x, y).$$

So, by applying the modified differential transform, we get

$$\sum_{r=0}^k \sum_{s=0}^h V(x, s)W(x, h - s) = U(x, h).$$

For $h = 0$, $V(x, 0)W(x, 0) = U(x, 0)$ gives $W(x, 0) = \frac{U(x, 0)}{V(x, 0)}$.

For $h = 1$, $V(x, 1)W(x, 0) + V(x, 0)W(x, 1) = U(x, 1)$.

Then

$$W(x, 1) = \frac{U(x, 1) - V(x, 1)W(x, 0)}{V(x, 0)}.$$

For $h = 2$,

$$W(x, 2) = \frac{U(x, 2) - V(x, 2)W(x, 0) - V(x, 1)W(x, 1)}{V(x, 0)}.$$

Finally,

$$W(x, h) = \frac{U(x, h) - \sum_{i=0}^{h-1} W(x, i)V(x, h - i)}{V(x, 0)}, \quad h \geq 1.$$

Corollary 4.1 (MDTM) *If*

$$w(x, y) = \frac{x^m y^n}{v(x, y)}$$

and $V(x, 0) \neq 0$, then the modified differential transform version is

$$W(x, h) = \begin{cases} \frac{x^m \delta(n)}{V(x, 0)}, & h = 0, \\ \frac{x^m \delta(h - n) - \sum_{i=0}^{h-1} W(x, i)V(x, h - i)}{V(x, 0)}, & h \geq 1. \end{cases}$$

Corollary 4.2 (MDTM) *If*

$$w(x, y) = \frac{1}{v(x, y)}$$

and $V(x, 0) \neq 0$, then the modified differential transform version is

$$W(x, h) = \begin{cases} \frac{1}{V(x, 0)}, & h = 0, \\ \frac{-\sum_{i=0}^{h-1} W(x, i)V(x, h - i)}{V(x, 0)}, & h \geq 1. \end{cases}$$

Theorem 4.2 (MDTM) *If*

$$w(x, y) = \frac{u(x, y)}{x^m y^n}, \quad (x, y) \neq (0, 0),$$

then the modified differential transform version of $w(x, y)$ is

$$W(x, h) = \frac{U(x, h + n)}{x^m}.$$

Proof. We have

$$x^m y^n w(x, y) = u(x, y), \quad (x, y) \neq (0, 0).$$

From Table 2, we get $x^m W(x, h - n) = U(x, h)$. Then

$$W(x, h) = \frac{U(x, h + n)}{x^m}.$$

Corollary 4.3 (MDTM) *If*

$$w(x, y) = \frac{u(x, y)}{x}, \quad x \neq 0,$$

then the modified differential transform version is

$$W(x, h) = \frac{U(x, h)}{x}.$$

Corollary 4.4 (MDTM) *If*

$$w(x, y) = \frac{u(x, y)}{y}, \quad y \neq 0.$$

then the modified differential transform version is

$$W(x, h) = U(x, h + 1).$$

Theorem 4.3

$$w(x, y) = \frac{u(x, y)}{v(x, y)}.$$

Then the reduced differential transform version is

$$W_k(x) = \begin{cases} \frac{U_0(x)}{V_0(x)}, & k = 0, \\ \frac{U_k(x) - \sum_{i=0}^{k-1} W_i(x)V_{k-i}(x)}{V_0(x)}, & k \geq 1. \end{cases}$$

Proof. The proof is similar to the previous one (Theorem 4.2).

Corollary 4.5 (MDTM) *If*

$$w(x, y) = \frac{x^m y^n}{v(x, y)}$$

and $V_0(x) \neq 0$, then the reduced differential transform version is

$$W_k(x) = \begin{cases} \frac{x^m \delta(n)}{V_0(x)}, & k = 0, \\ \frac{x^m \delta(k - n) - \sum_{i=0}^{k-1} W_i(x)V_{k-i}(x)}{V_0(x)}, & k \geq 1. \end{cases}$$

Corollary 4.6 (MDTM) *If*

$$w(x, y) = \frac{1}{v(x, y)}$$

and $V_0(x) \neq 0$, then the reduced differential transform version is

$$W_k(x) = \begin{cases} \frac{1}{V_0(x)}, & k = 0, \\ \frac{-\sum_{i=0}^{k-1} W_i(x)V_{k-i}(x)}{V_0(x)} & k \geq 1. \end{cases}$$

Theorem 4.4 *If*

$$w(x, y) = \frac{u(x, y)}{x^m y^n}, \quad (x, y) \neq (0, 0),$$

then the reduced differential transform version of $w(x, y)$ is

$$W_k(x) = \frac{U_{k+n}(x)}{x^m}.$$

Proof. We have

$$x^m y^n w(x, y) = u(x, y), \quad (x, y) \neq (0, 0).$$

From Table 3, we get $x^m W_{k-n}(x) = U_k(x)$.

Then

$$W_k(x) = \frac{U_{k+n}(x)}{x^m}.$$

Corollary 4.7 (MDTM) *If*

$$w(x, y) = \frac{u(x, y)}{x}, \quad x \neq 0,$$

then the reduced differential transform version is

$$W_k(x) = \frac{U_k(x)}{x}.$$

Corollary 4.8 (MDTM) *If*

$$w(x, y) = \frac{u(x, y)}{y}, \quad y \neq 0,$$

then the reduced differential transform version is

$$W_k(x) = \frac{U_{k+1}(x)}{x}.$$

5 Applications

5.1 Modified differential transform method

Example 5.1 First, we consider the nonlinear Lane-Emden equation

$$u_{xx} + \frac{3}{x}u_x + u_{yy} + \frac{4}{y}u_y - 14e^{-u} = 0 \tag{8}$$

subject to the initial conditions

$$u(x, 0) = 2\ln x, \quad u_y(x, 0) = 0. \tag{9}$$

From Table 2 and Corollaries 4.7, 4.8, the modified differential transform version of (8) is

$$U(x, h + 2) = \frac{-1}{(h + 5)(h + 2)} \left[\frac{\partial^2 U(x, h)}{\partial x^2} + \frac{3}{x} \frac{\partial U(x, h)}{\partial x} - 14W(x, h) \right],$$

where $W(x, h)$ is the modified differential transform version of e^{-u} (Table 2) such that

$$W(x, h) = \begin{cases} e^{-U(x,0)} = \frac{1}{x^2}, & h = 0, \\ -\sum_{s=0}^{h-1} \frac{s+1}{h} U(x, s+1)W(x, h-s-1), & h \geq 1. \end{cases}$$

Also, the modified differential transform version of initial conditions (9) is

$$U(x, 0) = 2\ln x, \quad U(x, 1) = 0,$$

then, for $h = 0$,

$$U(x, 2) = \frac{-1}{10x} \left[\frac{\partial^2 U(x, 0)}{\partial x^2} + \frac{3}{x} \frac{\partial U(x, 0)}{\partial x} - 14W(x, 0) \right] = \frac{1}{x^2}.$$

For $h = 1$ ($W(x, 1) = 0$),

$$U(x, 3) = \frac{-1}{18x} \left[\frac{\partial^2 U(x, 1)}{\partial x^2} + \frac{3}{x} \frac{\partial U(x, 1)}{\partial x} - 14W(x, 1) \right] = 0.$$

For $h = 2$,

$$U(x, 4) = \frac{-1}{28} \left[\frac{\partial^2 U(x, 2)}{\partial x^2} + \frac{3}{x} \frac{\partial U(x, 2)}{\partial x} - 14W(x, 2) \right] = \frac{-1}{2x^4},$$

where $W(x, 2) = \frac{-1}{x^4}$.

For $h = 3$,

$$U(x, 5) = \frac{-1}{40} \left[\frac{\partial^2 U(x, 3)}{\partial x^2} + \frac{3}{x} \frac{\partial U(x, 3)}{\partial x} - 14W(x, 3) \right] = 0.$$

For $h = 4$,

$$U(x, 6) = \frac{-1}{54} \left[\frac{\partial^2 U(x, 4)}{\partial x^2} + \frac{3}{x} \frac{\partial U(x, 4)}{\partial x} - 14W(x, 4) \right] = \frac{1}{3x^6}.$$

Then, by substituting the quantities $U(x, h)$ in Eq.(7), we get the series solution

$$u(x, y) = 2\ln x + \left(\frac{y}{x}\right)^2 - \frac{1}{2} \left(\frac{y}{x}\right)^4 + \frac{1}{3} \left(\frac{y}{x}\right)^6 + \dots \quad (10)$$

and the exact solution is

$$u(x, y) = \ln(x^2 + y^2). \quad (11)$$

The solution is also obtained by the Adomian decomposition method in [8].

Example 5.2 Second, we consider the nonlinear Lane-Emden equation

$$u_{xx} + \frac{3}{x}u_x + u_{yy} + \frac{3}{y}u_y - 7u^{-1} = 0 \quad (12)$$

subject to the initial conditions

$$u(x, 0) = x, \quad u_y(x, 0) = 0. \quad (13)$$

From Table 2 and Corollaries 4.7, 4.8, the modified differential transform version of (12) is

$$\frac{\partial^2 U(x, h)}{\partial x^2} + \frac{3}{x} \frac{\partial U(x, h)}{\partial x} + (h+4)(h+2)U(x, h+2) - 7W(x, h) = 0.$$

where $W(x, h)$ is the modified differential transform version of u^{-1} (Corollary 4.2) such that

$$W(x, h) = \begin{cases} \frac{1}{x}, & h = 0, \\ -\frac{\sum_{i=0}^{h-1} W(x, i)U(x, h-i)}{x}, & h \geq 1. \end{cases}$$

From (13), we get $U(x, 0) = x$, $U(x, 1) = 0$, then $W(x, 1) = 0$.

$$U(x, h + 2) = \frac{-1}{(h + 4)(h + 2)} \left[\frac{\partial^2 U(x, h)}{\partial x^2} + \frac{3}{x} \frac{\partial U(x, h)}{\partial x} - 7W(x, h) \right].$$

For $h=0$, we get

$$U(x, 2) = \frac{-1}{8} \left[\frac{\partial^2 U(x, 0)}{\partial x^2} + \frac{3}{x} \frac{\partial U(x, 0)}{\partial x} - \frac{7}{x} \right] = \frac{4}{8x} = \frac{1}{2x}.$$

For $h = 1$, because $U(x, 1) = 0$, we have $W(x, 1) = 0$, so

$$U(x, 3) = \frac{-1}{15} \left[\frac{\partial^2 U(x, 1)}{\partial x^2} + \frac{3}{x} \frac{\partial U(x, 1)}{\partial x} - 7W(x, 1) \right] = 0.$$

For $h = 2$, we have $W(x, 2) = \frac{-1}{2x^3}$, so

$$U(x, 4) = \frac{-1}{24} \left[\frac{\partial^2 U(x, 2)}{\partial x^2} + \frac{3}{x} \frac{\partial U(x, 2)}{\partial x} - 7W(x, 2) \right] = \frac{-3}{24x^3} = \frac{-1}{8x^3}.$$

And

$$U(x, 5) = 0, \quad U(x, 6) = \frac{1}{16x^5}.$$

Then, by substituting the quantities $U(x, h)$ in (7), we get the following series solution:

$$u(x, y) = x + \frac{1}{2} \left(\frac{y^2}{x} \right) - \frac{1}{8} \left(\frac{y^4}{x^3} \right) + \frac{1}{16} \left(\frac{y^6}{x^5} \right) + \dots \tag{14}$$

And the exact solution is

$$u(x, y) = \sqrt{x^2 + y^2}. \tag{15}$$

Example 5.3 We consider now the nonlinear Lane-Emden equation

$$u_{xx} + \frac{4}{x}u_x + u_{yy} + \frac{4}{y}u_y - (5 + 4x^2y^2)(x^2 + y^2)u^{-3} = 0 \tag{16}$$

subject to the initial conditions

$$u(x, 0) = 1, \quad u_y(x, 0) = 0. \tag{17}$$

From (17), we get

$$U(x, 0) = 1 \quad U(x, 1) = 0.$$

From Table 2 and Corollaries 4.7, 4.8, the modified differential transform version of (16) gives

$$U(x, h + 2) = \frac{1}{(h + 5)(h + 2)} \left[\frac{\partial^2 U(x, h)}{\partial x^2} + \frac{4}{x} \frac{\partial U(x, h)}{\partial x} - (5x^2W(x, h) + 5W(x, h - 2) + 4x^4W(x, h - 2) + 4x^2W(x, h - 4)) \right],$$

where $W(x, h)$ is the modified differential transform version of u^{-3} (Table 2) such that

$$W(x, h) = \begin{cases} \frac{1}{U^3(x, 0)} = 1, & h = 0, \\ -\sum_{i=0}^{h-1} W(x, i) U_1(x, h-i), & h \geq 1 \end{cases}$$

$$U_1(x, h) = \sum_{r=0}^h \sum_{s=0}^r U(x, h-r) U(x, s) U(x, r-s).$$

Then

$$W(x, h) = \begin{cases} \frac{1}{U^3(x, 0)} = 1, & h = 0, \\ -\sum_{i=0}^{h-1} W(x, i) \sum_{r=0}^{h-i} \sum_{s=0}^r U(x, h-i-r) U(x, s) U(x, r-s), & h \geq 1. \end{cases}$$

For $h = 0$, we get

$$\frac{\partial^2 U(x, 0)}{\partial x^2} + \frac{4}{x} \frac{\partial U(x, 0)}{\partial x} + 10U(x, 2) - 5x^2 W(x, 0) = 0.$$

Then

$$U(x, 2) = \frac{5x^2}{10} = \frac{x^2}{2}.$$

For $h = 1$,

$$\frac{\partial^2 U(x, 1)}{\partial x^2} + \frac{4}{x} \frac{\partial U(x, 1)}{\partial x} + 18U(x, 3) - 5x^2 W(x, 1) = 0,$$

where

$$W(x, 1) = -\sum_{i=0}^0 W(x, i) \sum_{r=0}^{1-i} \sum_{s=0}^r U(x, 1-i-r) U(x, s) U(x, r-s)$$

$$= -W(x, 0) [U(x, 1)U(x, 0)U(x, 0) + U(x, 0)U(x, 0)U(x, 1) + U(x, 0)U(x, 1)U(x, 0)] = 0$$

Then $18U(x, 3) = 0$. So, $U(x, 3) = 0$.

For $h = 2$,

$$\frac{\partial^2 U(x, 2)}{\partial x^2} + \frac{4}{x} \frac{\partial U(x, 2)}{\partial x} + 28U(x, 4) - 5x^2 W(x, 2) - 5W(x, 0) - 4x^4 W(x, 0) = 0. \quad (18)$$

We first calculate

$$W(x, 2) = -\sum_{i=0}^1 W(x, i) \sum_{r=0}^{2-i} \sum_{s=0}^r U(x, 2-i-r) U(x, s) U(x, r-s)$$

$$= -W(x, 0) [U(x, 2)U(x, 0)U(x, 0) + U(x, 1)U(x, 0)U(x, 1) + U(x, 0)U(x, 0)U(x, 2)$$

$$+ U(x, 0)U(x, 1)U(x, 1) + U(x, 0)U(x, 2)U(x, 0)] = -\left(\frac{x^2}{2} + \frac{x^2}{2} + \frac{x^2}{2}\right) = -\frac{3x^2}{2}.$$

Then Eq.(18) becomes

$$1 + 4 + 28U(x, 4) + 5x^2 \left(\frac{3x^2}{2} \right) - 5 - 4x^4 = 0.$$

So,

$$28U(x, 4) = \frac{-7x^4}{2} \Rightarrow U(x, 4) = \frac{-x^4}{8}.$$

And

$$U(x, 5) = 0, \quad U(x, 6) = \frac{x^6}{16}, \quad U(x, 7) = 0, \quad U(x, 8) = \frac{-5x^8}{128}, \quad \dots$$

Then, by substituting the quantities $U(x, h)$ in Eq.(7), we get the following series solution:

$$u(x, y) = 1 + \frac{x^2y^2}{2} - \frac{x^4y^4}{8} + \frac{x^6y^6}{16} - \frac{5x^8y^8}{128} + \dots$$

And the exact solution is

$$u(x, y) = \sqrt{1 + x^2y^2}.$$

The exact solution is not obtained by the Adomian method in [8], only the approximate solution is mentioned.

Remark 5.1 The application of the reduced differential transform method gives the same coefficients of power series and same steps of computation.

Remark 5.2 The nonlinear two-dimensional Lane–Emden system of equations can be introduced and solved by the RDTM and MDTM using the same computation steps.

$$\begin{cases} u_{xx} + \frac{\alpha}{x}u_x + u_{yy} + \frac{\beta}{y}u_y + f(x, y, v) = 0, \\ v_{xx} + \frac{\gamma}{x}v_x + v_{yy} + \frac{\theta}{y}v_y + g(x, y, u) = 0, \end{cases}$$

$$x > 0, \quad y > 0, \quad \alpha > 0, \quad \beta > 0, \quad \gamma > 0, \quad \theta > 0,$$

$$u(x, 0) = h(x), \quad u_y(x, 0) = 0, \quad v(x, 0) = k(x), \quad v_y(x, 0) = 0.$$

6 Conclusion

In this paper, the Reduced Differential Transform Method (RDTM) and Modified Differential Transformation Method (MDTM) have been successfully applied for obtaining exact solutions to the nonlinear forms of two-dimensional Lane–Emden type equations, by proving and applying new product and quotient properties for different differential transform methods (RDTM and MDTM). This paper is the first to provide an exact solution by the DTM (Differential transform method) in the case, where the Adomian method gives an approximative solution. We also introduce the two-dimensional Lane–Emden system of equations and obtain exact analytic solutions.

References

- [1] F. Ayaz. On two-dimensional differential transform method. *Appl. Math. Comput.* **143** (2003) 361–374.
- [2] F. Ayaz. Solution of the system of differential equations by differential transform method. *Appl. Math. Comput.* **147** (2004) 547–567.
- [3] C. K. Chen and S. H. Ho. Solving partial differential equations by two-dimensional differential transform method. *Appl. Math. Comput.* **106** (1999) 171–179.
- [4] B. Ibis and M. Bayram. Approximate solutions for some nonlinear evolutions equations by using the reduced differential transform method. *Int. J. Appl. Math. Res.* **1** (3) (2012) 288–302.
- [5] M. J. Jang, C. L. Chen and Y. C. Liu. Two-dimensional differential transform for partial differential equations. *Appl. Math. Comput.* **121** (2001) 261–270.
- [6] A. S. V. R. Kanth and K. Aruna. Comparison of two Dimensional DTM and PDTM for solving Time-Dependent Emden-Fowler Type Equations. *Int. J. Nonlinear Sci.* **13** (2012) 228–239.
- [7] L. Maia, G. Nornberg and F. Pacella. A dynamical system approach for Lane–Emden type problems. *Books in Bytes.*, (2021) Brazil.
- [8] A. M. Wazwaz, R. Rach. and J. S. Duan. Solving the two-dimensional Lane–Emden type equations by the Adomian decomposition method. *J. Appl. Math. Stat.* **3** (1) (2016) 15–26.

CAMBRIDGE SCIENTIFIC PUBLISHERS

AN INTERNATIONAL BOOK SERIES
STABILITY OSCILLATIONS AND OPTIMIZATION OF SYSTEMS

Stability Analysis of Nonlinear Systems under Structural Perturbations

Stability, Oscillations and Optimization of Systems: 2014, Volume 8, 252 pp.

ISBN 978-1-908106-37-7 £55 /\$100 /€ 80

A.A. Martynyuk

Institute of Mechanics, National Academy of Sciences of Ukraine, Kyiv, Ukraine

V.G. Miladzhanov

Andizhan University, Andizhan, O'zbekiston

This book focuses on some problems of stability theory of nonlinear large-scale systems. The purpose of this book is to describe some new applications of Liapunov matrix-valued functions method to the stability of evolution problems governed by nonlinear continuous systems, discrete-time systems, impulsive systems and singularly perturbed systems under nonclassical structural perturbations. The authors take a challenging and original approach based on concept of structural perturbations combined with direct Liapunov's method. This new approach will lead to results that cannot be obtained by standard theories of stability in the field.

The **Stability Analysis of Nonlinear Systems under Structural Perturbations** addresses to specialists in dynamical systems, applied differential equations, and the stability theory. It may be useful for graduated students in mathematics, control theory, and mechanical engineering.

CONTENTS

Preface • Generalities • Continuous Systems under Nonclassical Structural Perturbations • Discrete-Time Systems under Nonclassical Structural Perturbations • Impulsive Systems under Nonclassical Structural Perturbations • Singularly Perturbed Systems under Nonclassical Structural Perturbations • References • Subject Index

Please send order form to:

Cambridge Scientific Publishers

PO Box 806, Cottenham, Cambridge CB4 8RT Telephone: +44 (0) 1954 251283
Fax: +44 (0) 1954 252517 Email: janie.wardle@cambridgescientificpublishers.com

Or buy direct from our secure website: www.cambridgescientificpublishers.com

CAMBRIDGE SCIENTIFIC PUBLISHERS

AN INTERNATIONAL BOOK SERIES
STABILITY OSCILLATIONS AND OPTIMIZATION OF SYSTEMS

Advances in Stability and Control Theory for Uncertain Dynamical Systems

Stability, Oscillations and Optimization of Systems: Volume 11

317+xxii pp., 2021 ISBN 978-1-908106-73-5 £60/\$80/€67

C. Cruz-Hernández (Ed.)

Department of Electronics and Telecommunications, Scientific Research and Advanced Studies Center of Ensenada (CICESE), Ensenada, México.

A.A. Martynyuk (Ed.)

Institute of Mechanics, National Academy of Sciences of Ukraine, Kyiv, Ukraine

A.G. Mazko (Ed.)

Institute of Mathematics, National Academy of Sciences of Ukraine, Kyiv, Ukraine

This volume presents the latest investigations in stability and control theory for uncertain dynamical systems, incorporating the main engineering applications. The volume consists of 16 chapters containing the results of theoretical research and engineering applications of some uncertain systems and provides new trends for future promising researches. Some issues covered in the volume include:

- stability and control in uncertain systems: optimal design of robust control, generalization of direct Lyapunov method, robust output feedback stabilization and optimization of control systems, optimal control of nonlinear systems over an infinite horizon;
- stability and stabilization in discrete-time systems: stability conditions for discrete-time positive switched systems with delay, quadratic stabilization for nonlinear perturbed discrete time-delay systems, robust output feedback stabilization and optimization of discrete-time control systems, stability of singularly perturbed nonlinear Lur'e discrete-time systems;
- synchronization in dynamical systems: function projective dual synchronization of chaotic systems with uncertain parameters, anti-synchronization and hybrid synchronization of 3D discrete generalized Hénon map, adaptive hybrid function projective synchronization;
- engineering applications: attitude stabilization of a rigid body, adaptive control of continuous bioreactors, wavelet adaptive tracking control, adaptive fuzzy control of nonlinear systems, robust active control for structural systems with structured uncertainties.

The **Advances in Stability and Control Theory for Uncertain Dynamical Systems** may be useful for graduate students and researchers in applied mathematics and physics, control, nonlinear science, and engineering.

CONTENTS: Introduction to the series • Preface • Contributors • An Overview • Stability and Control in Uncertain Systems • Stability and Stabilization in Discrete-Time Systems • Synchronization in Dynamical Systems • Engineering applications • Index

Please send order form to:

Cambridge Scientific Publishers

45 Margett Street, Cottenham, Cambridge CB24 8QY, UK

Telephone: +44 (0) 1954 251283; Fax: +44 (0) 1954 252517

Email: janie.wardle@cambridgescientificpublishers.com

Or buy direct from our secure website: www.cambridgescientificpublishers.com
